RHIC Multi-Year Beam Use Request For Run7 – Run 9

The STAR Collaboration

August 24, 2006

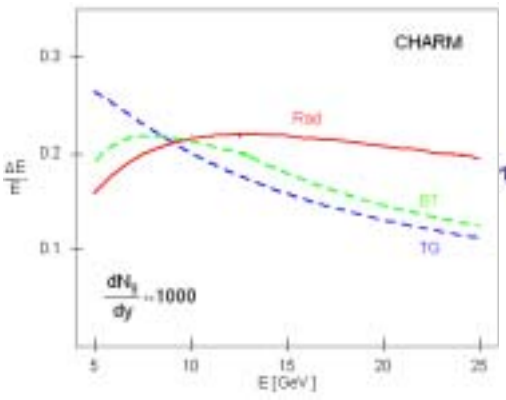

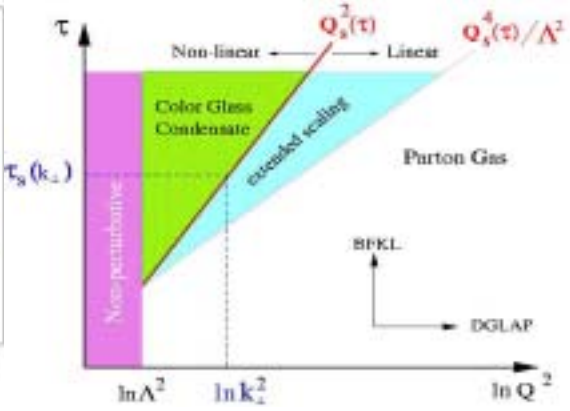

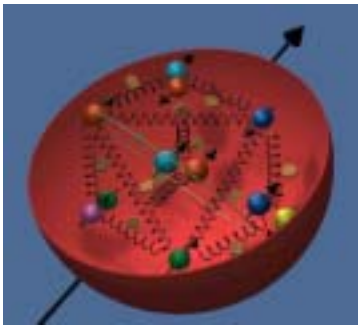

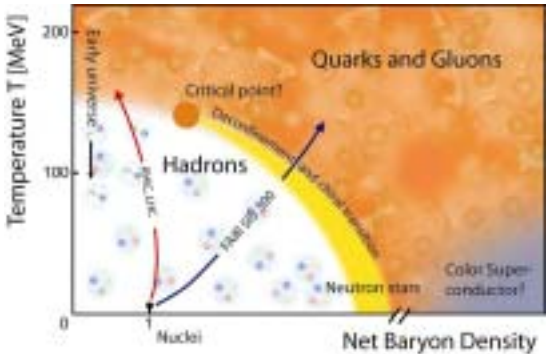

Table of Contents

	Executive Summary	4
1.	Report on polarized proton data taking in Run 6	6
1.1	Improvements in RHIC Collider performance	7
1.2	Improvements in STAR Detector Capability	8
1.3	Summary of performance in Run 6	10
2.0	Recent spin physics results and expected results from Run 6	11
2.1	Longitudinal spin physics program	11
2.2	Transverse spin physics program	19
3.	Multi-year spin physics beam use request for Run7 – Run 9	24
4.0	Recent heavy ion physics results and beam use proposal for Run 7	29
4.1	Recent relativistic heavy ion physics results	29
4.2	Au+Au beam use request for Run 7	39
4.3	Recent d+Au physics results and measurements proposed for Run 7	45
4.4	d+Au beam use request for Run 7	51
4.5	Modifications to the STAR Detector configuration for Run 7	53
5.0	Beam use proposal for Run 8	55
5.1	Mapping the spin dependent parton distributions of the proton	55
5.2	Forward Tagged Proton Studies in STAR: polarized p+p elastic Scattering ($p\uparrow + p\uparrow \rightarrow p + p$)	57
5.2.1	Spin averaged observables	57
5.2.2	Spin dependent observables	58
5.3	Diffractive processes $pp \rightarrow p + X + p$	59

5.3.1	Central production through double Pomeron exchange (DPE) process	59
5.3.2	Hard and soft diffraction	60
5.3.3	Central production of glueballs	60
5.4	Forward tagged proton implementation plan	61
5.5	Forward tagged proton beam use request	61
5.6	Integration of pp2pp DAQ and Trigger with STAR	62
6.0	Beam use proposal for Run 9 (2008-2009)	63
6.1	The search for the QCD critical point	64
6.2	Polarized proton request for Run 9	69
7.0	Collaboration Readiness	69
	References	70

RHIC Multi-Year Beam Use Request
For Run7 – Run 9
The STAR Collaboration

August 24, 2006

Executive Summary

The STAR Collaboration, in order to achieve its spin and relativistic heavy ion physics goals on a timescale consistent with intense international interest and competition in these areas, as well as to utilize RHIC beams effectively taking full advantage of planned improvements in machine and detector capability as a function of time, makes the following 3 year beam use proposal:

Run	Energy	System	Goal
7	$\sqrt{s_{NN}}$ = 200 GeV	Au + Au	300 μb^{-1} sampled 60 Mevts usable (10 + 2 weeks)
	$\sqrt{s_{NN}}$ = 9 GeV	Au + Au	(1 + 1 weeks) (machine dev.)
	$\sqrt{s_{NN}}$ = 200 GeV	d + Au	(10 + 3 weeks) 120 nb^{-1} sampled
8	$\sqrt{s}$ = 200 GeV	$p_{\rightarrow} p_{\rightarrow}$	20 + 3 weeks
	$\sqrt{s}$ = 200 GeV	$p_{\rightarrow} p_{\rightarrow}$	pp2pp
	$\sqrt{s}$ = 500 GeV	$p_{\rightarrow} p_{\rightarrow}$	2 weeks commissioning
9	Low $\sqrt{s_{NN}}$	Au + Au	12 + 2 weeks
	$\sqrt{s_{NN}}$ = 200 GeV	Au + Au	3 weeks*
	$\sqrt{s}$ = 200 GeV	$p_{\rightarrow} p_{\rightarrow}$	10+2 weeks

* Performance based, contingent on finishing QCD Critical Point Search

The primary physics goals of the proposed program are:

Run 7 Definitive results on the saturation scale for the gluon distribution in relativistic heavy nuclei

Decisive test of gluon saturation as the origin of particle suppression at forward pseudorapidity

Qualitative advance in understanding the origin of the suppression of non-photonic electrons from D, B semi-leptonic decays

Run 8	First significant measurement of the x dependence of gluon polarization in the proton, $\Delta G(x)$
	Qualitative advance in study of pp elastic scattering
Run 9	Definitive search for the existence and location of the QCD Critical Point
	Precision tests of the properties of quark-gluon matter

The STAR Collaboration feels strongly that the proposed plan is optimal to make the most efficient use of RHIC beam time for timely progress in determining the properties of the new state of matter produced at RHIC, determining the scale for and impact of gluon saturation in relativistic heavy nuclei, mapping the x dependence of the gluon polarization in the proton, $\Delta G(x)$, and performing a definitive search for the existence and location of the QCD critical point.

In Run 7, the STAR Collaboration proposes a Au+Au run of 10+2 weeks duration at $\sqrt{s_{NN}}$ = 200 GeV, 10+3 weeks of d+Au running at $\sqrt{s_{NN}}$ = 200 GeV, and a run of (1+1) weeks duration for low energy commissioning and background studies in preparation for a future QCD critical point search. The primary physics goal of the $\sqrt{s_{NN}}$ = 200 GeV Au+Au run will be to make a significant advance in understanding the origin of the suppression of non-photonic electrons, and the response of the medium to penetrating high pt probes. It is anticipated that improved vertex selection using an upgraded vertex position detector will yield 20-30% more usable events per unit integrated luminosity than in previous runs. The proposed d+Au run will yield definitive results on the gluon saturation scale in relativistic Au nuclei, and a decisive test of gluon saturation as the mechanism for inclusive particle suppression at forward pseudorapidity. The requested d + Au running will also provide reference data essential to the study of heavy flavor suppression in $\sqrt{s_{NN}}$ = 200 GeV Au+Au collisions.

Building on the outstanding success in Run 6, an optimal run plan for the STAR spin physics program calls for roughly 30 weeks of collision time to be divided between 2008 and 2009. The time will be devoted primarily to longitudinal spin running at $\sqrt{s}$ = 200 GeV, allowing a significant map of the *x*-dependence of the gluon polarization, within the approximate range $0.03 < x < 0.3$. Smaller values of *x* will subsequently be probed in 500 GeV running. During Run 7, STAR supports continued pp collision beam development time, as can be accommodated in a run with both Au+Au and d+Au running. In particular, STAR strongly supports continued polarization development of proton beams in the AGS, in parallel with RHIC stores.

1. Report on polarized proton data taking in Run 6

The scientific priority for the STAR program in Run 6 was to obtain a deeper understanding of the spin structure and dynamics of the proton by studying how the intrinsic spin of the proton is distributed among its underlying constituents (quarks, anti-quarks, and gluons). The data acquisition targets for Run 6 are shown in Table 1. As shown in the table, the goals for Run 6 were all substantially met.

Table I: Data acquisition goals for Run 6

Energy $\sqrt{s_{NN}}$ (GeV)	Trigger	System	Acquired	Goal
200 (longitudinal)	Rare (BEMC /EEMC Triggered)	p + p	8.5 pb^{-1}, P ~ 60% FOM ~ 830 nb^{-1}	10 pb^{-1}, P ~ 50% FOM ~ 625 nb^{-1}
200 (transverse)	Rare (Di-Jet)	p + p	3.34 pb^{-1} sampled, P ~ 60%	~3 pb^{-1} sampled* P ~ 50%
200	L2 J/Ψ	p + p	3.17 M events	3 M events
62.4	Minimum Bias	p + p	16.2 M events	15 M events

* This goal decreased from 5 pb^{-1} due to a very good L2 Di-jet Trigger

STAR sampled a total of approximately 8.5 pb^{-1} with longitudinal beam polarization and approximately 3.4 pb^{-1} (slow detector) / 6.8pb^{-1} (fast detectors) with transverse beam polarization at $\sqrt{s}$ = 200 GeV. In addition, at the end of Run 6, STAR collected a total of 0.1 pb^{-1} at $\sqrt{s}$ = 62 GeV using transversely polarized beams. The longitudinal data sample was split between an initial sample of 2.1 pb^{-1} during the beginning of Run 6 and 6.4 pb^{-1} at the end of the 200 GeV data taking period. These two samples were separated by data taking with transversely polarized beams. Beginning with the start of the transverse running period at $\sqrt{s}$ = 200 GeV, the average beam polarization in both RHIC beams was ~60%.

During Run 6, significant improvements in RHIC's capability as a polarized proton-proton collider as well as in STAR detector acceptance and trigger capability resulted in a qualitative change in the quality, magnitude, and richness of the spin data acquired. Table 2 shows the evolution of the recorded luminosity at STAR during longitudinal and transverse running modes at $\sqrt{s}$ = 200 GeV together with the average beam polarization from 2002 until 2006. The simultaneous improvements in integrated luminosity and polarization in 2006 yield a large gain compared to 2005 in the figure of merit LP^4 for the measurement of any double spin asymmetry (e.g., by a factor of ~ 6 for longitudinal asymmetries).

1.1 Improvements in RHIC Collider performance

Various improvements and developments of the RHIC polarized proton-proton collider complex contributed to the enormous success of Run 6. The number of bunches was increased to 111 with an average number of protons per bunch of $1.4 \cdot 10^{11}$. Further improvements in the number of protons per bunch to $2.0 \cdot 10^{11}$ and a reduction in the emittance growth are expected to allow an increase by a factor of three in the peak luminosity from $30 \cdot 10^{30} cm^{-2} s^{-1}$ in Run 6 to the design value of $90 \cdot 10^{30}$ $cm^{-2} s^{-1}$ [1] over the coming years. Figure 1 shows the integrated luminosity delivered to the two major RHIC experiments, PHENIX and STAR, as a function of time during Run 6. The delivered luminosity falls in between the minimum and maximum luminosity

Year	Long. recorded luminosity [pb^{-1}]	Trans. recorded luminosity [pb^{-1}]	Beam polarization [%]
2002 (Run 2)	0.3	0.15	15
2003 (Run 3)	0.3	0.25	30
2004 (Run 4)	0.4	0	40-45
2005 (Run 5)	3.1	0.1	45-50
2006 (Run 6)	8.5	3.4/6.8	60

Table 2: Evolution of the recorded luminosity at STAR during longitudinal and transverse running modes at $\sqrt{s}$ = 200 GeV together with the average beam polarization from 2002 until 2006.

performance for Run 6 that was projected based on the achievements during Run 5. The actual delivered luminosity reached its projected maximum of roughly 7 pb^{-1} per week at the end of the Run 6 data taking period at $\sqrt{s}$ = 200 GeV. The substantial improvement in the RHIC beam polarization was due to the installation and successful commissioning of a cold Siberian snake magnet in the AGS. Further improvements in the AGS and the transfer efficiency at injection from the AGS into RHIC are expected to increase the RHIC beam polarization to the design value of 70%.

At the end of Run 6, a short period of time was devoted to accelerate polarized protons to 250 GeV to explore the polarization transmission efficiency. Between 100 GeV and 250 GeV in beam energy, several large depolarizing resonances occur. Non-zero polarization was measured with the CNI polarimeters at 250 GeV, although their absolute calibration is not yet known at this energy. Several offline studies are underway to understand why polarization was lost for some, but not all, of the significant depolarization resonances above 100GeV. It will be critical to devote sufficient time in the next 1-2 years to fully develop the 250GeV ramp.

1.2 Improvements in STAR detector capability

In STAR, the addition of shielding in the east and west tunnels greatly reduced beam backgrounds and, it is expected, the systematic instrumental asymmetries they may introduce as well.

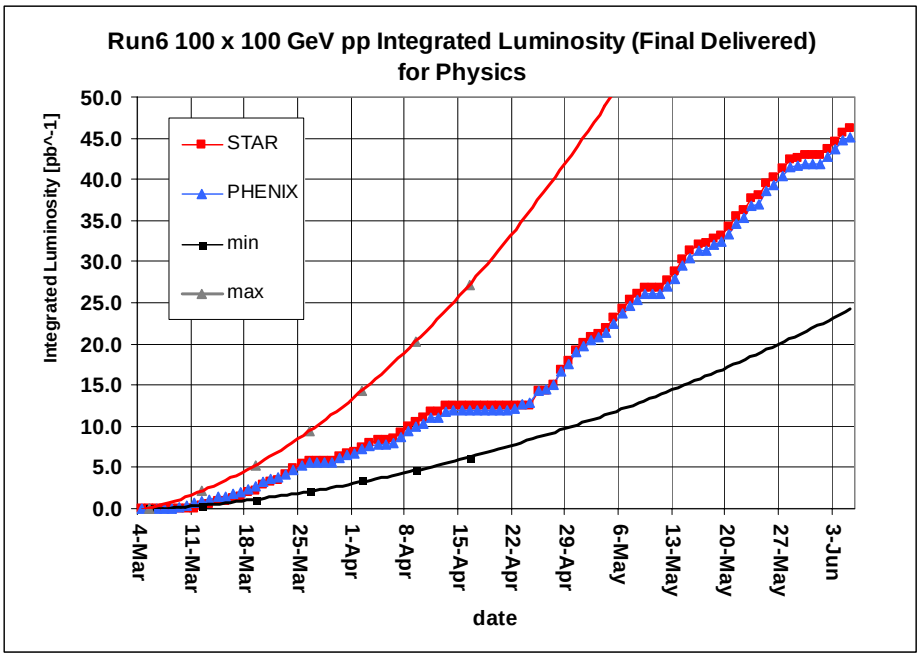

Figure 1: Integrated luminosity delivered to PHENIX and STAR during Run 6 as a function of time. More details are provided in the text.

Detailed analysis of Run 5 data—including the development of new software to reconstruct TPC tracks that do not originate from the event origin, but propagate from far upstream—indicated that the calorimeters were particularly sensitive to the 'spray' of particles produced from beam interactions with the quad triplets located just upstream of STAR. The EEMC, for example, positioned at the west end of the TPC, showed substantial energy deposition in certain azimuthal regions due to halo in the blue beam. Based on these analyses, shielding was installed in both rings prior to Run 6. This dramatically increased the quality of the data taken, and is expected to reduce systematic errors due to background contributions, both in 'false' triggers and in excess energy deposition in 'true' triggered events. In addition, an arsenal of software tools was generated to understand and correct for this large background which allowed for the observation of more subtle effects as Run 6 progressed. With the dominant source of background reduced by approximately an order of magnitude, comparison of event samples with and without a minimum-bias requirement showed additional localized 'hot spots' becoming apparent in the BEMC, particularly on the east end near mid-plane. This is shown in Figure 2. In close cooperation with the Collider-Accelerator Department, new

shielding was installed during an extended access, which effectively blocked these background particles, although subsequently less intense background sources from symmetric locations in the two rings became apparent.

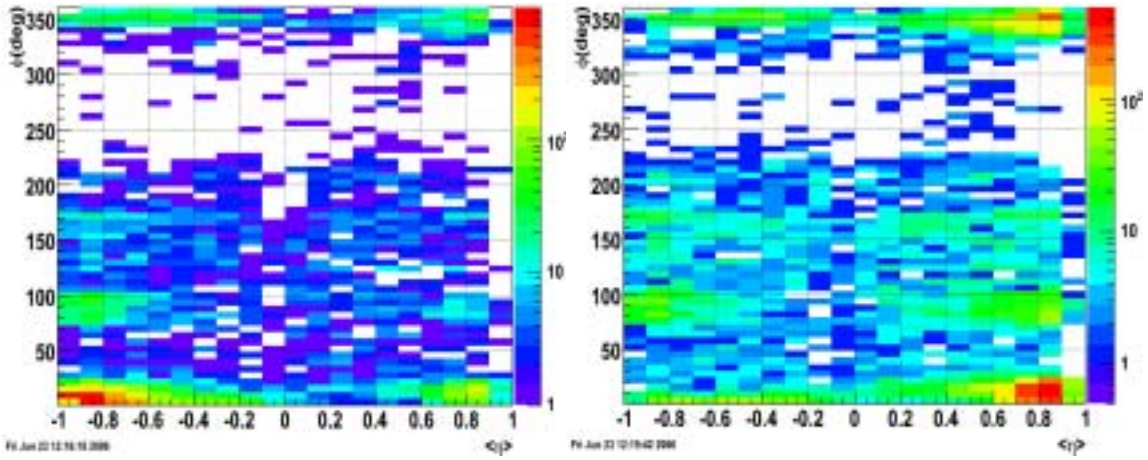

Figure 2: 'Hot spots' observed in the BEMC before (left) and after (right) installation of new shielding during Run 6. Due to automatic z-scaling (which prevents quantitative comparison between the panels) new hot spots only emerge (right panel) once the most intense backgrounds (left) have been suppressed.

Improved online monitoring and the development of beam background pattern recognition algorithms has also allowed for the determination of where to place additional shielding to reduce these problems further in future runs. The required additional shielding will be installed prior to Run 7.

The completion of the BEMC and the expansion of FPD coverage, together with more sophisticated exploitation of STAR triggering capabilities, led to a dramatic improvement in trigger-level acceptance for kinematic coincidence events. The BEMC coverage was only 1/2 (3/4) complete during Run 4 (Run 5). Combined with full exploitation of STAR's L0 and L2 trigger capabilities, the expanded calorimetry acceptance in Run 6 provided STAR with an enormously enhanced sample of di-jets for both transverse and longitudinal spin analyses. The readout electronics for the BEMC, providing full azimuthal coverage over the range $-1 < \eta < 1$, is now complete for the BEMC towers, the embedded shower maximum detectors, and the associated pre-shower layers. The extended reach of the towers allows for efficient triggering and electromagnetic energy measurements for jets and neutral mesons (principally π^0's and η's) over substantial portions of phase space, while the SMD planes provide the spatial localization of showers required for neutral meson reconstruction.

Additional electromagnetic calorimetry was also provided by the newly expanded Forward Pion Detectors, FPD++, which span the region $3.2 < |\eta| < 3.7$. Use of the full BEMC, EEMC, and FPD gave STAR almost hermetic coverage from $\eta = -1$ to $\eta = 4$.

This, in conjunction with the enhanced triggering capabilities, allowed for highly efficient measurements of coincident processes (di-jets, photon-jet, etc.) over a large kinematic regime.

Perhaps the most dramatic increase in STAR's data-taking efficiency,—the ability to select the events most useful for physics—resulted from increased sophistication in trigger definition and implementation. A complete re-work of the lowest-level (L0) triggers for the EMC's provided access to energy depositions from the smallest scale (single towers), through trigger patches (0.2 x 0.2 in η,ϕ), 'jet' patches (1 x 1), to sums over a large fraction of the available coverage. More importantly, all of the BEMC and EEMC tower information was available at L2, including the capability for pedestal subtraction and gain correction. This not only enabled searches for localized regions of electromagnetic energy indicative, *e.g.*, of high-p_T neutral pions or photons, but also allowed for primitive jet reconstruction at L2, based solely on electromagnetic energy deposition. Once found, broad kinematic correlations could be imposed to enhance selection of di-jets, for example. The significant processing power available at Level-2 also enabled a new generation of online diagnostic and monitoring tools. In addition to the detection of background events as discussed above, calorimeter towers that had gone 'dead' or 'hot' were identified much more quickly, and could be effectively removed from the L0 trigger, enhancing our overall trigger efficiency and event selection.

1.3 Summary of performance in Run 6

The result of these advances in the quality of the beam delivered and STAR's ability to mine the collisions is a Run 6 data set that far surpasses all previous polarized proton runs in terms of physics content. The combination of extended calorimetric coverage, reduction of the background trigger rate, and more intelligent triggering decisions increased the size the recorded di-jet sample by almost an order-of-magnitude per unit integrated luminosity compared to 2005. The impact, in terms of kinematic coverage, is readily apparent in Figure 3, which shows both the locations in η and the azimuthal opening angle distribution of the two jets found at L2. The importance of determining the direction of *both* jets produced in a given partonic scattering, and the constraints this provides on the initial-state parton x values, will be discussed below.

In summary, it is anticipated that the 3.3 pb^{-1} of transversely polarized collisions collected in Run 6 should yield 15 -20 M STAR (TPC) events, plus an even larger sample of 'fast detector only' data, which represent enormous increases over all previous runs. From these data, quantitative estimates of the magnitudes of the gluon and quark Sivers functions in several kinematic regions will be extracted to compare to existing results from semi-inclusive DIS [2,3]. Data taken with the FPD will allow STAR to map out the x_F and p_T dependences of the large neutral pion spin asymmetries observed earlier in STAR at high rapidity, and to search for jets and direct photons in this regime. The longitudinally polarized runs will extend the existing STAR results on A_{LL} for inclusive jets and neutral pions to higher p_T, and, due to improvements in triggering, will provide

the first substantial sample of di-jets. The Run 6 data set should also yield the first useful sample of photon-jet coincidences will which be crucial to the development of

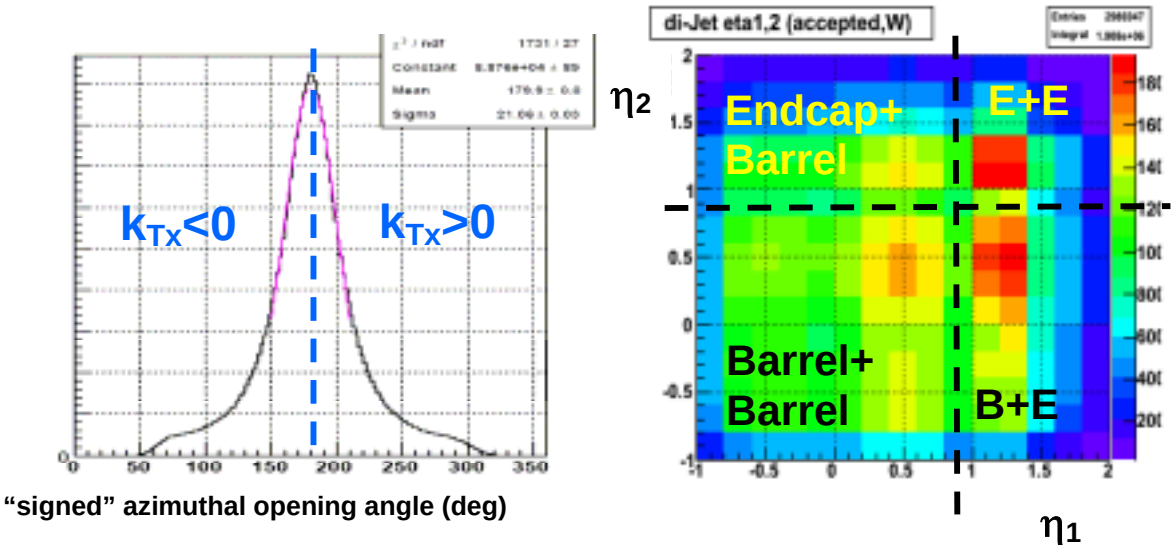

Figure 3: Angle correlations between pairs of jets reconstructed from calorimeter information as part of the Level 2 trigger decision: left—the distribution of azimuthal opening angle (defined to be greater or lesser than 180° based on the x-projection of the bisector of the two jet thrust axes); right—the correlation of jet pseudorapidities. A total of 3 million di-jet events were processed via this L2 trigger during 3 weeks of transverse spin running at STAR, permitting a trigger-level analysis of Sivers asymmetries for quark-gluon and gluon-gluon scattering.

algorithms for identifying direct photons in the EMC's in order to reconstruct the photon-jet events to probe the gluon helicity preference at very low x. Further details on plans and challenges of the Run 6 physics analysis will be discussed in the next section.

2 Recent spin physics results and expected results from Run 6

2.1 Longitudinal spin physics program

The longitudinal STAR spin physics program profits enormously from the unique capabilities of the STAR experiment for large acceptance jet production, identified hadron production and photon production. The first longitudinal double-spin asymmetry measurement for inclusive jet production and the associated inclusive jet cross-section measurement at mid-rapidity have recently been completed and submitted for publication to Physical Review Letters [4]. In addition, the STAR collaboration has recently released a preliminary result on the inclusive neutral pion production cross-section at mid-rapidity [5]. The (unpolarized) cross-section measurements support the asymmetry measurements at RHIC by validating the applicability of pQCD.

The first measurement of the longitudinal double-spin asymmetry for inclusive jet production and the associated inclusive jet cross-section measurement are based on data taken during 3 week beam periods in Run 3 and Run 4. The integrated luminosity for the analyzed 2003 and 2004 data sets was $0.18pb^{-1}$ and $0.12pb^{-1}$ respectively. The average proton beam polarization in both cases was 30-40%. Jets were reconstructed using a midpoint-cone algorithm that clusters reconstructed TPC tracks and BEMC energy deposits within a cone of radius r_{cone}=0.4 in η and ϕ, starting from energy seeds of at least 0.5 GeV. The jet data were collected with a minimum bias (MB) and a high tower (HT) calorimeter trigger condition. The MB trigger, based on a coincidence of the STAR Beam-Beam Counters (BBC), required a proton collision event. It was highly pre-

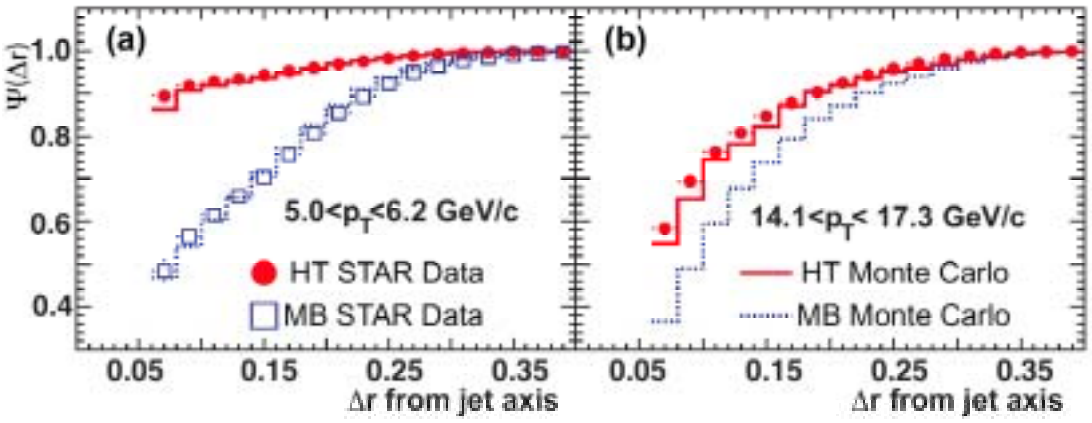

Figure 4: Jet profile $\Psi(\Delta r, r_{cone}, p_T)$ versus the inner cone size at r_{cone}=0.4 for MB (open squares) and HT (filled circles) data compared with STAR MC simulations for two different p_T bins.

scaled. The HT trigger required, in addition, a signal from at least one BEMC tower of size $\Delta\eta \times \Delta\phi = 0.05 \times 0.05$ above a transverse energy (E_T) threshold of 2.2 GeV in 2003 (2.2 - 3.4 GeV at η=0-1 in 2004). In total, $2.1 \cdot 10^6$ MB and $3.0 \cdot 10^6$ HT events were analyzed. (In Run 5 the commissioning of a jet patch (JP) trigger was completed, which allowed a more efficient way to trigger on jets compared to a HT trigger.) Figure 4 shows the jet profile $\Psi(\Delta r, r_{cone}, p_T)$, defined as the average fraction of jet E_T inside a coaxial inner cone of radius $\Delta r < r_{cone}$, for the combined 2003-2004 data set for MB and HT data separately. The HT trigger, providing increased selectivity for jets, causes a bias towards jets with hard fragmentation that produce an electromagnetic shower. The distributions are well described by a PYTHIA-based MC simulation using the 'CDF Tune A' settings.

The differential inclusive cross sections were determined separately for the MB and HT trigger samples. The measured p_T spectra were corrected based on MC simulations. Figure 5a shows the MB and HT cross-sections averaged over 2003 and 2004 data versus jet p_T. The MB and HT data are in good agreement for overlapping jet p_T. The curves show the result of NLO pQCD calculations [6] evaluated at equal factorization and

renormalizations scales, $\mu \equiv \mu_F = \mu_R = p_T$, using the CTEQ6 parton distribution functions. The normalization uncertainty amounts to 8%. The total systematic uncertainty of 48% on the measured jet yield is dominated by a 9% uncertainty on the jet energy scale.

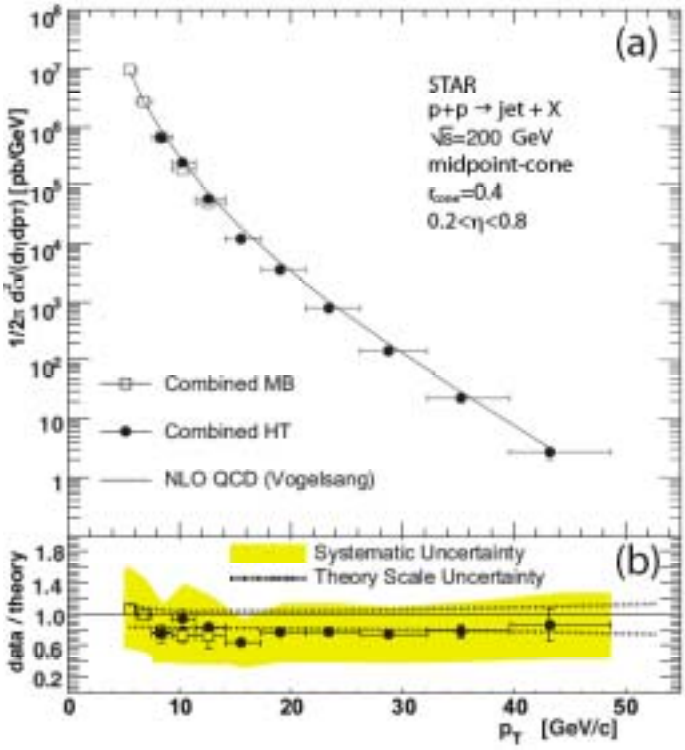

Figure 5: (a) Inclusive differential cross-section for $p + p \to jet + X$ versus p_T for a jet cone radius of 0.4. The symbols show MB (open squares) and HT (filled circles) data from the years 2003 and 2004 combined. The curves show the result of a NLO calculation [6]. (b) Comparison of data and theory. The band indicates the experimental systematic uncertainty, while the dashed lines indicate the variation of NLO calculations for two different scales of $\mu = p_T/2$ ($\mu = 2p_T$).

Figure 6 shows the 2003-2004 measured longitudinal double-spin asymmetry A_{LL} in $p + p \to jet + X$ versus jet p_T. The uncertainty on the data points is statistical. The grey band indicates the systematic uncertainty from the beam polarization measurement, and the hatched band the total systematic uncertainty. The curves in Figure 6 show theoretical evaluations at $\mu_F = \mu_R = p_T$ for the commonly used polarized parton distribution functions. Those are based on a best fit to polarized DIS data, the so-called GRSV-standard gluon polarization (black curve). Furthermore, the case for a vanishing gluon polarization (blue curve) and the case of a maximally positive (red curve) or negative

(green curve) gluon polarization are also shown. The measured asymmetries are consistent with NLO pQCD calculations based on DIS polarized lepton-nucleon data, and disfavor a large positive value of the gluon polarization in the nucleon. Clearly, more data are needed to improve on the statistically dominated uncertainties. The impact of the Run 5 and Run 6 data analysis of inclusive jet production will be discussed below.

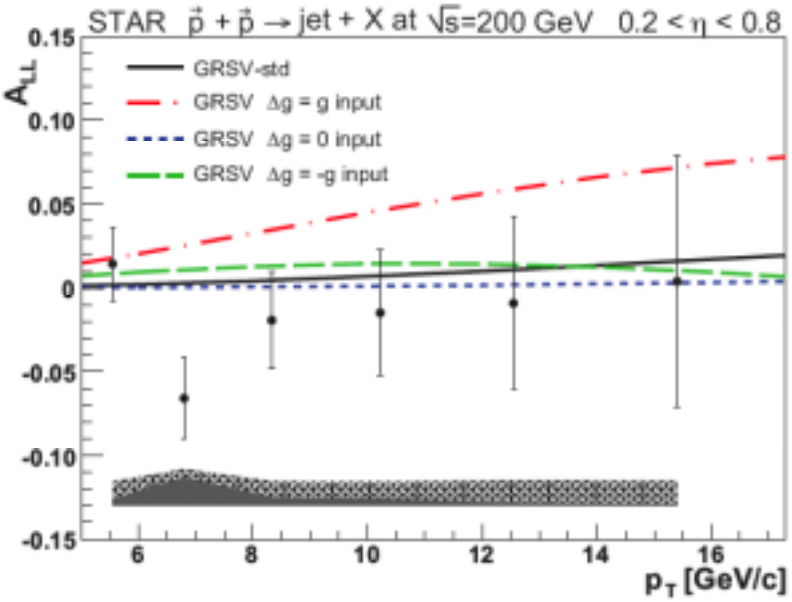

Figure 6: The longitudinal double-spin asymmetry A_{LL} for 2003-4 data on $p+p\rightarrow jet+X$ versus jet p_T. The uncertainties on the data points are statistical. The grey band indicates the systematic uncertainty from the beam polarization measurement, and the hatched band the total systematic uncertainty. The curves show predications based on deep-inelastic scattering parameterization of the gluon polarization [6,7].

A substantial increase in precision is expected from the measurement of A_{LL} in inclusive jet production based on the Run 5 data sample which will be reported at SPIN2006. The current analysis effort focuses on a better understanding of systematic uncertainties. The projected statistical precision for inclusive jet production based on a jet patch trigger in Run 5 is shown in Figure 7 in comparison to those expected in Run 6. More details on the improvements needed in systematic uncertainties are provided in Section 3.

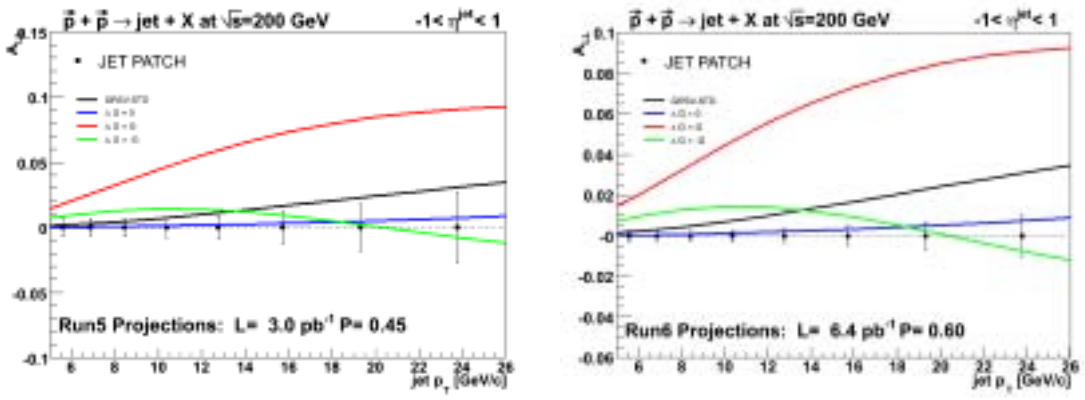

Figure 7: Projected statistical uncertainties for the Run 5 (left) and Run 6 (right) longitudinal data sample based on Jet Patch triggers.

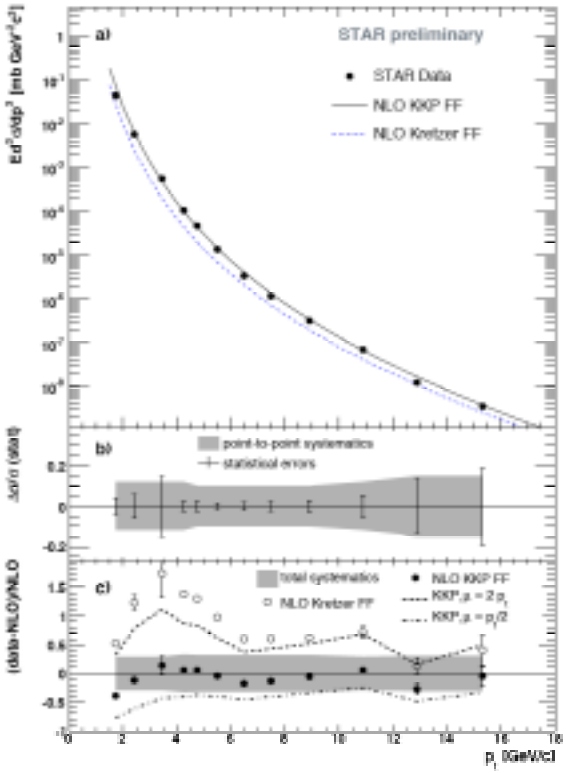

Figure 8: (a) Preliminary cross section for inclusive neutral pion production for $0.1<\eta<0.9$. (b) Relative statistical errors of the data points are shown as error bars and the preliminary point-to-point systematic errors are shown as shaded bands. (c) Relative difference of the measured cross section from the NLO pQCD calculations [6] for both Kretzer [8] and KKP [9] fragmentation functions.

Additional constraints on the gluon polarization can be obtained from hadron production in longitudinal polarized proton-proton collisions. One has to keep in mind, however, the additional uncertainty from the fragmentation function for a given observed hadron. The first preliminary result from STAR for the differential cross section for inclusive neutral pion production near mid-rapidity has recently been presented [5]. Neutral pions near mid-rapidity are detected with the BEMC. For the 2005 running period, half of the BEMC was fully installed and commissioned, providing a coverage of $0 < \eta < 1$ for all azimuthal angles ϕ. For the reconstruction of high p_T neutral pions the identification of two decay photons with a small opening angle is crucial. This is achieved using the shower maximum detector SMD, a wire proportional counter with cathode strip readout at ~$5X_0$ depth inside a given BEMC tower. The analyzed data sample is based on HT triggers with thresholds of ~2.8 GeV and ~3.6 GeV. For the preliminary neutral pion cross section, subsets of the available 2005 data with an integrated luminosity of 44 μb^{-1} for MB events and $0.4 pb^{-1}$ for HT triggers were analyzed. The measured p_T distribution for identified neutral pions was corrected for acceptance, reconstruction and trigger efficiency using a PYTHIA MC sample passed through the full STAR GEANT detector simulation. Figure 8 shows the inclusive cross section for neutral pions at mid-rapidity. The measured cross-section is compared to NLO pQCD calculations [6] using the Kretzer [8] and KKP [9] fragmentation functions. The pQCD calculations are performed with a factorization scale $\mu=p_T$, unless stated otherwise. Figure 8a shows the preliminary cross section for inclusive neutral pion production for $0.1 < \eta < 0.9$. Figure 8b show the relative statistical errors of the data points as error bars and the preliminary point-to-point systematic errors as shaded bands. Figure 8c shows the relative difference of the measured cross section from the NLO pQCD calculations for both Kretzer and the KKP fragmentation functions. The NLO calculations using the KKP fragmentation function show excellent agreement with the data. The Kretzer fragmentation functions consistently underpredict the data. This result constrains the neutral pion fragmentation function which is an additional uncertainty in neutral pion production in comparison to inclusive jet production. This analysis will be extended to the measurement of the longitudinal double-spin asymmetry, which is expected to be presented at SPIN 2006.

Other analyses in preparation for SPIN 2006 which provide additional constraints on the gluon polarization in the proton include:

- The measurement of inclusive neutral pion production using the EEMC covering more forward rapidities ($1 < \eta < 2$): this measurement probes a different composition of underlying gluon-gluon, quark-gluon and quark-quark initiated processes in comparison to the mid-rapidity region.
- Charged pion production: this analysis provides a unique channel in that the ordering of the measurements of A_{LL} for positive and negative pions is sensitive to the sign of the gluon polarization, while at moderate p_T the gluon-gluon dominated inclusive jet production is relatively insensitive to the sign. STAR has already established the procedure for the identification of charged pions and the calculation of their production cross sections over a broad kinematic range. A critical aspect of this

analysis is the evaluation of a systematic bias introduced by the selection of charged pions based on a HT trigger caused generally by a different particle.

Finally, one additional analysis that has been submitted for presentation at the SPIN 2006 concerns the longitudinal spin transfer in inclusive Λ and $\overline{\Lambda}$ production in singly polarized proton-proton collisions at $\sqrt{s}$ = 200 GeV. In this analysis the Λ and $\overline{\Lambda}$ are reconstructed via the dominant decay channel into protons and pions. The Λ and $\overline{\Lambda}$ polarization is determined from angular correlations in the weak decay. Since the Λ and $\overline{\Lambda}$ contain a strange (anti-)quark and this quark is expected to contribute to Λ and $\overline{\Lambda}$ spin, such measurements may give sensitivity to the polarization of strange (anti-) quarks in the polarized proton. A phenomenological study in the framework of perturbative QCD for RHIC conditions shows that spin transfer measurements in inclusive $\overline{\Lambda}$ production becomes increasingly sensitive to the anti-strange polarization with increasing large transverse momenta p_T, more so than to the details of spin transfer in the fragmentation process [10]. Measurements at large transverse momentum may thus help constrain the polarization of strange (anti-) quarks in the polarized proton, and yield new insights into polarized fragmentation functions. A proof-of-principle analysis, based on the small sample collected in 2003 and 2004, has been presented at the PANIC-2005 conference [11]. The results are displayed in Figure 9. Although these data are presently statistics limited and cover small only non-perturbative p_T we anticipate that future RHIC running periods will deliver adequate data to perform sensitive measurements.

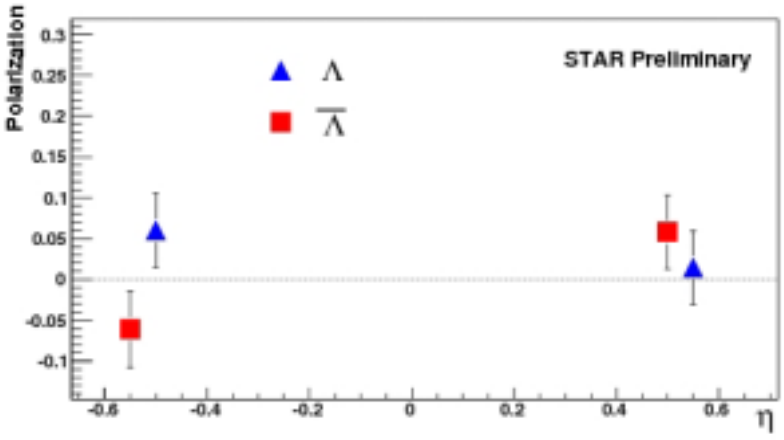

Figure 9: Preliminary STAR data on the spin transfer D_{LL} in inclusive Λ and $\overline{\Lambda}$ production versus pseudo-rapidity η. Positve η is taken along the directioin of the polarized proton beam. Mean $|x_F|$=8.10-3 and p_T=1.3 GeV/c. The indicated uncertainties are statistical.

All of the above measurements will benefit enormously from the much larger data sample collected during Run 6.

The next important step for the STAR spin physics program is the study of correlation measurements such as di-jet production and di-hadron production. Those analyses will profit yet again from the wide acceptance calorimetry coverage at STAR. Correlation measurements offer a direct handle on the underlying parton kinematics. The need for such measurements has been clearly pointed out by Stratmann [12].

The sensitivity of the above inclusive measurements to the underlying gluon polarization is shown in Figure 10 in comparison to inclusive photon production. The sensitivity in the case of inclusive photon production is particularly large, due to its dominance by the quark-gluon Compton process in proton-proton collisions. Photon-jet coincidence measurements will allow in addition a direct handle on the underlying partonic kinematics. The analysis of Run 6 data on photon, photon-jet, jet-jet and hadron-hadron

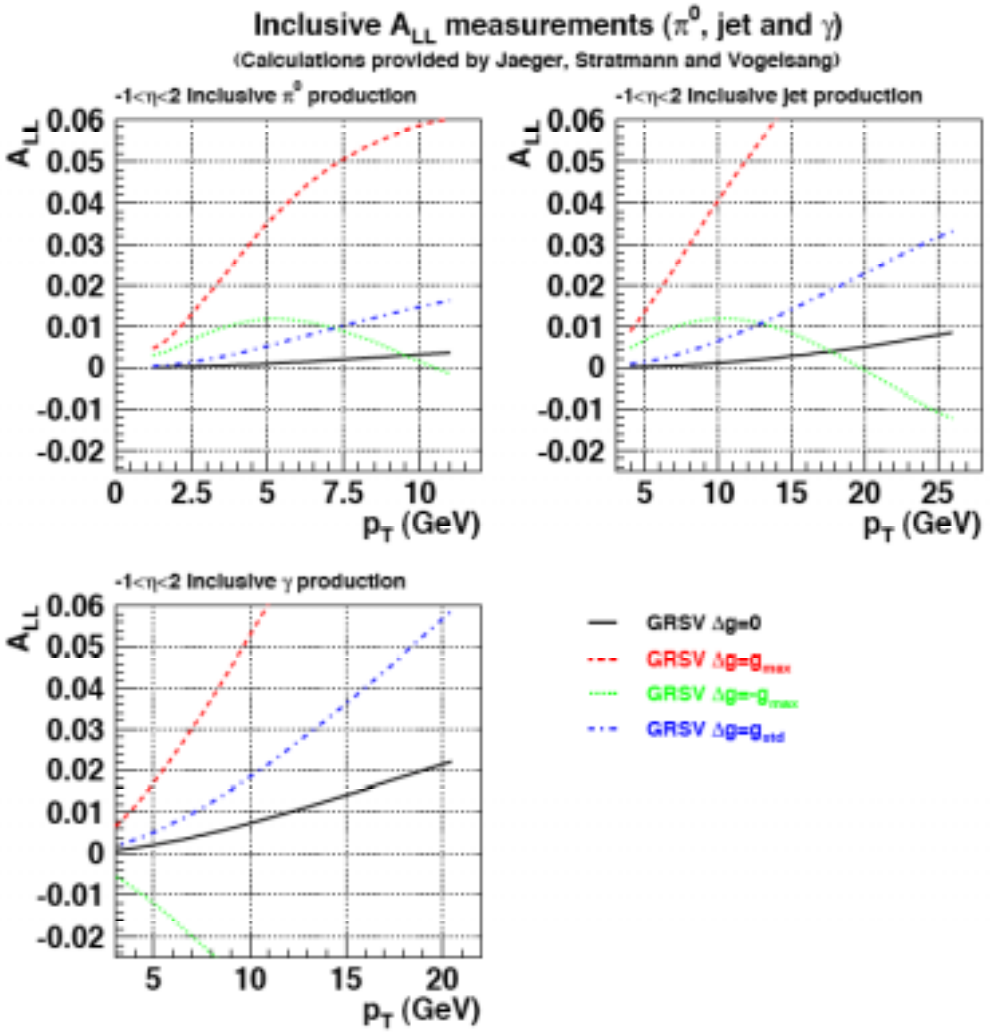

Figure 10: Theoretical predictions for A_{LL} for inclusive jets, π^0 and photon production for different assumptions on the underlying polarized gluon distribution.

production channels will focus at first on delineating the most productive channels to pursue with limited STAR trigger bandwidth in future pp runs in order to constrain $\Delta G(x)$ as well as possible. The specific analysis issues to be explored will be described further in Section 3.

2.2 Transverse spin physics program

There is a nontrivial difference when the proton spin is longitudinal versus when it is transverse to its momentum vector because the up and down quarks are nearly massless and the boosts and rotations required to transform longitudinal spin to transverse spin do not commute. The aim of the transverse spin program at STAR is to tackle the spin puzzle when the proton spin is perpendicular to its momentum. The ultimate goals are to isolate the transversity distribution (related to transverse polarization of quarks and antiquarks within a transversely polarized proton) and possible orbital angular momentum contributions of quarks, antiquarks and gluons to the spin of the proton.

The transverse spin program at STAR fits into a world-wide context of ongoing experimental and theoretical work. The present theoretical understanding is that large transverse single spin asymmetries (SSA) observed in hard scattering processes are produced through either initial-state or final-state effects. Initial-state effects that are part of the proton wave function correspond to a correlation between the parton intrinsic transverse momentum (k_T) and the proton spin. These spin- and k_T-dependent distribution functions, when combined with a requisite initial-state or final-state interaction [13], correspond to the 'Sivers effect' [14]. Alternatively, if there is non-zero transversity, hard-scattering processes must transfer initial-state quark and antiquark polarization to the final state. Transverse SSA arise in this scenario by the fragmentation of the quark or antiquark back to hadrons via a correlation between k_T of the hadron relative to the thrust axis and the quark or antiquark spin. This corresponds to the Collins/Heppelmann effect [15]. The past few years have seen rapid theoretical progress in the understanding of transverse SSA concurrent with ongoing experimental efforts at RHIC, in semi-inclusive deep inelastic scattering (SIDIS) from transversely polarized targets and by the Belle collaboration, through their observation of azimuthal asymmetries of dihadron production in e^+e collisions [16]. The Belle results are the first direct observation of a non-zero Collins fragmentation function. Its existence may then provide access to transversity at RHIC. The HERMES collaboration have observed non-zero and separated contributions from both the Collins and Sivers effects from their measurements of SIDIS from transversely polarized targets [2].

Transverse single spin asymmetries (SSA) have been measured at STAR (Figure 11) for inclusive π^0 [17,18] and charged hadron production near midrapidity. Statistical sensitivities for $1 < p_T < 3$ GeV/c are comparable for midrapidity charged hadron production and large rapidity π^0 production. Invariant cross sections (Figure 12) are found to be in agreement with the best next-to-leading order perturbative QCD calculations for $p_T \geq 2$ GeV/c at both midrapidity and $|\eta| < 4$ [19], thereby providing a strong foundation for understanding the spin effects. Non-zero SSA are found only at

large rapidity; SSA for midrapidity particle production at comparable p_T are measured to be zero. The present understanding is that non-zero SSA for particles produced at large rapidity arise primarily through the 'Sivers' effect. But existing data cannot rule out contributions for inclusive particle production from the Collins/Heppelmann effect.

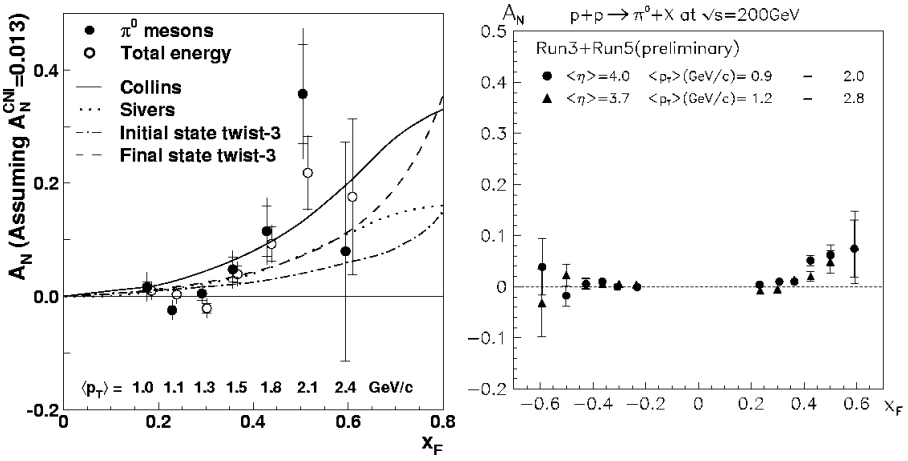

Figure 11: (left) First results for p↑ + p→ π^0+X analyzing powers (A_N) at√s=200 GeV compared to theoretical predictions available prior to the measurements [20]; (right) More precise results for A_N obtained in subsequent runs using on-line measurements of the beam polarization [18].

The large rapidity π^0 measurements have been completed, to date, with modular lead-glass calorimeters viewing particles produced by ion collisions through the holes in the STAR magnet poletips. These holes provide a clear view of forward angle particle production. The original detectors were smaller lead-glass matrices known as the Forward Pion Detector (FPD). In RHIC Run 6, as an engineering test of the planned STAR Forward Meson Spectrometer, the area of the modular forward calorimeters west

	Run2	**Run3**	**Run5**	**Run6**
Detector	EEMC and FPD prototypes	6 matrices of FPD	full FPD (8 matrices)	East FPD West FPD++
P_{beam}, %	~15	~30	~45	~60
Sampled, $\int L$ dt, pb^{-1}	0.15	0.25	0.1	6.8
<η> spanned	3.8	±3.3/±4.0	±3.7/±4.0	±3.2/±3.7

Table 3: Summary of data samples acquired with forward calorimeters at STAR.

of the STAR interaction point was increased by almost an order of magnitude. Data obtained with the increased forward calorimetry coverage will permit measurement of transverse SSA for multi-photon, 'jet-like' events in the same rapidity interval where large analyzing powers for π^0 production are observed.

In addition, the greater coverage will permit the determination of the p_T dependence of A_N for forward π^0 production in x_F bins to compare against QCD models developed to explain these spin effects. Table 3 shows the accumulated integrated luminosity and beam polarizations used for prior transverse SSA measurements and for the data set acquired in RHIC Run 6. The latter has more than ten times the number of events and almost twice the average beam polarization as the earlier data. Calibrations of the smaller lead glass detectors of the FPD++ are complete. The event distribution in the x_F-p_T plane for $\tilde{\pi}$ production is shown in Figure 12. Preliminary results for the separated x_F and p_T dependence of transverse SSA for forward π^0 production from Run 6 are planned for release at the upcoming SPIN2006 symposium.

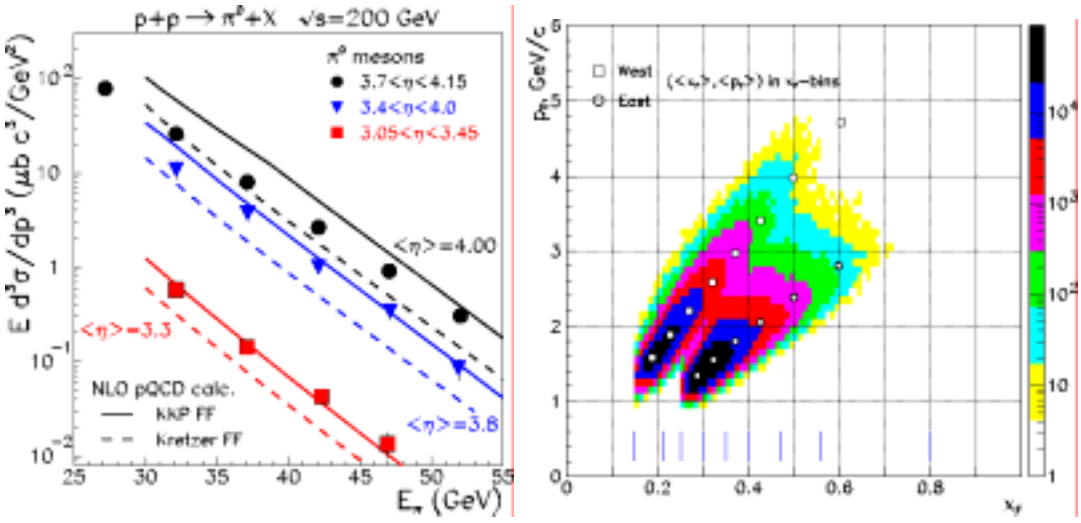

Figure 12: (left) Cross sections for p+p→$\tilde{\pi}$+X at √s = 200 GeV compared to NLO pQCD calculations. In the 45 < E_π < 50 GeV bin, <p_T> (<η>) = 1.7 (4.0); 2.1 (3.8); and 3.4 (3.3) GeV/c. (right) Distribution of reconstructed $\tilde{\pi}$ events in the x_F-p_T plane for ~20% of the data obtained with transverse beam polarization in RHIC Run 6.

In addition to the large rapidity studies, STAR has begun a program of measurements of Sivers SSA for midrapidity di-jet production. The di-jet measurement is conceptually simple and very well suited to the STAR detector. The effect of initial-state k_T is an event-by-event kinematic boost that smears the azimuthal correlation between the two jets; a k_T directional preference would lead to a systematic tilt of the jets toward the preferred direction, hence, to a spin-dependent average deviation from 180° azimuthal

opening angle [21]. We thus define, event by event, a "signed" opening angle ζ between two detected jets that is chosen to be > 180° if the jets tilt toward the south in STAR (i.e., their bisector has a positive *x*-component, with the blue beam direction chosen as +*z* and an upward beam spin direction as +*y*) and < 180° if they tilt toward the

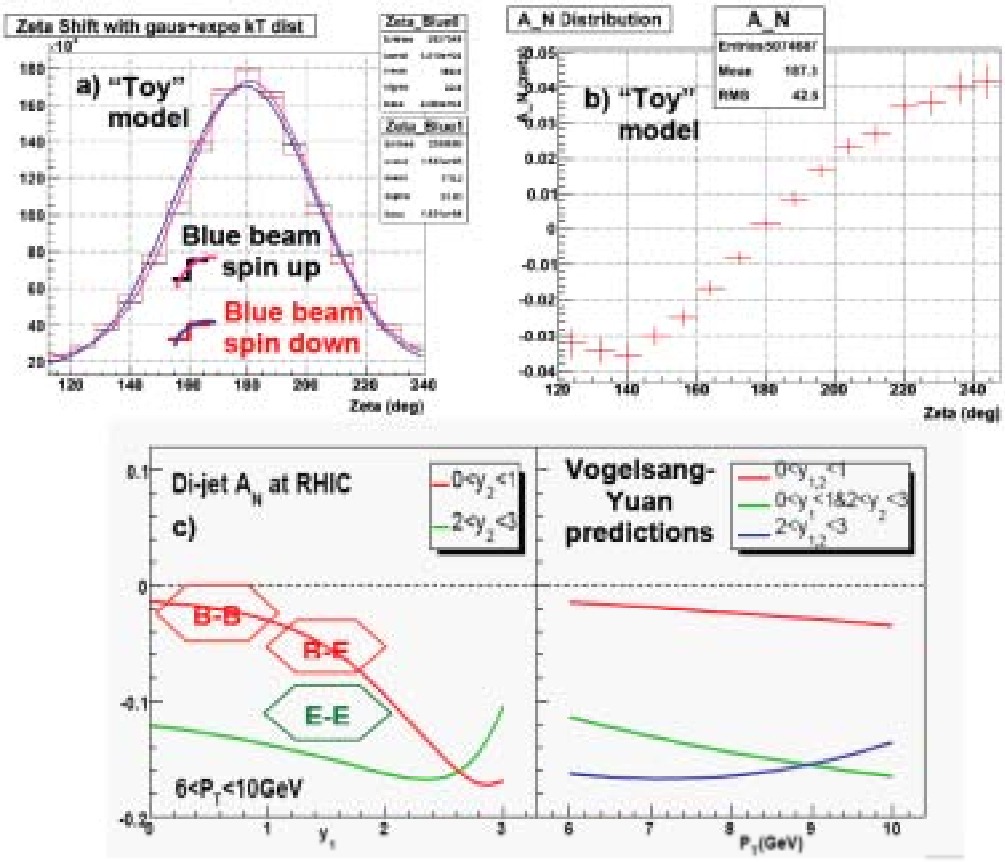

Figure 13: Toy model Monte-Carlo simulations demonstrate the measurable effects of a spin-dependent k_T distribution centroid on (a) the azimuthal opening angle (ζ) distribution of di-jet events and (b) the resulting single-spin transverse asymmetry as a function of ζ. Frame (c) shows di-jet asymmetries (integrated over the intrinsic k_T distribution for $k_T^x < 0$) predicted [3] on the basis of u and d quark Sivers functions fitted to HERMES SIDIS transverse spin asymmetries [2]. The labels in the lower left plot indicate the regions of pseudo-rapidity and predicted Sivers asymmetries covered by barrel-barrel (B-B), barrel-endcap (B-E) and endcap-endcap (E-E) EMC-triggered di-jets in STAR.

north. The zeroth-order effect of a Sivers function would be to cause a centroid shift in the ζ distribution when one beam spin direction or the other is reversed. This effect is illustrated in Figure 13 by "toy" model simulations in which each colliding parton is assigned a k_T^y component chosen randomly from a Gaussian distribution (with symmetric

exponential tails added) centered about zero and a k_T^x component chosen randomly from a similar distribution centered about ±40 MeV/c, with the sign correlated with the randomly assigned vertical spin orientation of the parent proton. The width of the k_T-distribution in these simulations and the p_T slope of the thrown parton scattering events are chosen to match approximately the *observed* ζ (Figure 3) and E_T distributions for di-jets in the 2006 run.

Figure 13 also shows that the analyzing power that would result from a ±40 MeV/c spin-dependent shift in the k_T distribution centroid is comparable in magnitude to (or smaller than) those predicted for STAR by Vogelsang and Yuan [3] on the basis of quark Sivers functions fitted to the HERMES SIDIS asymmetries. These particular predictions ignore effects of gluon Sivers functions and possible Sudakov suppression of the asymmetries [21]. The predicted asymmetries grow as the jets are boosted to higher rapidity ($y_{1,2}$), because the production becomes more dominated by quark-gluon scattering, with the quark provided preferentially by the proton assumed in these calculations to be polarized. In STAR's measurements, both beams were polarized. Then we can probe both quark and gluon Sivers functions for these forward-boosted di-jets, by measuring the respective sensitivities to spin-flip of the blue and yellow beams. When both jets are near mid-rapidity, the blue and yellow beam asymmetries should become equal but opposite in sign (since the two proton momenta are opposite in sign), and both become dominated at moderate p_T by gluon Sivers sensitivity.

Summing over several relevant triggers, STAR collected roughly 5 million di-jet events with transversely polarized protons in 2006. This sample will provide statistical uncertainties typically an order of magnitude smaller than the asymmetries predicted in Figure 13, allowing a very significant test of universality of the quark Sivers functions and search for gluon Sivers functions. While the eventual analysis of these data will be based on full jet reconstruction, including both charged-track and electromagnetic shower energies, the measurement of azimuthal opening angle can already be made utilizing the EMC energy deposits alone, with a resolution much better than the k_T-induced width of the ζ distribution (and hence, very little effect on the measured asymmetries). Thus, the EMC information saved at trigger level for the 3 million di-jet events that passed the level 2 di-jet trigger described in Section 1 will already permit a significant preliminary result for the Sivers asymmetries to be presented at the SPIN2006 conference. This analysis will be based upon spin-sorting of level 2 ζ distributions, such as that shown above in Figure 3. Event entries into these distributions will be weighted by the cosine of the bisector angle of the two jet thrust axes (as is done also in Figs. 13 (a) and (b)), in order to take into account that only k_T^x components (perpendicular to the beam spin and momentum directions) are sensitive to Sivers functions.

Detailed plans for transverse spin measurements in Runs 8 and 9 must await completion of the analysis of the extensive Run 6 data sample. Here, we anticipate some aspects of what measurements will be feasible. In Runs 8 and 9, the STAR detector will have nearly continuous electromagnetic calorimetry with its barrel and endcap EMC and the

completed Forward Meson Spectrometer. These subsystems will cover the complete azimuth for $-1 < \eta < +4$. With this calorimetry, STAR will be uniquely positioned to measure the correlation between transverse spin and relative transverse momentum as determined by observing either pairs of jets or pairs of hadrons. The back-to-back di-jet asymmetry studies can be extended to span larger η, including the range in which sizable transverse SSA are observed for inclusive π production. The larger η measurements will isolate the quark Sivers distribution. The transverse spin dependence of near-side di-hadron correlations can be used to probe for non-zero transversity through the Collins effect. The original estimates were that data samples with ~70% beam polarization and 30 pb^{-1} of integrated luminosity would be required to gain sensitivity to transversity in di-hadron measurements at STAR. Data samples of this magnitude will also provide access to transverse SSA for inclusive photon production. It is anticipated that polarized proton collisions at $\sqrt{s}$ = 200 GeV in Runs 8 and 9 will attain the luminosity and polarization goals stated for the RHIC spin program. In developing the *Research Plan for Spin Physics at RHIC* [22], it was assumed that approximately 25% of the polarized proton collision time would be spent with transverse polarization. A data sample recorded with only the STAR calorimeters, corresponding to 30 pb^{-1} sampled, could be achieved in several weeks of running at full luminosity.

3. Multi-year spin physics beam use request for Run 7 – Run 9

STAR's spin physics goals for the 2007-9 period remain focused on the primary goal of mapping the gluon polarization in a polarized proton as a function of Bjorken x. Toward this end, we feel that two additional long pp runs at $\sqrt{s}$ = 200 GeV are needed to provide the desired experimental uncertainties. However, faced with the very significant analysis task list presented by the highly productive 2006 run (Section 2) and competing priorities in the heavy ion physics program, we argue here that the optimal run plan should place these long pp runs in 2008 and 2009. This allows addressing other high-priority physics goals in the 2007 run, while in parallel carrying out pp analyses that should lead to several high-impact papers and to an optimization of the trigger mix for accomplishing the remaining spin goals at 200 GeV as efficiently as possible. The efficiency will be further aided by removal of STAR's Silicon Vertex Tracker after the 2007 run, since the SVT material budget compromises direct photon detection in the important kinematic region near $\eta = 2$. It is furthermore anticipated that STAR's DAQ1000 upgrade will be in place for the 2009 run, enhancing the trigger bandwidth and reducing the dead time for pp data collection.

Significant improvements to the constraints on $\Delta G(x)$ over the data we have already collected in 2006 are most likely to come from the following sources: (1) improving the statistical precision for high-p_T (15-30 GeV/c) inclusive jets; (2) collecting a statistically meaningful sample of photon-jet coincidences, providing event-by-event information on the Bjorken x-values of the colliding partons, coupled with leading-order dominance of quark-gluon interactions; (3) di-jet coincidences, which will give better statistical

sensitivity than photon-jet coincidences, but less constrained parton kinematic information (the ratio x_1/x_2 for the two colliding partons should be well determined, but resolution on p_T, hence x, absolute scales will be coarse). Along the way toward these goals, we may also extract inclusive direct photon asymmetries, but these will never compete statistically with inclusive jet production, and are likely to provide only a somewhat coarse crosscheck on the pQCD analyses. As STAR has always argued, photon-jet coincidences provide better sensitivity to $\Delta G(x)$ than inclusive photon asymmetries, despite giving a smaller total event sample, because the possibility to extract initial-state parton kinematic information permits emphasizing events in regions of phase space that involve both sizable quark polarizations and large parton-level two-spin asymmetries. Future STAR pp runs should thus devote most of the limited available trigger bandwidth to photon and coincidence triggers; but the optimal mix of these triggers will be dictated by data analysis results obtained during 2007.

Among the most important issues for future run plans to be addressed in analyzing 2006 data are the following.

Evaluation of systematic errors in inclusive jet asymmetries: While statistical uncertainties in A_{LL} for inclusively produced jets were very significantly improved from 2003-4 to 2005, systematic uncertainties have not yet been similarly reduced. At low p_T the dominant systematic uncertainty in 2005 is comparable to the achieved statistical errors, and is associated with hints (at the 2—3 σ level of statistical precision) of longitudinal single-spin asymmetries expected to be zero (an order of magnitude larger than expected theoretically from W and Z exchange interference), for which we have not yet succeeded in delineating a clear instrumental cause. It is conceivable that these hints will disappear in 2006 data due to better statistics or better shielding against backgrounds, but that is yet to be demonstrated. At higher p_T a comparable systematic uncertainty arises from resolution-induced bin smearing, coupled with the so far uncertain p_T-dependence of A_{LL}. The latter effect should shrink as the statistical errors on A_{LL} are reduced and the p_T-dependence becomes better defined by STAR data. Until we have seen that systematic uncertainties were reduced in 2006, or learned how to reduce them for subsequent runs, it is difficult to estimate how much of the trigger bandwidth should be devoted to improving statistics for this channel. The jet p_T range where we can certainly improve our ΔG sensitivity, even if we do not improve systematic uncertainties further, is roughly between 15 and 30 GeV (above 30 GeV, quark-quark scattering starts to dominate, and we lose sensitivity to ΔG).

Evaluation of γ-jet and jet-jet sensitivity to $\Delta G(x)$: The interpretation of A_{LL} data for inclusive channels is subject to model-dependence regarding the assumed shape of $\Delta G(x)$, since different p_T bins integrate over broad, and substantially overlapping, x-ranges. Photon-jet and di-jet coincidences offer complementary strengths in reducing this model-dependence. The former is kinematically preferred because the resolution attainable on p_T, hence on x, is far better for photons than for jets. But attaining a statistically sufficient photon-jet data set with realistic integrated luminosities will be challenging. Since both channels demand new analyses, we do not yet have clear demonstrations of

their anticipated sensitivity levels, and so cannot yet optimize the compromises that will be needed to accommodate both within the limited trigger bandwidth.

One physics source for the complementarity between the two channels is illustrated in Figure 14, which plots a leading-order parton-level statistical "figure of merit" for ΔG sensitivity, defined as the product of the invariant amplitude squared and the partonic $\hat{a}_{LL}^2$, for $qg \to qg$ and $qg \to q\gamma$ as a function of the partonic c.m. angle θ*. The plot assumes that parton scattering at both $\pm\cos\theta^*$ contributes incoherently to the observed coincidences at given pseudorapidities $\eta_{1,2}$. This is valid for di-jets because it is difficult in practice (though possible in principle) to distinguish quark from gluon jets. In the Compton scattering case, the photon can of course be distinguished from the quark jet, and an effective discrimination between forward and backward scattering is then provided by the quark vs. gluon distribution functions for some regions of phase space.

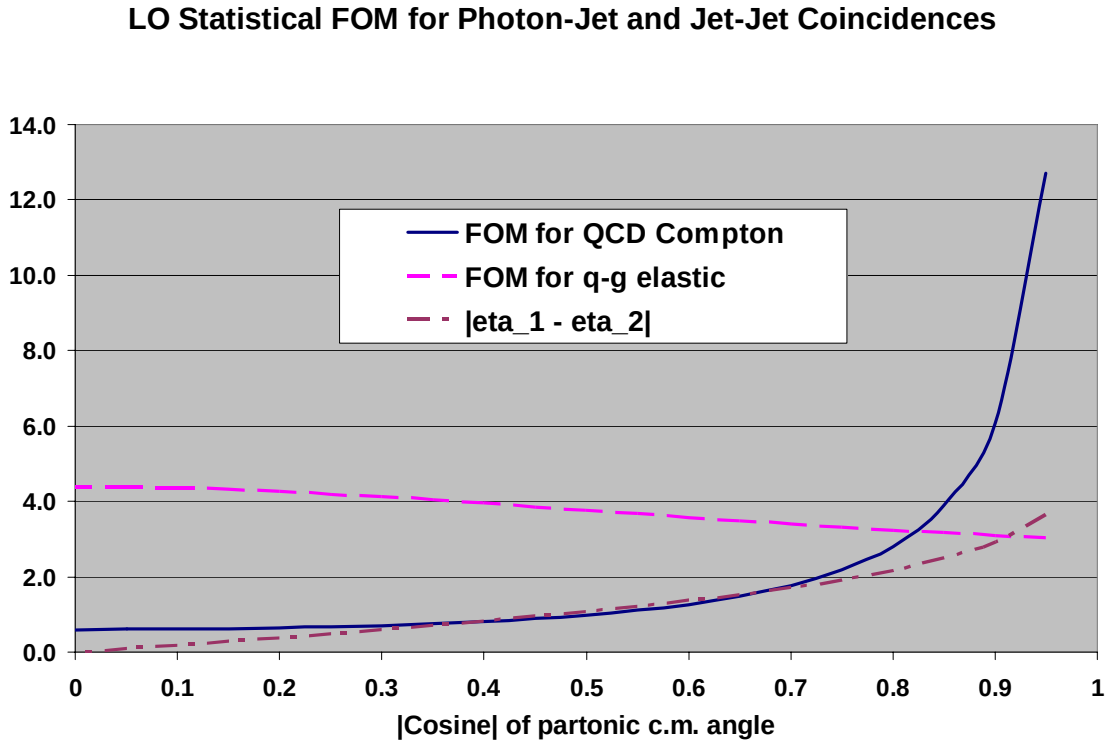

Figure 14: LO pQCD parton-level figure of merit (defined as $\overline{|M|^2}\hat{a}_{LL}^2$) for QCD Compton scattering (solid curve) and quark-gluon elastic scattering (dashed curve). The squared amplitude is taken as the sum, and $\hat{a}_{LL}$ as the weighted average, of values at $\pm\cos\theta^*$. The dot-dashed curve is the kinematic relation $|\eta_1 - \eta_2| = 2\tanh^{-1}(\cos\theta^*)$.

But in any case the photon production sensitivity is optimized at far backward c.m. angles ($|\cos\theta^*| \approx 1$ in the figure) by peaks in both cross section and spin asymmetry. In contrast, the presence of a *t*-channel gluon-exchange pole for the *qg* elastic scattering couples a

strong forward peak in the cross section with very small spin sensitivity, leading to a modest θ* dependence of the figure of merit, with a maximum at 90°. As also illustrated in the figure, these different sensitivities imply that photon-jet coincidences are most powerful for $|\eta_1 - \eta_2| > \approx 2$, while di-jet coincidences favor smaller values. In both cases, one is most interested in asymmetric partonic collisions, $|\eta_1 + \eta_2| = |\ln(x_1 / x_2)| > \approx 1$, in order to probe low-$x$ gluons with high-x (hence highly polarized) quarks. With the FMS, STAR's coverage will extend over $-1 \leq \eta \leq 4$, providing an outstanding opportunity to map $\Delta G(x)$.

The curves in Figure 14 do not take into account the factor $e_q^2 \alpha_{em} / \alpha_s << 1$ that appears in the ratio of cross sections for the semi-electromagnetic to strong processes. In practice, at anticipated luminosities, we are likely to fill much of the bandwidth with triggers for either process. Thus, a critical aspect of the comparison is the fraction of triggers that lead to desired reconstructable coincidence events in each case. These fractions are influenced by physics – *e.g.*, the fraction of di-jet events arising from qg scattering under given kinematic conditions – but also depend on technical issues that can be quantitatively assessed for realistic detector performance in the analysis of 2006 data and related simulations: (1) What levels of γ retention and π^0 rejection can be attained to optimize signal/background for photon-jet coincidences? (2) How low in p_T can direct photons be identified in the presence of a growing π^0 background? (3) Does low-mass background seen to date in π^0 reconstructions in STAR constitute an additional background for direct photon analyses? (4) Is an L2 coincidence trigger for γ-jet desirable, or will it enhance background more than signal? (5) How efficiently, and with what bias in extracted four-momenta, can jets be reconstructed beyond the barrel EMC region, despite the services gap (η=0.98 – 1.08) and rapidly decreasing TPC tracking performance? (6) What trigger biases on contributing partonic processes and x-ranges are imposed by the 2006 di-jet trigger?

One year from now, STAR will be better able to demonstrate the sensitivity to $\Delta G(x)$ attainable in given length runs at 200 GeV with an optimized trigger mix. As of now, we anticipate needing at least an additional 30 weeks of pp collision time at 200 GeV. If divided between 2008 and 2009, this would use the same time envisioned in the 2005 RHIC Spin Planning Document, but there spread over three years (2007-9). Three runs would provide an extra opportunity for the remaining beam development needed to attain the enhanced design goals for luminosity and polarization. But longer runs (e.g. 15 vs. 10 weeks) would deliver integrated luminosity more efficiently, since C-AD guidelines call for 8-week buildups to maximum luminosity for any given run. Thus, the integrated luminosity anticipated in two 15-week runs (2008+9) would be very nearly the same as for three 10-week runs (2007+8+9). STAR also strongly prefers devoting most of the 2008-9 pp collision time to 200 GeV, for two reasons: (1) attaining adequate coincidence statistics for a given x-range (≈ 0.04-0.08) at both 200 and 500 GeV will provide a powerful crosscheck on the pQCD analysis of RHIC spin data and will constrain the evolution of the gluon helicity distribution; (2) a forward tracking upgrade needed to optimize STAR's performance for 500 GeV W production physics will not yet be installed in 2009.

In summary, the optimal pp run plan for the STAR spin physics program would divide roughly 30 weeks of collision time between 2008 and 2009. The time would be devoted primarily to longitudinal spin running at $\sqrt{s} = 200$ GeV. These runs would allow a significant map of the *x*-dependence of the gluon polarization, within the approximate range $0.03 < x < 0.3$. Smaller values of *x* would be subsequently probed in 500 GeV running. During 2007 we support continued pp collision beam development time, as can be accommodated in a run with both Au+Au and d+Au running. In particular, we strongly support continued polarization development of proton beams in the AGS, in parallel with RHIC stores.

4. Recent heavy ion physics results and beam use proposal for Run 7

4.1 Recent relativistic heavy ion physics results

The reconstruction of the Au+Au dataset taken in Run 4 was completed in spring of 2006, while the reconstruction of the Cu+Cu dataset taken in Run 5 was completed in the summer of 2006. Preliminary results from a fraction of the Cu+Cu dataset have been presented in a number of conferences, while many analyses from the Au+Au dataset have reached completion and have been submitted for publication.

Recent measurements have focused on testing the phenomenon of jet quenching through systematic studies of suppression with system size and hadron species. As seen in Figure 15, suppression of high p_T charged particles in Cu+Cu is significant and consistent with that of peripheral Au+Au data at the same number of participants (N_{part}). The greater precision possible in controlling the collision geometry in Cu+Cu compared to peripheral Au+Au collisions results in higher precision in the suppression measurement, allowing stringent tests of the evolution with increasing system size.

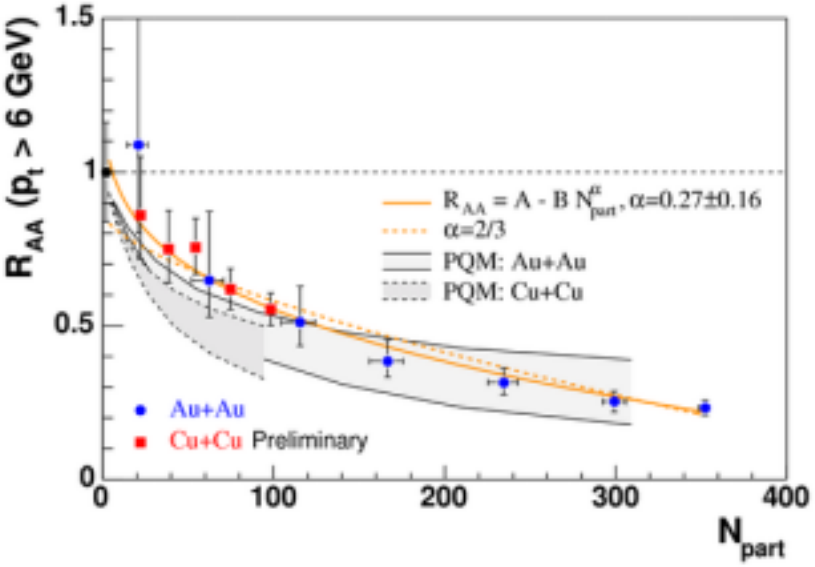

Figure 15: Nuclear modification factor R_{AA} for p_T > 6 GeV/c as a function of N_{part} for Cu+Cu and Au+Au. Error bars for Cu+Cu and Au+Au data include statistical and point-to-point systematic uncertainties, which are dominated by uncertainties in the modeling of the collision geometry. Common uncertainties from the p+p reference dataset have been folded into the p+p data point at the left.

Identification of the hadron species at high p_T provides important tests of the mechanism of jet quenching. An important advance in the past few years in STAR was to combine TOF information from a prototype detector for the STAR barrel TOF upgrade with specific ionization (dE/dx) measured in the Time Projection Chamber (TPC) to enable measurement of electrons at intermediate p_T and identification of pions and protons from

low p_T (~ 0.5 GeV/c) out to p_T > ~ 12 GeV/c. This increased STAR's particle identification capability significantly extending the reach of measurements such as the baryon to meson ratio as a function of p_T .

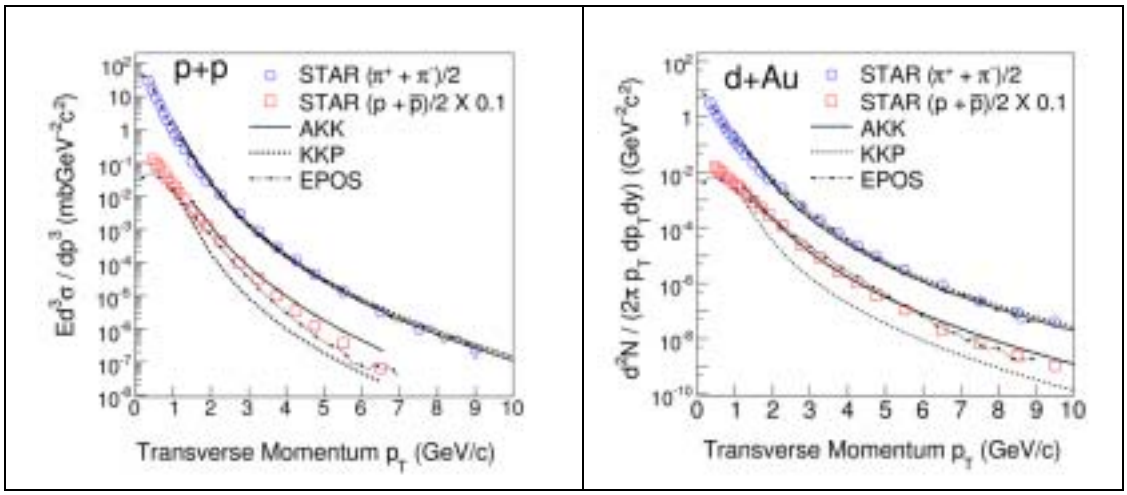

Figure 16: Identified hadron spectra in p+p and d+Au collisions, as compared to theoretical models. AKK [23] and KKP [24] describe perturbative QCD calculations incorporating either the AKK or KKP fragmentation functions. Figure is from Phys. Lett. B 637(2006) 161.

It is useful to calibrate penetrating probes of the medium in simpler systems before utilizing them in heavy ion collisions. Figure 16 shows a comparison to theoretical calculations of identified hadron spectra in p+p and d+Au collisions. Spectra for pions and protons are well described by perturbative QCD calculations, but, for the protons, only when the recent AKK [23] fragmentation functions are used. Within these calculations, the admixture of quark and gluon fragmentation is different for protons and pions: pions at large p_T have a significant contribution from fragmentation of light quarks, up to p_T of 10 GeV/c, while protons arise predominantly from gluons. Therefore, by measuring the suppression of protons separately from pions in Au+Au collisions sensitivity may be gained to the relative suppression of quarks and gluons. Gluons are expected to lose more energy in their interaction with matter due to the fundamentally stronger Casimir factor for gluon-gluon vs. quark-gluon or quark-quark interactions.

However, before applying partonic explanations to interpret measurements in heavy ion collision, it must be demonstrated that the dominant source of particle production is through parton fragmentation. It was first observed in Run 2 that at intermediate p_T (p_T < ~ 6 GeV/c) baryons behave differently in heavy ion collisions than mesons. This is shown clearly by Fig. 17, which shows the ratio of proton to pion spectra in both central Au+Au collisions and in p+p collisions. The large enhancement in Au+Au collisions of the ratio at intermediate p_T indicates that the dominant source of particle production in this p_T range

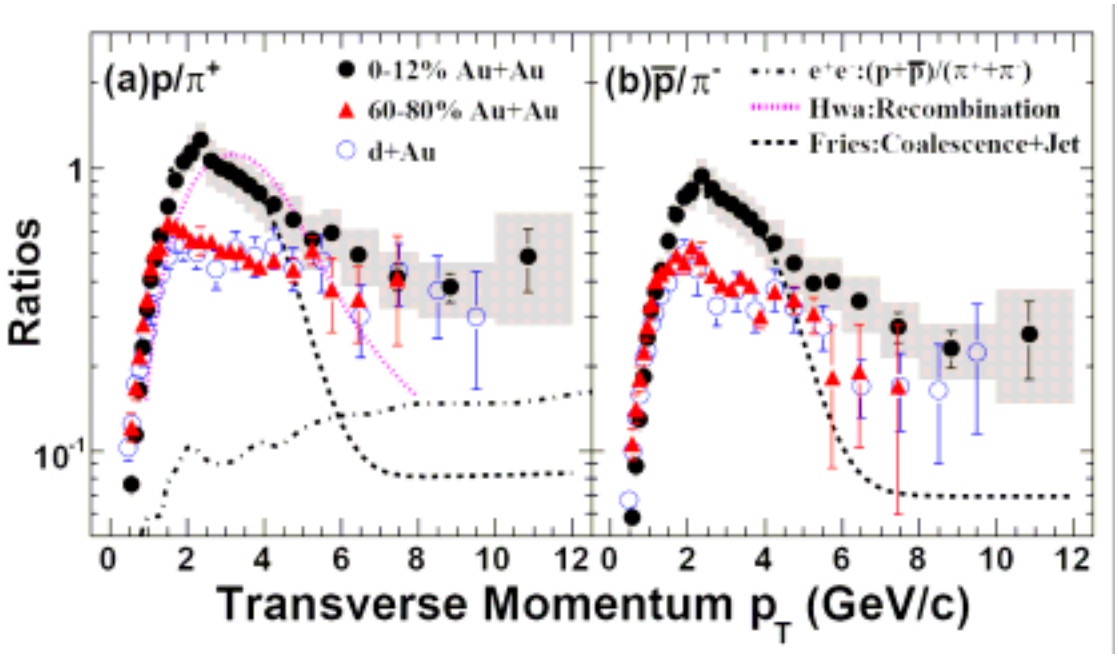

Figure 17: proton/π and antiproton/π ratios from d+Au and Au+Au collisions at $\sqrt{s_{NN}}$ = 200 GeV. The shaded boxes represent the systematic uncertainties in the top 12% central Au+Au collisions. The figure is taken from nucl-ex/0606003, submitted to Phys. Rev. Lett.

is not jet fragmentation in vacuum. Utilizing the high statistics obtained in Run 4 and STAR's particle identification capability, the enhancement is observed to be maximal for $p_T \sim$ 2-3 GeV/c, beyond which the ratio decreases towards the value observed in p+p and d+Au collisions.

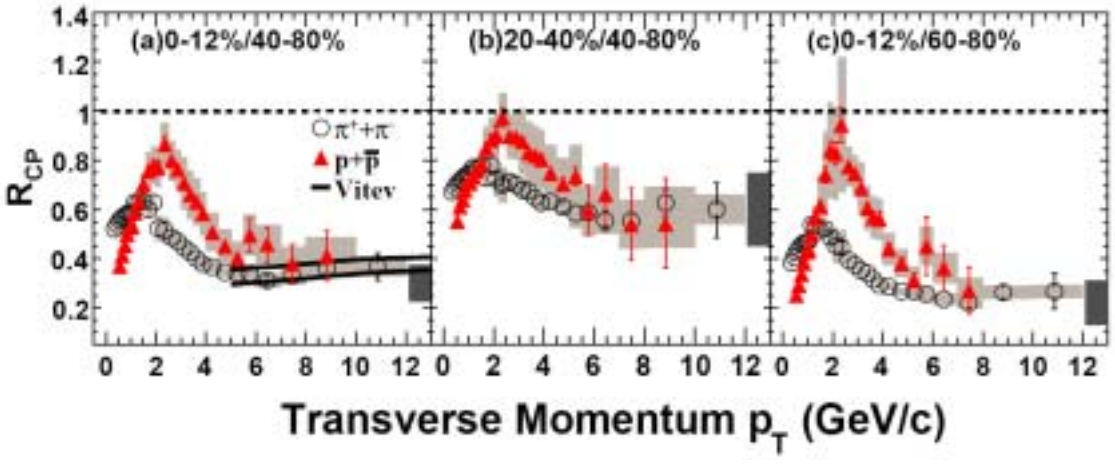

Figure 18: Nuclear modification factors RCP for protons and pions in 200 GeV Au+Au collisions. "Vitev" [25] denotes jet quenching predictions for pions. Figure is from nucl-ex/0606003, submitted to Phys. Rev. Lett.

The enhancement also is evident in the nuclear modification factor R_{CP}, the ratio between central and peripheral Au+Au collisions of N_{binary}-scaled spectra (Fig. 18). As with v_2, baryons and mesons are clearly differentiated in the behavior of R_{CP} as a function of p_T. Indications from previous runs that the dependence on hadron species disappears at high p_T were strengthened significantly based on analysis of the Run 4 dataset, supporting the applicability of models incorporating parton energy loss for $p_T > \sim 6$ GeV/c. However, no evidence is seen for stronger suppression of protons: instead, the results at high pT indicate that the partonic sources of pions and protons have similar energy loss when traversing the nuclear medium. Since the pions are expected to contain a larger contribution from quark fragmentation than the protons, this may indicate that gluons and quarks suffer similar levels of energy loss in the medium, contrary to expectations.

Another STAR capability which was dramatically increased in Runs 4 and 5 was the ability to measure heavy flavor. In large measure this was due to the commissioning of a large fraction (2π in azimuth, $0 < \eta < 1$) of the barrel electromagnetic calorimeter (BEMC). When combined with information from the main tracking detector (TPC), information on the electromagnetic energy deposited in the BEMC enables the measurement of electrons and photons out to high transverse momentum.

The radiative energy loss of heavy quarks (charm and bottom) in the dense medium created in heavy ion collisions is of prime interest. It is expected to be less than that of light quarks and gluons due to the large c and b quark masses. Therefore, the suppression of mesons containing heavy quarks may be used to test models which incorporate partonic energy loss as well its predicted dependence of on the density of the medium.

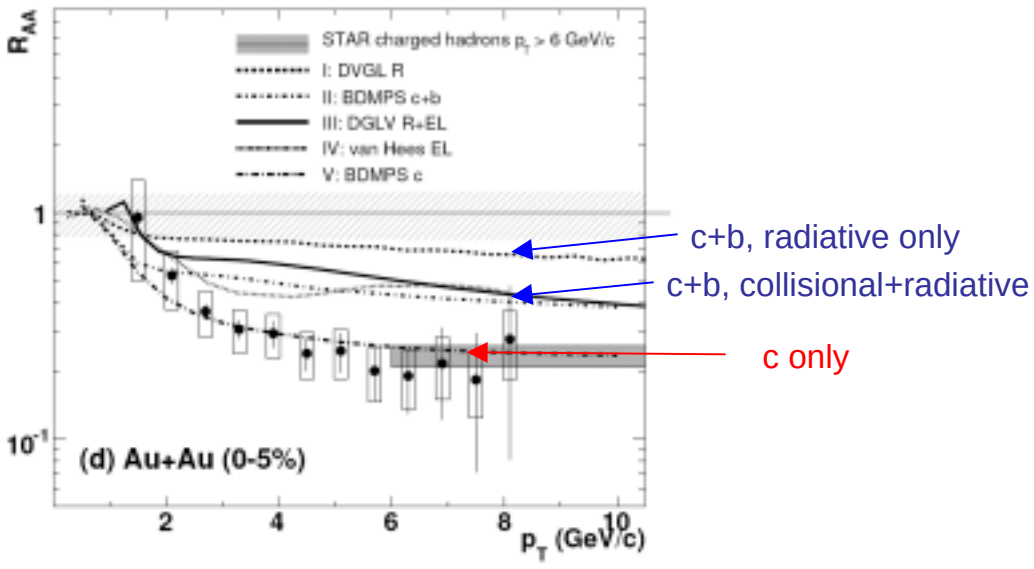

Figure 19: Nuclear modification factor R_{AA} for non-photonic electrons in central Au+Au collisions. The lines are theoretical calculations incorporating

models of energy loss. The figure is from nucl-ex/0607012, submitted to Phys. Rev. Lett.

Within STAR, heavy flavor can be accessed on a statistical basis through combinatoric subtraction of background from the distribution of invariant mass reconstructed from hadronic decay products (e.g. $D^0 \rightarrow k\pi$ at low p_T) or indirectly by measuring the spectrum of "non-photonic" electrons from semi-leptonic decays. The dominant source of electrons observed in the detector is the conversion of photons produced by hadronic decays (e.g. $\pi^0 \rightarrow \gamma\gamma$). Dalitz decays also play a role. These backgrounds can be subtracted using an invariant mass technique: the resulting non-photonic electrons are expected to come predominantly from the decay of mesons containing charm and bottom.

Figure 19 shows results on the p_T suppression of non-photonic electrons. The total cross-section of charm production, determined predominantly by the direct measurement of D° mesons at low p_T, is found to scale with N_{binary}, as expected for "hard probes" produced in the initial stages of the collision. At higher p_T however, surprisingly, strong suppression similar to that observed for light hadrons is observed out to $p_T \sim 8$ GeV/c. This result differs significantly from the suppression predicted (R_{AA}~0.5-0.6) for non-photonic electrons in this p_T range. The suppression can be reproduced assuming radiative energy loss in a medium of extreme density, but only if the contribution from bottom decays is assumed to be negligible. Resolving the true level of suppression for charm and bottom will ultimately depend on measuring their contributions separately.

One means to access the energy loss of a parton in the medium is to tag on a direct photon from a hard parton scattering, and then examine the fragmentation products of the away-side jet. Since the photon exits directly from the collision zone, this can be accomplished by examining the strength of the correlation in azimuth between the photon and fragmentation hadrons from the away-side jet for a given range of p_T. Experimentally, this measurement is complicated by large contributions from π^0 decay photons and the low cross section for γ + jet coincidences in a measurable range of p_T .

Figure 20 shows first results for this measurement from Run 4. A photon having E_T >10 GeV/c in the BEMC is tagged and correlated in azimuth with all hadrons having $4 < p_T < E_T^{trigger}$. For this result, 180M minimum bias events were presented to the trigger, corresponding to a sampled luminosity of ~ 25 μb^{-1}. Clear near and away-side peaks are seen as expected from high Q^2 parton-parton scattering. Separation of the contribution of direct and hadronic photons to the azimuthal correlation function is a work in progress. Ultimately, full exploitation of this technique will require the large increase in luminosity planned for RHIC II.

Another source of information is pair-wise correlations in azimuth and pseudorapidity between hadrons. Jet-like correlations have been found to persist to extremely low p_T (below 2 GeV/c), as shown in Fig. 21. Dramatic changes in the shapes of these correlations are seen in the progression from peripheral (lower right) to central (upper left) Au+Au collisions. The near-side peak widens substantially in η (by a factor of 2.3) from

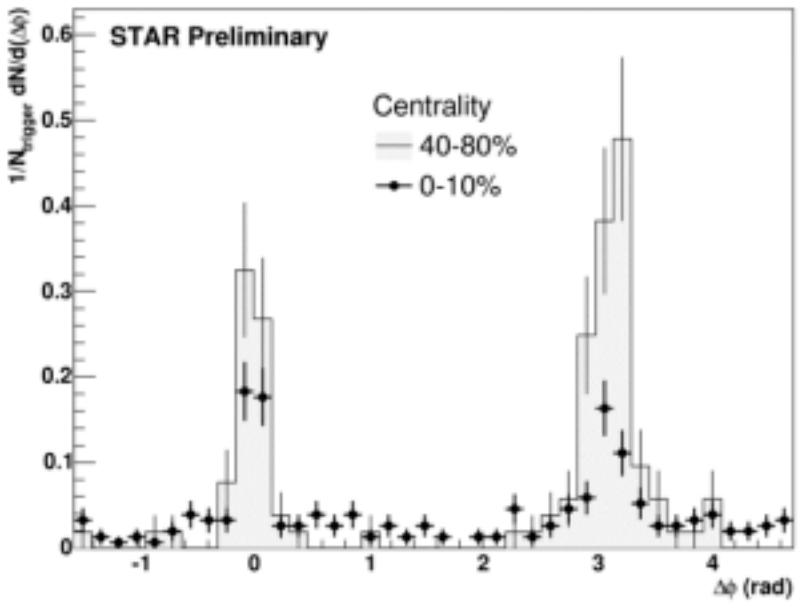

Figure 20: Au+Au collisions at $\sqrt{s_{NN}}$ = 200 GeV: per-trigger azimuthal correlation of charged hadrons associated with a trigger photon. The trigger photon has E_T>10 GeV/c, while the associated charged hadrons have 4 < p_T^{assoc} < $E_T^{trigger}$

peripheral to central collisions, indicating strong coupling between these correlated particles and the longitudinal expansion of the medium. Such measurements are possible because of the large η acceptance of the STAR TPC. The long-range correlation on the near side appears to persist in correlations between a trigger hadron and hadrons at intermediate p_T: the study of the spectrum and chemistry of particles within this long-range "ridge" have begun, and appear to identify the origin of the ridge as a bulk reaction of the medium to a trigger particle. Further studies with a larger sample of triggers and the identification capabilities of the barrel TOF will greatly increase the understanding of this new phenomenon in heavy ion collisions.

Somewhat higher in transverse momenta, when both the "trigger" hadron and the associated particles are in the intermediate p_T regime, strong modification of the away-side peak shape is seen. Figure 22 shows results for one choice of p_T threshold as a function of centrality. As the collisions become more central, the population of the two-particle correlation at intermediate angles (from ~1.5 to 2.5 radians) grows significantly. Various interpretations for the origin of this enhancement have been given including the possibility that energetic particles may exceed the speed of sound in the medium creating a shock front. This study is an area of very active investigation.

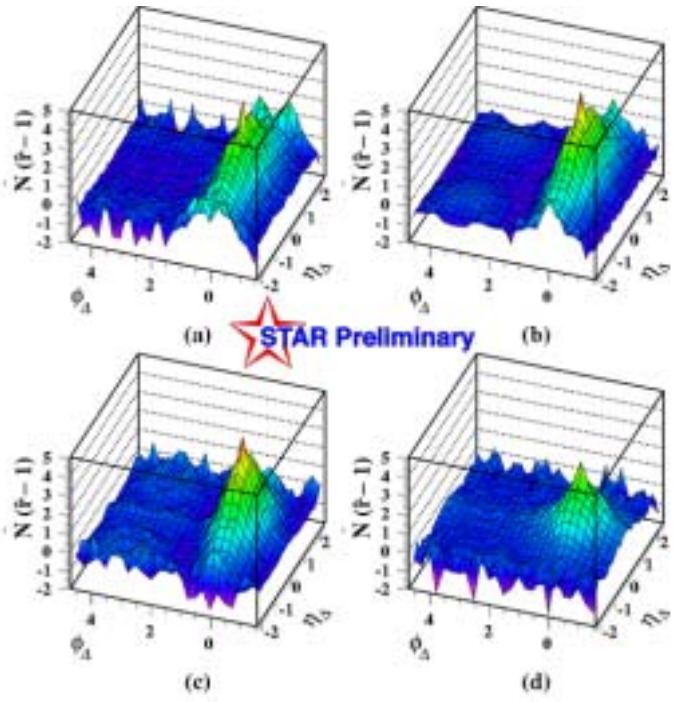

Figure 21: For Au+Au collisions at $\sqrt{s_{NN}}$ = 200 GeV: pair-wise correlations in azimuth (ϕ_Δ) and pseudorapidity (η_Δ) between soft particle pairs with 0.15 < p_T< 2 GeV/c for (a) central to (d) peripheral collisions. Independent first and second harmonics have been subtracted.

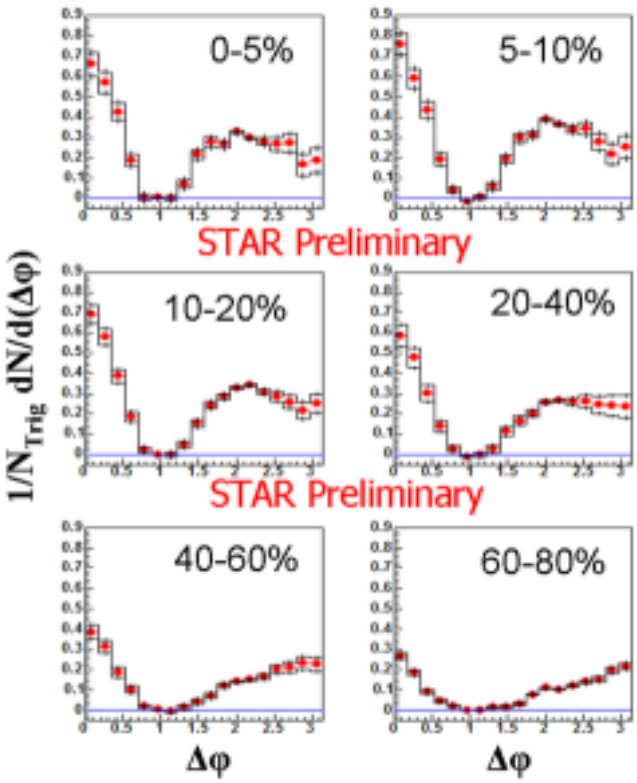

Figure 22: Au+Au collisions at $\sqrt{s_{NN}}$ = 200 GeV: per-trigger azimuthal correlations at different centralities with 2.5 < p_T^{trig} < 4.0 GeV/c, $|\eta^{trig}| < 0.7$, and 1 <p_T^{assoc} < 2.5 GeV/c, $|\eta^{assoc}| < 1$.

Deeper insight into the origin of this observation may be provided by three-particle correlations which tend to suppress trivial effects e.g. due to momentum conservation. Shown in Figure 23 are first results on 3-particle correlations for p+p reference data and central Au+Au collisions.

One interpretation of the additional population observed in the two-particle correlations at intermediate angles for central collisions is that it is due to conical flow induced by shock waves in the non-viscous medium created in heavy ion collisions. If so, sufficiently strong conical flow would result in an enhancement in the off-diagonal region (π-1, π+1 and π+1, π-1) in three-particle correlations. While no such enhancement is found at 1 radian, there are indications of an enhancement at off-diagonal distances of 1.4 radians, as shown in Figure 23. This is a complicated analysis which is ongoing, and an alternative method of subtracting the two-particle correlations to obtain true 3-particle correlations is currently under study. The analysis is statistically limited: future increases in sampled luminosity would help greatly.

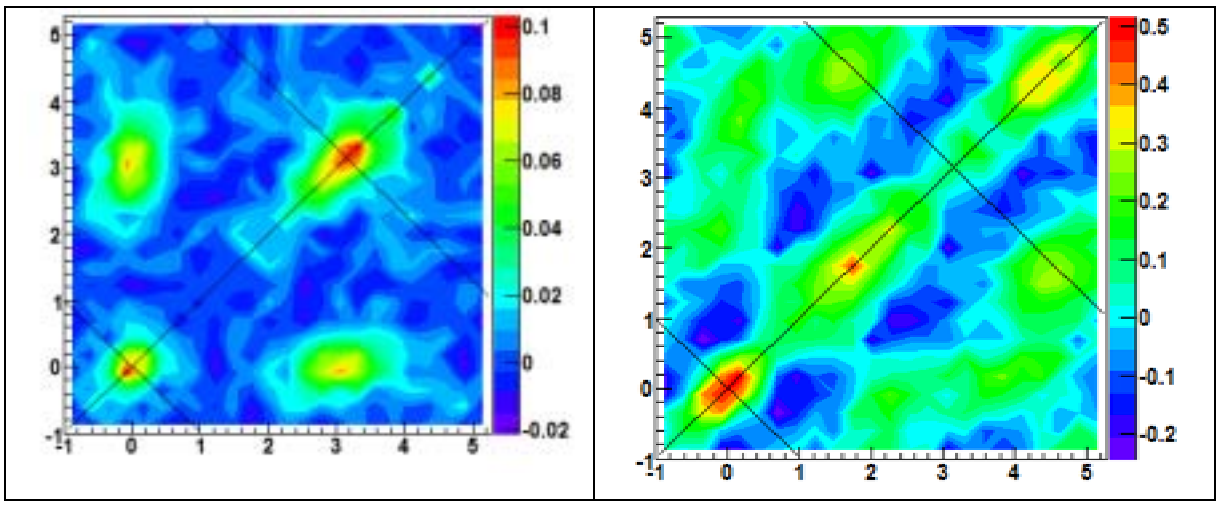

Figure 23: Three-particle correlations in minimum bias p+p collisions (left) and 12% central Au+Au collisions (right). The p_T ranges are $3 < p_T^{trig} < 4$ GeV/c and $1 < p_T^{assoc} < 2$ GeV/c. The figure is from at Hard Probes 2006 [26].

An important advance in the soft physics sector has been obtaining an improved understanding of the relative contribution of non-flow effects to the observed v_2 in Cu+Cu vs Au+Au collisions. This was accomplished by correlating particles at forward rapidity and mid-rapidity to minimize the non-flow contribution. The results are shown in Figure 24, in which it is seen that the non-flow component is relatively much stronger in the lighter Cu+Cu sytem.

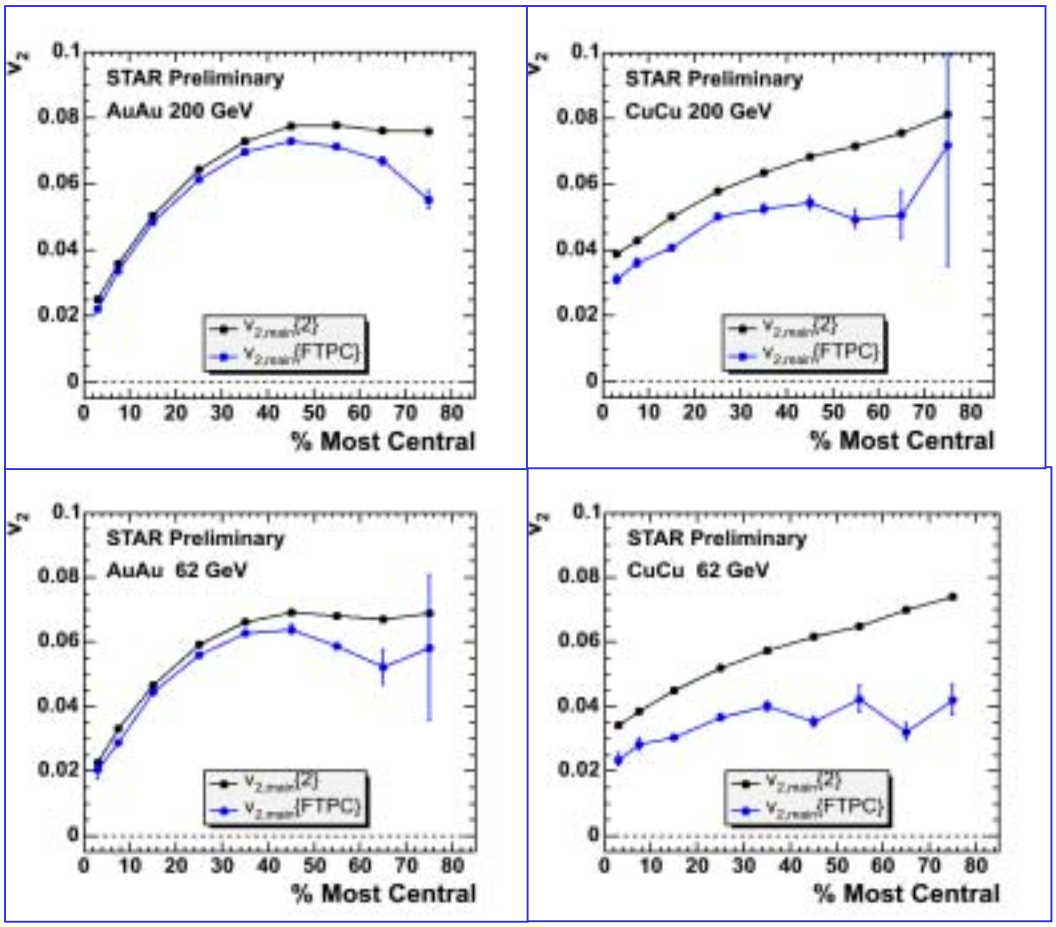

Figure 24. Comparison of the contribution of non-flow effects to the observed v_2 for Au+Au and Cu+Cu. The black curves are derived by correlating two random particles at mid-rapidity in the STAR TPC. The blue curves, for which non-flow effects are minimal, result from correlating particles at forward rapidity and mid-rapidity. The difference between the black and blue curves demonstrates that non-flow effects are relatively stronger for the lighter Cu+Cu system.

The higher statistics available from the Run 4 Au+Au data sample have allowed extension of hadronic correlation measurements to the high p_T region in which e.g. the baryon-meson splitting in R_{cp} is no longer apparent. Figure 25 shows two-particle azimuthal correlations in this region. Clear near and away-side peaks are seen. The combinatoric background upon which they sit is greatly reduced, negligible even in central Au+Au collisions for the highest p_T thresholds investigated. The strong modifications in the peak shapes observed for low p_T thresholds are not apparent for these higher p_T thresholds, indicating the correlations observed in this regime result primarily from the fragmentation of di-jets.

The clean identification of correlations generated by di-jets, allows investigation of hadron-triggered "fragmentation functions", by binning the correlations in z_T =

p_T^{assoc}/p_T^{trig} and integrating the near- and away-side peaks (Fig. 26). The near-side fragmentation function is unchanged from d+Au collisions to central Au+Au collisions, but the away-side fragmentation function is strongly suppressed, comparable to the level of suppression observed for single-particle inclusive spectra. Di-hadron correlations incorporate a completely different set of biases (induced by fragmentation and the geometry of the overlap region) than single-particle spectra. Therefore, such measurements place constraints on the density of the medium which are somewhat independent of those derived from the suppression of inclusive spectra.

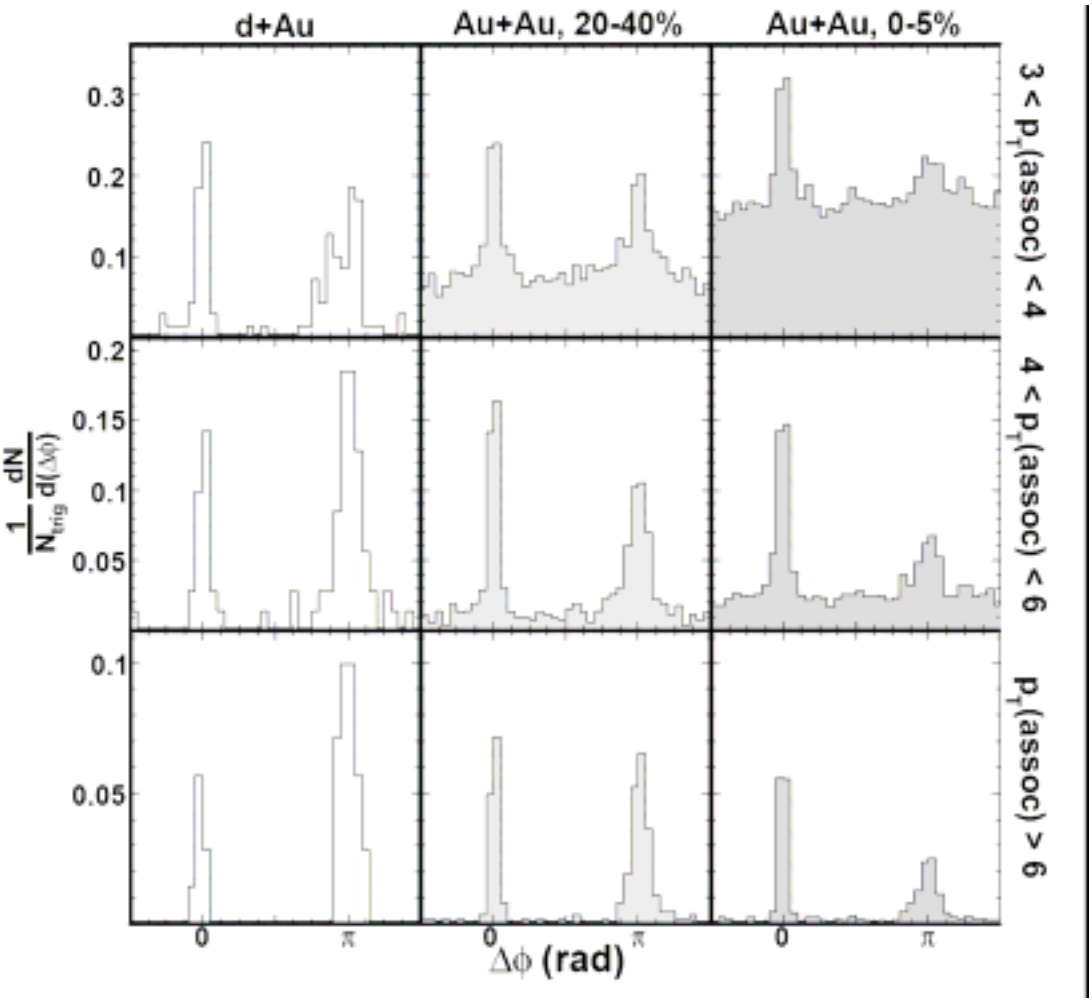

Figure 25: Per-trigger azimuthal correlations between charged hadrons for the systems indicated at $\sqrt{s_{NN}}$ = 200 GeV. The "trigger" hadron has $8 < p_T < 15$ GeV/c. The figure is from nucl-ex/0604018, submitted to Phys. Rev. Lett.

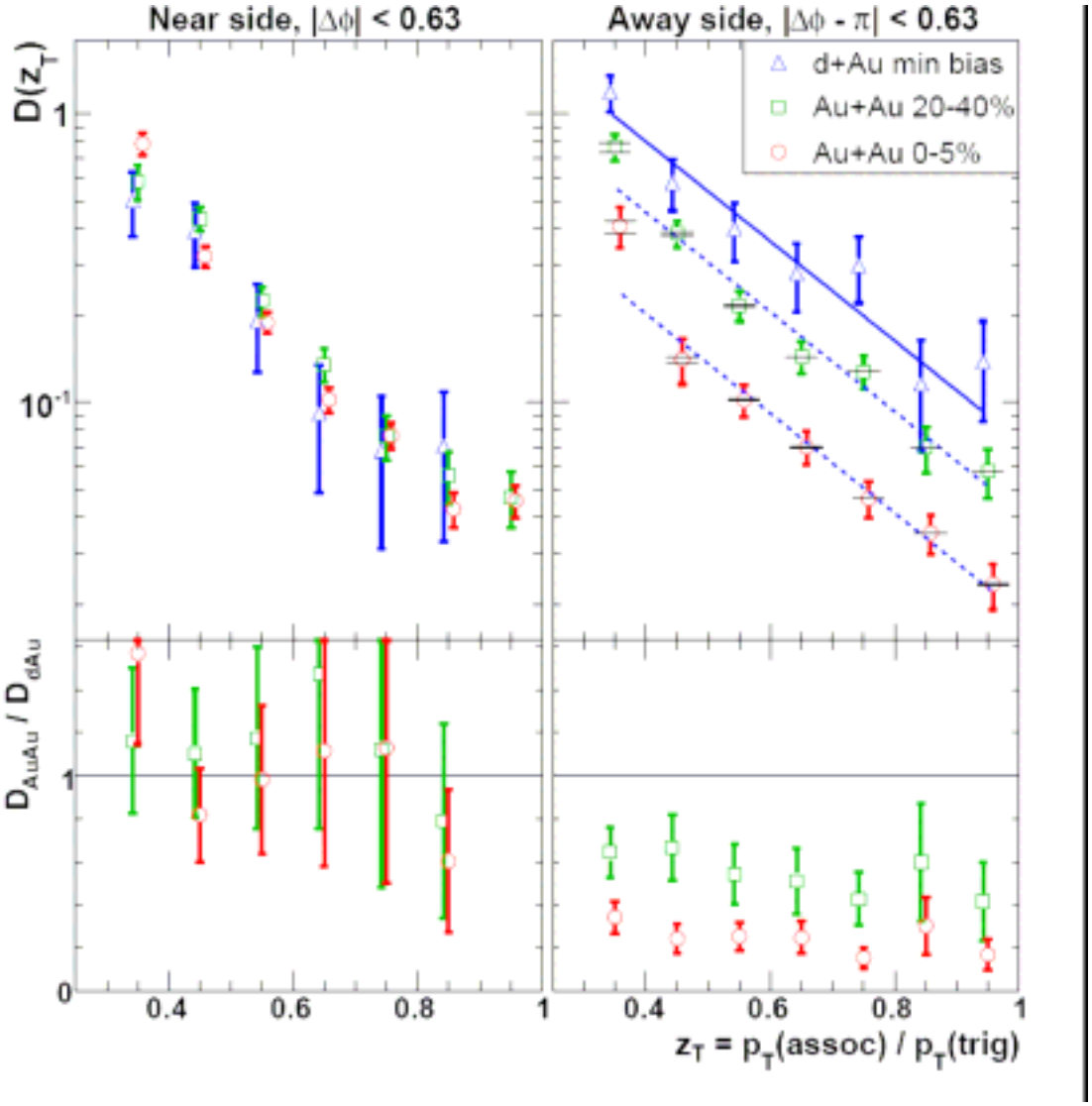

Figure 26: Top: Di-hadron "fragmentation functions" as a function of z_T for minimum bias d+Au collisions and Au+Au collisions at two centralities. The lines are from an exponential fit to the d+Au data, scaled down by a p_T-independent factor to results in Au+Au collisions. Bottom: ratio between results from Au+Au and d+Au collisions. The figure is nucl-ex/0604018, submitted to Phys. Rev. Lett.

4.2 Au+Au beam use request for Run 7

The STAR Collaboration proposes a Au+Au run of 10+2 weeks duration at $\sqrt{s_{NN}}$ = 200 GeV, and a run of (1+1) weeks duration for low energy commissioning and background studies in preparation for a future QCD critical point search. The primary physics goal of the $\sqrt{s_{NN}}$ = 200 GeV run will be to make a significant advance in understanding the origin

of the suppression of non-photonic electrons, and the response of the medium to penetrating high pt probes. It is anticipated that improved vertex selection using an upgraded vertex position detector will yield 20-30% more usable events per unit integrated luminosity than in previous runs.

A key motivation for a return to Au+Au at 200 GeV in Run 7 is to expand on measurements of heavy flavor suppression. The current situation is shown in Figure 19. Non-photonic electrons are suppressed to the same level as charged hadrons. This surprising result cannot be easily accommodated in frameworks in which the suppression is due to partonic energy loss, and has led to much activity in extending and expanding these frameworks.

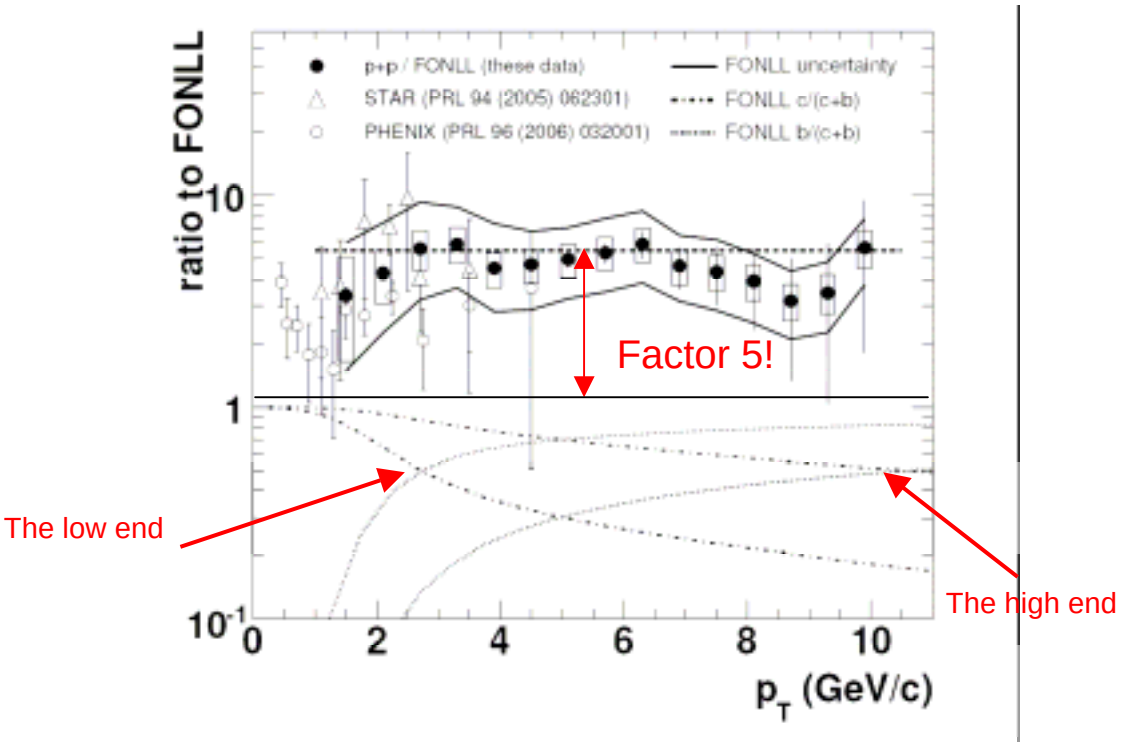

Figure 27: Comparison of non-photonic electron spectra in p+p to FONLL calculation. The figure is from nucl-ex/0607012, submitted to Phys. Rev. Lett.

A critical uncertainty in these investigations is the relative yield of charm and bottom resulting in non-photonic electrons from their semi-leptonic decays. Shown in Figure 27 is a comparison to the data of the most sophisticated calculation of non-photonic electron spectra from perturbative QCD, the Fixed Order Next-to-Leading Log (FONLL) calculation [27]. First, the calculation under predicts the measurement by a factor of 5. Secondly, within the framework of the calculation, the relative yield of charm and bottom contributing to the non-photonic electron spectrum is highly uncertain: the point at which bottom becomes the dominant source of non-photonic electrons ranges from a p_T of 3 to

10 GeV/c. Since bottom and charm are predicted to have different levels of energy loss in the medium, this produces difficulties in understanding the suppression pattern. At the extreme, as shown in the lowest calculation in Figure 19, if bottom were to have little contribution to the non-photonic electron spectra in the measured range of p_T, the suppression of non-photonic electrons could possibly be understood within the existing framework. Therefore, progress in separating the contributions from charm and bottom to non-photonic electrons is a very high priority.

One way to address this problem is to measure charm directly. STAR has directly reconstructed the charmed D hadron through the K+π decay channel in both Au+Au and d+Au. These measurements are currently statistically limited by the large combinatorial background under the D peak. In 16M d+Au events, the signal has a statistical significance of 6σ, while in 13M minimum bias Au+Au collisions the statistical significance is 4.5σ, limiting the measurements to p_T below 2-3 GeV/c. While such measurements are essential for constraining the total charm cross-section, and its scaling across collision systems, the uncertainties and reach in p_T do not allow for significant measurements of D flow or R_{AA} of D. Additional detector capability is needed in order to extend these measurements.

STAR has a detector system, composed of the Silicon Vertex Tracker (SVT) and Silicon Strip Detector (SSD), which in principle has adequate resolution to make progress in this direction. In the past year, significant progress has been made in the calibration of these detectors resulting in their performance coming very close to design. Shown in Figure 28 is the pointing accuracy to the vertex of this system: accuracies on the order of 150 um have been reached. The decay distance cτ of charm and bottom hadrons is on the same order (D^0: 123 um, D^+: 312 um, B^+: 501 um), so the addition of this full detector system in the Au+Au and d+Au collisions can potentially begin to address the separation of charm and bottom. In previous Au+Au and d+Au runs the SSD, which is critical for the performance of the full vertexing system, was not fully commissioned.

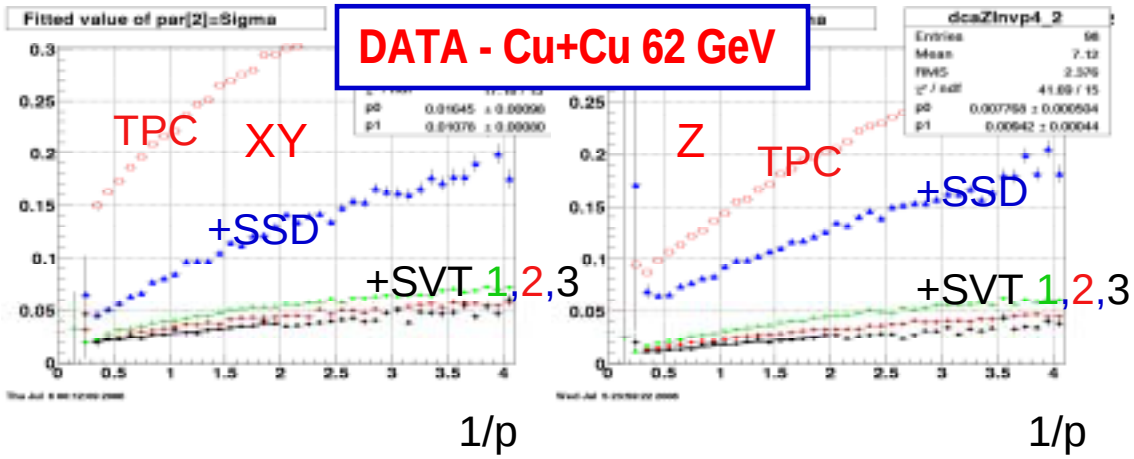

Figure 28: TPC, TPC+SSD, and TPC+SVT pointing resolution, in microns, to the interaction vertex as a function of 1/p in Run 5 Cu+Cu at 62 GeV

The addition of the full SVT+SSD vertexing system can decrease the combinatorial backgrounds, allowing for a substantial increase in the significance per event. With 60M minimum bias events, the p_T reach for D mesons is expected to increase to approximately 4 GeV/c. This improvement will also potentially allow measurement of D meson v_2 at low p_T with absolute errors of approximately 5%. Such measurements will provide a first look at such phenomena, but definitive measurements on charm flow and R_{AA} await the much greater reduction in background afforded by the STAR Heavy Flavor Tracker.

Large improvements are possible in the upcoming run in the integrated luminosity sampled by the trigger capability for rare probes provided by the Barrel Electromagnetic Calorimeter (BEMC). In the previous d+Au (Run 3) and Au+Au (Run 4) runs, the BEMC was only partially instrumented, leading to an effective acceptance of less than half of its current acceptance. In addition, the machine and detector performance in these runs led to an effective luminosity sampled of approximately 30 ub^{-1} in Au+Au and 370 ub^{-1} in d+Au. With the improvement in the machine luminosity envisioned for Run 7, combined with an effort to reduce the deadtime introduced in the trigger mix, it will be possible to sample 200-300 ub^{-1} in a 10-week Au+Au run and 15 nb^{-1} in a 10-week d+Au run. Combined with the increase in acceptance, this will provide a statistical enhancement by more than an order of magnitude in probes that can be triggered by the EMC.

There are three probes which will benefit from this increase in luminosity: Υ, γ, and non-photonic electrons. A dedicated Υ trigger has been used since Run 4, but to date the luminosity integrated by this trigger has led only to upper limits. With the increased acceptance of the BEMC and 300 ub^{-1} integrated luminosity in Au+Au collisions, on the order of 150 Υ should be obtained, leading to measurements with statistical accuracy of approximately 10%. Similar accuracy is expected in d+Au collisions from Run 7 and from the analysis of p+p collisions from Run 6. Combined, these measurements will give a first glimpse into the suppression (or lack thereof) of bottomonium at RHIC.

Correlations between prompt photons and hadrons will give key insight into the jet tomography of the collision zone. Such measurements require large amounts of integrated luminosity, and suffer from backgrounds in the photon tag from π^0 decays and fragmentation of jets. Inclusive photon-hadron correlations from Run 4 Au+Au collisions are shown in Figure 20; they are severely statistically limited. In Run 7, with 300 ub^{-1} integrated luminosity, and the full acceptance of the BEMC, several hundred tower-charged track pairs with $E_T^{tower} > 10$ GeV/c, $p_T^{assoc} > 4$ GeV/c should be obtained. This sample should be large enough to extract a first direct measurement of the photon-jet process in heavy-ion collisions. Ultimately, detailed examination of this process awaits the STAR DAQ1000 upgrade and further improvements in machine luminosity.

Additionally, large samples of trigger photons can help in other correlation measurements. Trigger towers at thresholds that would be able to sample the full luminosity available from the beam, approximately 5 GeV/c in E_T, arise predominantly from π^0 decay. While this is a disadvantage for prompt photon-hadron correlations, it is

an advantage for hadron-hadron correlations. Studies of jet-medium interactions, such as the 3-particle correlations in Figure 23 and correlations sensitive to the widening of the near-side peak in pseudorapidity shown in Figure 21, could use BEMC towers rather than charged hadrons in the TPC as the trigger. This would increase the statistical samples of such studies by more than an order of magnitude.

Improvements in the integrated luminosity for triggered non-photonic electrons will allow for differential measurements in the heavy flavor sector. The current statistical uncertainties for non-photonic electrons at high p_T are large: approximately 20% at 6 GeV/c ranging to 50% at 8 GeV/c for Au+Au collisions from Run 4, and approximately half that for d+Au collisions from Run 3. The improvements in sampled luminosity and acceptance in Run 7 should decrease these uncertainties by a factor of 5 in Au+Au and a factor of 10 in d+Au. This increased statistical power should allow for a first look at electron-hadron correlations in ion collisions, which may provide sensitivity to the relative contribution of charm and bottom to the electrons and, as in dihadron correlations, provide an alternative probe of partonic energy loss. The addition to these correlation measurements of vertexing using the SVT and SSD shows promise in constraining the relative abundance of charm and bottom: current simulations show sensitivities, with such a sample, at the 30% level to the bottom contribution to non-photonic electrons.

Additionally, with 60M minbias events a significant J/Psi measurement will be possible in Au+Au. A dedicated trigger will be used to obtain a significant J/Psi measurement in both d+Au and ultraperipheral Au+Au events for studies of gluon shadowing.

An additional dedicated trigger for ultraperipheral collisions will allow for studies of the ρ', providing the first step in the search for exotic mesons.

There is growing interest in running RHIC at extremely low energies, down to $\sqrt{s_{NN}}$ of 5 GeV, in order to search for the critical point of QCD. Fluctuations and correlations, specifically of identified kaons and protons at low p_T, have been proposed as signatures for this search. The capabilities of STAR are best matched to such an energy scan once the barrel TOF is in place, which will greatly increase particle identification capabilities in the crucial p_T region. Therefore, STAR proposes to delay the extended scan, over many energies, to Run 9. However, there are critical developments necessary both on the machine side and on the detector side in order to make this future run a success. On the detector side, developments are necessary to understand methods to trigger on collisions at these low energies and to characterize the associated background levels. We propose to dedicate 1 week to such developments at the energy which CAD considers the most informative for a future run. A likely target is 9 GeV, in which, based on a collision rate of 20 Hz, we could expect to obtain 4M events per week. A minimum of 5M events are needed for fluctuation studies. Extending the studies at this lower energy by one week would optimize the physics measurements at this energy.

The increased machine performance is expected to deliver luminosities of approximately 1.8 nb^{-1} in a 10-week Au+Au run and 120 nb^{-1} in a 10-week d+Au run. The deadtime of

STAR linearly increases with the rate of events to tape, with 100 Hz corresponding to 100% dead. STAR needs to run at 50 Hz for 10 weeks in order to reach a goal of 100M minimum bias events recorded, from which 60M will be usable for physics analysis. This loss in usability is due to the online selection of longitudinal vertex position, and may be improvable with a planned upgrade to the vertex triggering at L0, resulting in a

Year	Collision System	Sampled Luminosity	AB*Sampled Luminosity	BEMC Coverage
2003	D+Au	370 ub^{-1}	0.15 pb^{-1}	Half
2004	Au+Au	30 ub^{-1}	1.2 pb^{-1}	Half
2005	Cu+Cu	860 ub^{-1}	3.4 pb^{-1}	Half
2006	P+p	10 pb^{-1}	10 pb^{-1}	Full
2007 (projected)	Au+Au (10 weeks)	200-300 ub^{-1}	8-11 pb^{-1}	Full
	D+Au (10 weeks)	15 nb^{-1}	6 pb^{-1}	Full

Table 4: Integrated luminosities, usable for physics analysis, sampled by the rarest triggers, as achieved in previous runs, along with estimated luminosities for Run 7.

decrease in the sample of minimum bias events needed with a corresponding decrease in the necessary deadtime. Conservatively assuming a loss of a factor of 2 in STAR uptime, a factor of 2 in usable events due to the longitudinal spread of the vertex, and a factor of 2 from deadtime, the integrated luminosity sampled by the rare triggers in $\sqrt{s_{NN}}$ = 200 GeV Au+Au running in the upcoming run would be ~ 225 μb^{-1} . Improved triggering could increase this to approximately 300 μb^{-1}. Similar considerations apply to the d+Au run. A comparison of projected integrated luminosities in Run 7 to the results of previous runs is shown in Table 4. The comparison is quite favorable for a return to Au+Au and d+Au in Run 7.

It is important to note that **the use of d+Au collisions as a reference for heavy flavor measurements is highly preferred to the use of p+p collisions** for two reasons. First, the yield of hard processes per minimum bias event is enhanced by a factor of $<N_{binary}>$, which is 7.5 in d+Au collisions. The total number of minimum bias events that can be recorded in a given time period is limited by deadtime considerations, independent of the collision system. Therefore, the higher yield of hard processes per event in d+Au collisions increases the statistical sample of probes on which the BEMC cannot trigger, such as the D meson. Second, the higher multiplicity in d+Au increases the precision of event-wise vertex determination: while in p+p, the precision of the vertex determination is expected to be a limiting factor in the use of the SVT and SSD to tag displaced vertices from heavy flavor decays, the vertex precision in d+Au is not expected to be an issue. Nuclear effects at mid-rapidity are small, so from the reference standpoint d+Au and p+p are equivalent.

4.3 Recent d+Au physics results and measurements proposed for Run 7

The low-x structure of heavy nuclei is a fundamental question of great interest, both in its own right and because it determines the initial conditions in relativistic heavy ion collisions. For protons, data from HERA show that the low-x region is dominated by gluons and that gluon splitting causes the gluon density to increase dramatically as x is decreased. At a sufficiently small value of x, yet to be determined by experiment, the splitting is expected to become balanced by recombination as the gluons overlap in the transverse plane, resulting in gluon saturation. Indeed, some theorists have argued that the HERA results already point to an onset of gluon saturation effects in the proton in the region $x <\sim 0.01$. In contrast, others have argued that conventional DGLAP evolution, which should only be appropriate in the dilute regime, applies over the entire HERA kinematic domain. Overall, the picture is clouded by the lack of a well-defined "unsaturated" baseline system to which the HERA data can be compared.

The gluon density in a heavy nucleus is larger than that in the proton by a factor of $\sim A^{1/3}$. This makes heavy nuclei particularly attractive laboratories to look for saturation effects for two reasons. The increased gluon density implies saturation effects should become apparent at higher values of x in nuclei than in the nucleon. Meanwhile, the measured gluon density in the nucleon provides a well-defined reference for comparison.

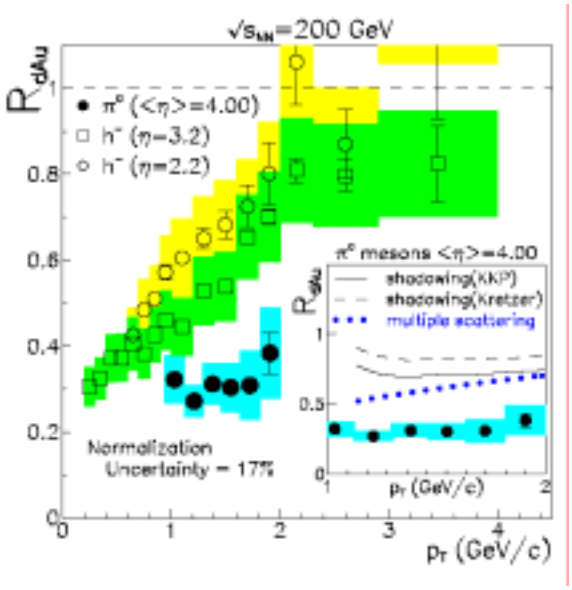

Figure 29: Nuclear modification factor R_{dAu} vs. p_T for identified π^0 at η=4 from STAR [28], compared to previous BRAHMS results for unidentified h^- at η=2.2 and 3.2 [29]. The inset shows the STAR results compared to several theoretical predictions. See [28] for details.

Measurements of inclusive particle production in d+Au collisions at RHIC have established that the yield of produced particles systematically decreases as their rapidity increases. For example, Fig. 29 shows recent results for the nuclear modification factor R_{dAu} for identified π^0 at η=4 from STAR [28], compared to previous results for

unidentified h^- from BRAHMS [29]. The inset shows a comparison of the STAR results to several theoretical predictions, all of which predict much less suppression than is observed. The BRAHMS results at forward rapidity have been described by calculations [30] based on the Color Glass Condensate (CGC) model that treats the Au nucleus as a saturated gluon field. As shown in Fig. 30, calculations within the CGC model [31] also provide a very good description of the p_T dependence of the π^0 cross section measured by STAR, although they overpredict the observed π^0 yield at η=4 by a factor of ~2 when they are scaled to match the BRAHMS results at η=3.2.

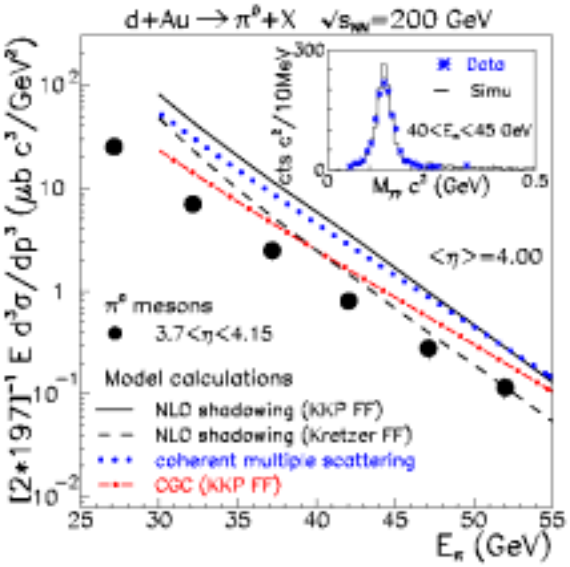

Figure 30: Inclusive π^0 cross section per binary collision for d+Au collisions at η=4. The curves are model calculations, and are described in detail in [28]. The inset shows a comparison between the uncorrected di-photon invariant mass spectra from data and from Monte Carlo simulations.

To further elucidate the dynamics underlying particle production in d+Au collisions at forward rapidity, STAR also performed exploratory measurements of forward-midrapidity di-hadron coincidences during Run 3 [28]. Many models that predict the yield of particles should be suppressed in d+Au collisions, including those that attribute the suppression to conventional leading-twist shadowing or initial-state energy loss, nonetheless expect that back-to-back correlations, characteristic of di-jets, should remain similar. In contrast, in the saturation picture, forward particles arise from energetic quarks in the deuteron that undergo multiple interactions in the dense gluon field of the Au nucleus, leading to an apparent "mono-jet" mechanism [32].

Figure 31 shows the probability of finding a leading charged particle with $p_T > 0.5$ GeV/c at midrapidity in coincidence with an identified π^0 at η=4. Results are shown for p+p and d+Au collisions, and for two different π^0 energy ranges. (Note that $p_T = E_\pi$ / cosh η.) A PYTHIA simulation predicts most of the features of the p+p data [28]. HIJING simulations with nuclear shadowing predict the d+Au correlations should be qualitatively similar to those in p+p. HIJING provides a reasonable description of the d+Au data in

the 30 < E_π < 55 GeV bin, including both the strength of the coincidence peak and the magnitude of the combinatoric background. In contrast, the low E_π data are not consistent with the HIJING expectations. Very recently PHENIX has published results of a similar d+Au forward-midrapidity correlation study [33]. However, the PHENIX measurements are sensitive to significantly larger x_g values than are sampled in the STAR study, so it is not clear that one should expect similar behavior.

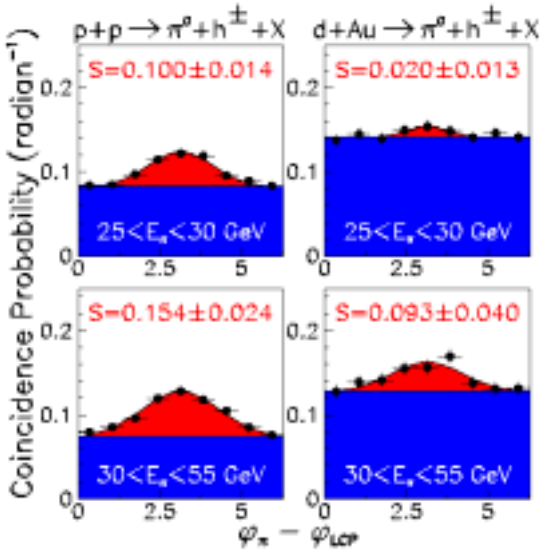

Figure 31: Coincidence probability vs. Δφ between a forward π^0 at η=4 and a leading charged particle with p_T > 0.5 GeV/c and |η| < 0.75. The curves show fits to a Gaussian centered at Δφ = π plus a constant background. *S* indicates the area of the back-to-back peak.

The existing d+Au results suggest that forward particle production at RHIC may be sensitive to the onset of gluon saturation. However, many alternate explanations of the observed effects have been offered – including limiting fragmentation, parton recombination, initial-state energy loss, and factorization breaking. In fact, there is even controversy regarding the kinematic range that is explored by the existing RHIC d+Au results. Perturbative QCD calculations predict that the $\langle x_g \rangle$ sampled by the BRAHMS measurement is ~0.02 [34], whereas CGC calculations imply the $\langle x_g \rangle$ ~ 0.001 [31]. Thus, evidence for gluon saturation at RHIC energies is not yet conclusive.

Unambiguous determination of the gluon density in a heavy nucleus requires going beyond inclusive particle production to explore particle correlations in order to elucidate the dynamics that underlie the observed suppression of the inclusive yields. Perturbative QCD is known to describe inclusive hadron yields at forward rapidity in p+p collisions at RHIC, especially for p_T >~ 2 GeV/c (e.g., see Fig. 32). In pQCD, triggering on particle production in the forward direction implies that the quarks from the deuteron beam are the predominant probes of the gluons in the Au nucleus. The gluon density in the Au

nucleus is probed at the lowest Bjorken x values when pairs of jets, or their hadronic surrogates, are both observed at large rapidity.

It is important to quantify whether the gluon density in the Au nucleus saturates at RHIC energies. Knowledge of the quark and gluon distributions in the gold nucleus is essential for understanding the initial state of a Au+Au collision, and how that state evolves on apparently very short time scales into a strongly interacting quark gluon plasma. We know that most of the mass of protons and neutrons arises from the very strong color fields carried by the gluons that bind the nearly massless up and down quarks. But, we

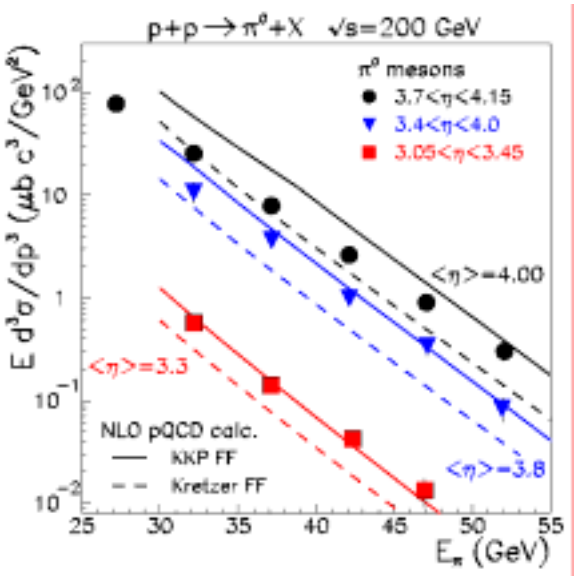

Figure 32: Inclusive π^0 cross section in p+p collisions vs. E_π, compared to NLO pQCD calculations that assume two different fragmentation functions. See [28] for details.

have essentially no knowledge about the gluon density in a heavy nucleus. It is expected that at the LHC a saturated gluon density will be manifest in p+p collisions in forward particle production and in ion collisions over the entire rapidity range, so it is timely to quantify the role of gluon saturation at RHIC prior to the start of operations of the LHC.

The low-x gluon density in the Au nucleus can be measured in d+Au collisions at RHIC through correlated particle measurements. In pQCD, *inclusive* forward particle production in high energy hadronic collisions probes the gluon density over a broad range of Bjorken x values [34]. The x value can be much better constrained through measurement of back-to-back pairs of particles. When an away-side hadron is detected in coincidence with a leading hadron or jet at forward rapidity, the pseudorapidity of the recoil jet or its hadronic surrogate reflects the x value probed. This is illustrated for p+p collisions in Fig. 33. The lowest x values are reached when both particles are detected in the forward direction [35].

The STAR Forward Meson Spectrometer (FMS) (Fig. 34) is being assembled to enable measurement of the gluon densities in the Au nucleus down to x values where saturation is expected to become apparent. It will be ready for commissioning when beam turns on for Run 7. The FMS will span the pseudorapidity interval $2.5 < \eta < 4.0$. This will give STAR nearly hermetic electromagnetic calorimetry over the range $-1 < \eta < 4$. This broad coverage will enable the mapping of the nuclear gluon density down to $x \sim 0.001$

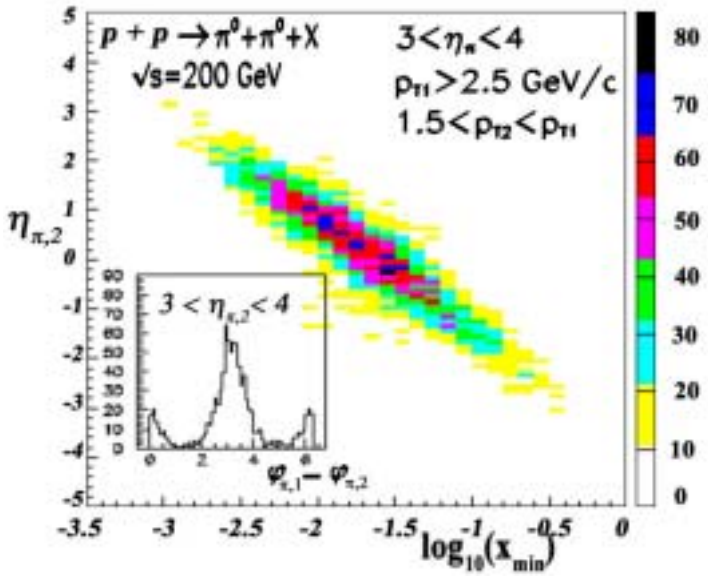

Figure 33: PYTHIA predictions for the correlation between η_2 and x_{min} for p+p $\rightarrow \pi^0 + \pi^0 + X$, where the first π^0 has $3 < \eta_1 < 4$ and $p_{T,1} > 2.5$ GeV/c, and the second π^0 obeys 1.5 GeV/c $< p_{T,2} < p_{T,1}$. The inset shows the corresponding $\Delta\varphi$ distribution.

utilizing particles with sufficiently high p_T that the corresponding p+p collisions are well described by pQCD.

The FMS will dramatically increase STAR's forward physics capabilities. The FMS will cover a solid angle nearly three times that of the FPD++, which it is replacing (and 16 times the area of the west FPD, which was replaced by the FPD++ prior to Run 6). At least as important, only a small fraction of the Pb-glass cells in the FPD++ participated in the trigger decisions. In contrast, all of the Pb-glass cells in the FMS will feed the trigger logic. This will provide nearly an order of magnitude increase in the trigger coverage. Preliminary data from Run 6, as shown in Fig. 35, provide an indication of the capabilities that can be expected from the FMS.

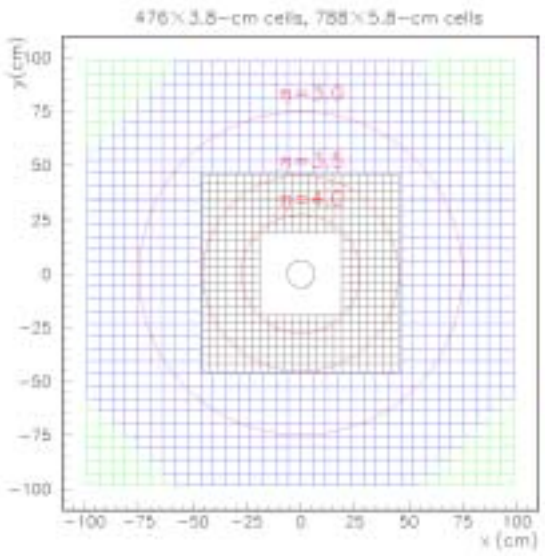

Figure 34: Front view of the STAR Forward Meson Spectrometer (FMS). The FMS will consist of 1264 Pb-glass cells and cover the pseudorapidity region $2.5 < \eta < 4$. The FMS will greatly expand STAR's acceptance for mesons decaying into photons and for meson coincidences in a kinematic region where particle production is dominated by contributions that are sensitive to low-x gluons in the Au nucleus.

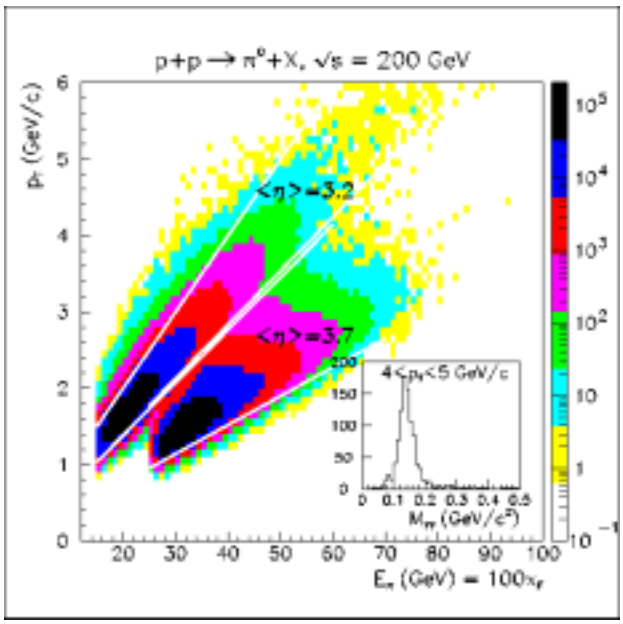

Figure 35: Kinematic coverage of the forward π^0 data from the 200 GeV p+p transverse spin period of Run 6. The η=3.7 band represents events that were detected by the east FPD. The η=3.2 band represents events that fell within the triggered fraction of the FPD++. The FMS will span this entire area, including the gap between the two regions. It will also extend the coverage to smaller η, providing even higher p_T reach at any given x_F. The inset shows the invariant mass spectrum for the 2-photon events with $4 < p_T < 5$ GeV/c, demonstrating the clean π^0 reconstruction.

4.4 d+Au beam use request for Run 7

The STAR Collaboration proposes 10+3 weeks of d+Au running at $\sqrt{s_{NN}}$ = 200 GeV to provide definitive results on the gluon saturation scale in relativistic Au nuclei, and to determine if gluon saturation accounts for the suppression of inclusive particles observed at forward pseudorapidity at RHIC. The requested data set will also provide reference data essential to the study of heavy flavor suppression in the $\sqrt{s_{NN}}$ = 200 GeV Au+Au run.

It is important for us to determine if gluon saturation is the correct explanation for the existing RHIC data. The saturation scale represents a fundamental property of hadrons and nuclei. Indeed, one saturation theory that has been quite successful, the Color Glass Condensate, predicts that there exists a universal wave function for hadronic matter at sufficiently high energy or small x. Even if gluon saturation does not prove to be the correct explanation, it is nonetheless crucial to determine the gluon density at small x in the Au nucleus if one hopes to understand the initial state in Au+Au collisions at RHIC and its rapid evolution from a highly non-equilibrated system to a thermalized one.

RHIC is uniquely situated to explore this phenomenon. We know that the gluon density ultimately must saturate, but a fundamental question is: *When does it occur?* For example, the gluon density at the saturation momentum controls such basic properties of heavy-ion collisions as the multiplicity. To observe the onset of saturation, it's essential to be able to turn it on and off. This will likely be possible at RHIC. This would also make RHIC the ideal laboratory to explore the underlying mechanism for saturation. In contrast, particle production in heavy-ion collisions at the LHC may occur deep within the saturation regime over most of the accessible kinematic region. If that proves to be the case, then (a) it will be very difficult to turn saturation effects off at the LHC, and (b) it will be essential to quantify the saturation effects independently in order to distinguish between initial-state saturation effects vs. final-state plasma effects in Pb+Pb collisions at the LHC.

STAR proposes to have a 10-week d+Au physics run at $\sqrt{s_{NN}}$ = 200 GeV during Run 7. It is ***essential that this run must follow the Au+Au run*** in order to provide the necessary time to commission the read-out electronics and trigger system for the FMS.

It is timely to have a second d+Au run during RHIC Run 7, both to quantify the role of gluon saturation at RHIC energies and to explore the relative contributions of charm vs. bottom to non-photonic electron spectra. The *RHIC Collider Projections (FY2007-2008)* document indicates that we can expect RHIC to deliver ~120 nb^{-1} of d+Au collisions at $\sqrt{s_{NN}}$ = 200 GeV during a 10-week physics run. (This is the average of the projected minimum and maximum performance estimates.) STAR proposes to utilize the d+Au collisions as follows:

- Fast-detector data (e.g., FMS, BEMC, EEMC, BBC, etc.) will be recorded with essentially 100% livetime for events that include an intermediate- or high-p_T π^0 in the FMS. Previous analyses of FPD and FPD++ data indicate that a very high fraction of these events will be usable.

- Slow-detector data (e.g., events that include read-out of the TPC, SVT, SSD, FTPC, etc.) will be recorded at 50 Hz, leading to 50% livetime. The approximate division of this bandwidth will be:
  - Minbias: 30 Hz
  - BEMC and EEMC high-tower triggers: 10 Hz
  - FMS triggers: 10 Hz

Detailed simulations, such as those in Fig. 36, have established that the fast-detector events will permit STAR to map out the gluon density in the gold nucleus over the range $0.001 \leq x \leq 0.1$. If we assume $R_{dAu} \sim 0.5$ for the trigger π^0 in Fig. 36 obtained by extrapolating the results in Fig. 29 to the trigger kinematics, and also assume that $2 \rightarrow 2$ partonic scattering dominates particle production as would be expected in pQCD, the requested luminosity would yield approximately 10,000 ± 170 events in the coincidence peak. The region $1 < \eta_{\pi,2} < 4$ in Fig. 36 corresponds approximately to the region $0.001 \lesssim x \lesssim 0.01$ where we might hope to find evidence for gluon saturation. This sample will be sufficient to allow examination of the x dependence of the gluon density in 3~4 centrality bins, even if the recorded statistics end up much reduced because gluon saturation effects are found. It will also facilitate important cross-checks of the conclusions. For example, the kinematic coverage will be sufficiently broad so that the same x_g will be sampled with trigger π^0 over a range of x_F values. The latter closely approximate the x of the scattered quark from the deuteron beam, so this study will provide an independent means to distinguish between gluon saturation and incident quark energy loss. Data will be taken concurrently in the region $-1 < \eta_{\pi,2} < 1$, corresponding to $0.01 \lesssim x \lesssim 0.1$. These data will be compared to existing nuclear deep-inelastic lepton scattering measurements to provide an important universality check.

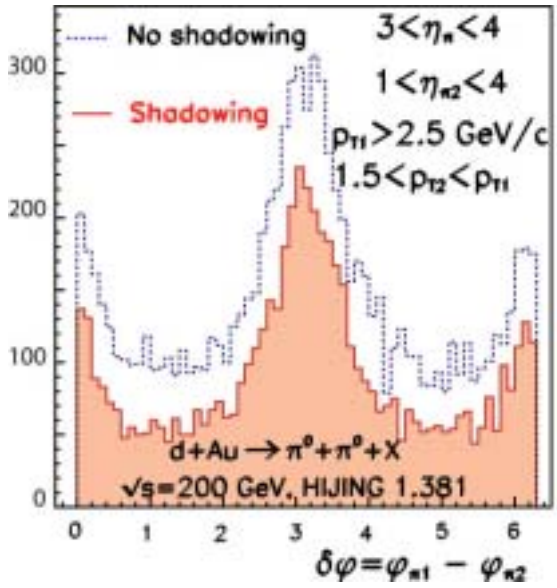

Figure 36: HIJING predictions for the Δφ distribution in d+Au collisions, with and without shadowing. HIJING includes leading-twist shadowing, which leads to a reduction in the coincident peak yield, without a significant change in its structure.

As noted above, the ability to compare results from d+Au collisions to reference results from p+p collisions is very important. The initial analyses of the Run 7 d+Au data will use p+p data that were taken during Run 6 to provide a baseline. Ultimately, to exploit the Run 7 d+Au results fully, p+p data will be required over a broader kinematic range than are available from Run 6. The additional reference data will be taken during the proposed long p+p run in Run 8.

The proposed 30 Hz of slow-detector minbias data will provide 60M events. These will be used to obtain a D spectrum from d+Au collisions for comparison to the D spectrum that will be obtained during the Au+Au run. The high-tower triggered data will provide a dramatic improvement in the STAR measurements of non-photonic electrons in d+Au, as discussed above. Notably, when combined with the vertexing capability of the SVT+SSD, these events will constrain the relative contributions of D vs. B mesons to the non-photonic electron spectrum in "elementary" collisions. Finally, the 10 Hz of slow-detector data triggered with the FMS will provide measurements of correlations between triggered π^0 and coincident charged particles to complement the π^0 - π^0 correlations that will be obtained from the fast-detector data and will facilitate important studies of the near-side jet structure, utilizing the pseudorapidity coverage of the FTPC. They will also open the possibility to measure forward J/ψ by combining the complementary features of the FMS and FTPC.

4.5 Modifications to the STAR Detector configuration for Run 7

A continuing problem in recent runs has been the reliability of readout boxes for the STAR Silicon Vertex Tracker. Typically several readout boxes fail during the period of a run. The channels served by those readout boxes are then dead for the remainder of the run since the boxes are physically located inside the poletips of the STAR magnet and can not be accessed. Attempts to characterize the failure mode on the bench have led to the conclusion that the problem probably lies within the Field Programmable Gate Array (FPGA) used in the design, although it has not been possible to develop a robust solution since the failure mode can not be reliably reproduced.

As a consequence, due to the focus in Run 7 on optimization of the performance of the of the SVT+SSD to improve the significance of STAR's measurement of D meson yields and spectra, the readout boxes for the SVT will be relocated outside the poletips of the STAR magnet. They will be mounted on the exterior of the poletip at the 3 o'clock (9'oclock) location looking east (west). This is a major undertaking requiring re-routing of existing cables that presently go from the readout boxes to the support platform, as well as the fabrication of new cables to take the signals from the detector to the readout boxes at their new location. This work is being performed by the STAR Operations Group in collaboration with Wayne State University and Yale University. It is expected to be complete in time for the start of Run 7.

Another important upgrade will be the implementation of an upgraded Vertex Position Detector (VPD) to improve event selection at trigger Level 0, so that less events are rejected in offline analysis. The potential gain from this upgrade is as large as 20-30% in the numbers of events which pass the vertex selection cut in offline analysis.

The plan to upgrade the STAR VPD for Run7 is to use either the anode outputs from the existing TOF pVPD or to install a new array of PMTs surrounding the beampipe approximately at the longitudinal location of the Forward Pion Detector. The upgraded VPD will use existing electronics and detector components. For electronics, the plan is to use 16 channels per side (East or West), using existing TAC boards to feed CDBs which subsequently output into DSMs (data storage and manipulation boards). Tests performed indicate the CDB-TAC-CDB-DSM chain is stable to better than 65ps, indicating that the PMT signals may ultimately be the limiting resolution, although they may be better than 65ps as well. The electronics will reside in the existing Multi Wire Chamber VME crate where space and cabling into the last DSM module already exists. Trigger-level code will be developed to find the earliest particle hit on each side of the interaction vertex in real time. This is straightforward to implement, but requires care to insure the leading edge response of the detectors has been optimized. Periodically, throughout the run, recalibration will be performed to insure against deterioration of the response.

The final major modification to the detector for Run 7 will be the construction of the Forward Meson Spectrometer.

The STAR Forward Meson Spectrometer will consist of lead glass detectors in a hermetic stack positioned 750 cm from the interaction point (Fig. 34). The inner calorimeter is built from 476 detectors obtained from IHEP, Protvino. Each lead-glass bar of the inner calorimeter has dimensions of 3.8cm × 3.8cm × 45 cm corresponding to 18 radiation lengths. These detectors are stacked into a 24 × 24 matrix having a central 10 × 10 element hole for the beams. The outer calorimeter is built from 788 detectors built from Schott F2 glass obtained from FermiLab. Each lead-glass bar of the outer calorimeter has dimensions of 5.8cm × 5.8cm × 60 cm and also corresponds to 18 radiation lengths. They are stacked into a 34 × 34 matrix with a central 16 × 16 element hole into which the inner calorimeter fits. The FMS is positioned west of STAR on a platform extension of the tunnel entrance into the Wide Angle Hall. Its distance from the interaction point is limited by the DX magnet to the west of STAR. The FMS views reaction products from the colliding beams through the hole in the STAR magnet poletip and will face the oncoming deuteron beam in d+Au collisions. The FMS will span the full azimuth for $2.5 < \eta < 4.0$. The addition of the FMS will provide STAR with nearly contiguous electromagnetic calorimetry, including the barrel and endcap EMC, spanning the full azimuth for the rapidity range $-1 < \eta < +4$.

The 1264 detectors of the FMS will be housed in enclosure halves mounted on the north and south sides of the vacuum pipe. A rail system on the tunnel extension platform allows the enclosure halves to be moved away from the beam pipe for servicing the vacuum system at the STAR interaction point.

Smaller matrices of the 3.8cm × 3.8cm cross section IHEP, Protvino detectors have been operated since RHIC Run 2 in the modular STAR Forward Pion Detector. Cerenkov photons from showers in the lead glass are detected by FEU-84 photomultiplier tubes powered by resistive voltage dividers. Given the distance from the interaction point, single photons can be resolved from pairs of photons produced in the decay of neutral pions for energies up to 60 GeV.

An engineering test of the FMS was conducted during RHIC Run 6. Symmetric modular calorimeters were positioned left and right of the beams on the FMS platform. Each module was 14 × 14 matrix of the 5.8cm × 5.8cm cross section Schott F2 glass with a central 4 × 4 element hole filled by a 6 × 6 matrix of IHEP lead-glass detectors. Each Schott F2 glass was viewed by an XP2202 photomultiplier tube powered by a resistive voltage divider employing Zener diodes to provide the voltage drops across the last four dynodes. Stability was continuously monitored during the run by light pulses delivered to individual detectors by fiber optics from blue light-emitting diodes. Performance during polarized proton collisions at interaction rates approaching 1 MHz matched tests done prior to assembly of the calorimeters thereby providing confidence that these detectors will result in robust operation of the FMS.

To limit the dissipated power, the FEU-84 that will be used in the FMS will be powered by a Cockcroft-Walton (CW) base under development at Penn State University. Extensive tests performed indicate the stability and linearity of their CW design exceeds that of the resistive dividers that have been previously used.

Readout of the FMS detectors will be performed using 12-bit analog-to-digitial converters (ADC) that are under development at the University of California, Berkeley / Space Sciences Institute. A 32-channel 9U VME prototype board has been produced and is undergoing final tests. The ADC are clocked at 9.38 MHz and present their data to on-board field-programmable gate arrays for readout and bit manipulations as an interface to the STAR trigger system. Each board presents 32 bits of information every 107 ns to a tree of data storage and manipulation (DSM) boards for triggering on either large energy deposition in single detectors (high towers) or on large energy sums observed in the FMS.

The construction of the FMS is expected to be complete in time for it to be operational in Run 7.

5.0 Beam use proposal for Run 8

5.1 Mapping the spin dependent parton distributions of the proton

The STAR Collaboration proposes a polarized p+p run of (20+3) weeks. The major goal of this run is to map out the spin-dependent gluon distribution of the proton using longitudinal polarization. Additionally, two weeks of dedicated $\sqrt{s}$ = 500 GeV

commissioning and 1 week of dedicated running for forward tagged proton studies are also requested.

The goals of the STAR spin program in Run 8 and Run 9 have been discussed in detail in Section 3. An optimal pp run plan for the STAR spin physics program would divide of order 30 weeks of collision time between these runs. The time would be devoted primarily to longitudinal spin running at $\sqrt{s} = 200$ GeV. These runs would allow a significant map of the x-dependence of the gluon polarization, within the approximate range $0.03 < x < 0.3$. Smaller values of x would be subsequently probed in 500 GeV running. During 2007 STAR supports continued pp collision beam development time, as can be accommodated in a run with both Au+Au and d+Au running. In particular, we strongly support continued polarization development of proton beams in the AGS, in parallel with RHIC stores.

A critical aspect of the preparation for Run 8 will be learning from the analysis of Run 6. Technical issues that can be quantitatively assessed for realistic detector performance in the analysis of 2006 data and related simulations include: (1) What levels of γ retention and π^0 rejection can be attained to optimize signal/background for photon-jet coincidences? (2) How low in p_T can direct photons be identified in the presence of a growing π^0 background? (3) Does low-mass background seen to date in π^0 reconstructions in STAR constitute an additional background for direct photon analyses? (4) Is an L2 coincidence trigger for γ-jet desirable, or will it enhance background more than signal? (5) How efficiently, and with what bias in extracted four-momenta, can jets be reconstructed beyond the barrel EMC region, despite the services gap (η=0.98 – 1.08) and rapidly decreasing TPC tracking performance? (6) What trigger biases on contributing partonic processes and x-ranges are imposed by the 2006 di-jet trigger?

One year from now, STAR will be better able to demonstrate the sensitivity to $\Delta G(x)$ attainable in given length runs at 200 GeV with an optimized trigger mix. As of now, we anticipate needing at least an additional 30 weeks of pp collision time at 200 GeV. If divided roughly between 2008 and 2009, this would use the same time envisioned in the 2005 RHIC Spin Planning Document, but there spread over three years (2007-9). Three runs would provide an extra opportunity for the remaining beam development needed to attain the enhanced design goals for luminosity and polarization. But longer runs (15 vs. 10 weeks) deliver integrated luminosity more efficiently, since C-AD guidelines call for 8-week buildups to maximum luminosity for any given run. Thus, the integrated luminosity anticipated in two 15-week runs (2008+9) is very nearly the same as for three 10-week runs (2007+8+9). STAR also strongly prefers devoting most of the 2008-9 pp collision time to 200 GeV, for two reasons: (1) attaining adequate coincidence statistics for a given x-range ($\approx$ 0.04-0.08) at both 200 and 500 GeV will provide a powerful crosscheck on the pQCD analysis of RHIC spin data and will constrain the evolution of the gluon helicity distribution; (2) a forward tracking upgrade needed to optimize STAR's performance for 500 GeV W production physics will not yet be installed in 2009.

The proposed polarized proton run will also provide reference data crucial as a control measurement for the gluon saturation studies carried out in Run 7 with the Forward Meson Spectrometer.

In addition to the beam time devoted to studies of the helicity preference of gluons in the proton, STAR proposes a dedicated run of one week to carry out the program of forward tagged proton physics studies discussed in the following section and 2 weeks to be devoted to $\sqrt{s}$ = 500 GeV $p_{\rightarrow} + p_{\rightarrow}$ machine development.

5.2 Forward Tagged Proton Studies in STAR

Polarized proton-proton elastic scattering ($p^{\uparrow}p^{\uparrow} \rightarrow pp$)

As part of its scientific program, the STAR Collaboration proposed to investigate the non-perturbative regime of QCD using polarized proton beams at RHIC, the STAR detector and the Roman Pots of the pp2pp experiment [36,47,38]. The pp2pp Roman Pot detectors will be used to tag very forward protons, thus selecting processes in which the proton stays intact, and the exchange has quantum numbers of the vacuum,—so called Pomeron (IP) exchange. For these events, the probability of measuring reactions where colorless gluonic matter dominates the exchange is enhanced. The use of polarized proton beams, unique at RHIC, will allow exploring unknown spin dependence of diffraction including both elastic, Fig. 37, and inelastic processes, Fig. 38. As the entire energy range of this proposal has been inaccessible to proton-proton (elastic) scattering in the past, new results of high quality will be produced. A more detailed description of the physics can be found in [39, 40, 41].

5.2.1 Spin averaged observables

The measurement of the differential pp cross section $d\sigma/dt$ over the extended t-range will include the region at the lower |t| that is particularly sensitive to the ρ-parameter. Hence we will measure: 1) the ρ-parameter; 2) the nuclear slope parameter b in a combined fit to the differential cross section, and 3) the total cross section $\sigma_{\mathbf{tot}}$.

An asymptotic difference between the differential and total cross sections for pp and $p\bar{p}$ could be explained by a contribution of the Odderon to the scattering amplitude. The absence of an Odderon contribution would lead to identical cross sections, approaching each other roughly as $s^{1/2}$. Also, our measurement of the total cross section, $\sigma_{\mathbf{tot}}$ **,** at the highest possible energy will probe the prevalent assumption that the cross sections for pp and $p\bar{p}$ scattering are asymptotically identical.

With the expected $20 \cdot 10^6$ elastic events an estimated error on the slope parameter is $\Delta b = 0.31$ $(GeV/c)^{-2}$ and on the ratio of the real to imaginary part $\Delta\rho = 0.01$, which is

comparable to the existing measurements from the pp and p $\bar{p}$ data. The $\Delta\sigma_{tot}$ = 2-3 mb, where the largest contribution is from the error on the luminosity measurement.

5.2.2 Spin dependent observables

By measuring spin related asymmetries one will be able to determine elastic scattering at the amplitude level [42,43,44]. The availability of longitudinal polarization at STAR will allow measuring A_{LL} in addition to A_{NN}, A_{SS}, and A_N resulting in a significant improvement of the scientific reach of these measurements. Full azimuthal coverage of the elastic events that we are planning to have will assure high efficiency and small errors in the measurements.

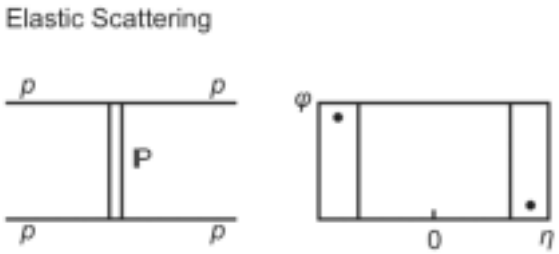

Fig. 37. Diagram of the elastic scattering process in the t-channel.

One of the physics motivations to measure A_N is the possibility of the rise with energy of the spin-flip to spin-nonflip amplitudes ratio. In other words it may occur that a small contribution from hadronic spin-flip to the spin single-spin asymmetry, measured with a polarized jet target at 100 GeV/c, could increase at $\sqrt{s}$=200 GeV. This will help to address the long standing problem of the energy dependence of the spin flip amplitude, which is best answered experimentally.

Reaching such a small |t|-value allows measuring the single spin analyzing power A_N close to its maximum at |t| =0.0024 $(GeV/c)^2$, where A_{max} = 0.04, at $\sqrt{s}$ = 200 GeV. The A_N and its t-dependence in the covered range are sensitive to a possible contribution of the single spin-flip amplitude, ϕ_5, from the interference between the hadronic spin-flip amplitude with the electromagnetic non-flip amplitude.

An additional contribution of the hypothetical Odderon to the pp scattering amplitude can be probed by measuring the double spin-flip asymmetry, A_{NN} [45]. Their calculation shows that A_{NN} is sensitive to contributions of the real and imaginary parts to the double spin-flip amplitude, ϕ_2, in the range $0.003 < |t| < 0.010$ $(GeV/c)^2$. At a higher value of |t| the difference between a pure Pomeron contribution and an equal mixture of Pomeron and Odderon at the five percent level are hard to distinguish, while a pure Odderon contribution would lead to a very small double spin-flip asymmetry.

The useful interval with 100% acceptance for elastic scattering is $0.003 < |t| < 0.024$. Given polarization of 60%, and 2.3mb cross section within our acceptance, we shall get

$20 \cdot 10^6$ events. For four t subintervals we shall have $5 \cdot 10^6$ events in each. The corresponding errors are $\delta An=0.0017$, $\delta A_{NN}=\delta A_{SS}=0.003$.

5.3 Diffractive processes pp → p + X + p

In the double Pomeron exchange process each proton "emits" a Pomeron and the two Pomerons interact producing a massive system M_X. The massive system could form resonances or consist of jet pairs. Because of the constraints provided by the double Pomeron interaction, states coupling preferentially to gluons will be produced with much reduced backgrounds compared to standard hadronic production processes.

The gluonic processes (IP exchanges) begin to dominate when the rapidity gap between the forward protons and the system produced at center rapidity is $\Delta y > 3$. This is achieved at RHIC with masses M_X up to 10 GeV. The STAR detector at RHIC equipped with Roman Pots is ideally suited for studying of the processes where the M_X decays in all charged particles. In addition one can study at RHIC processes with leading high p_T particles in the center rapidity, which are equivalent to jet studies.

5.3.1 Central production through double Pomeron exchange (DPE) process.

The above processes are commonly characterized by using variables t, ξ and M_X, where t is four-momentum transfer between the incoming and outgoing protons, $\xi = \Delta p/p$ is the momentum fraction carried off by the Pomeron and M_X is invariant mass of the system produced. In case of double Pomeron exchange, separate t and ξ variables exist for each proton-Pomeron vertex.

Tagging and measuring forward protons is important since it removes the ambiguity of a (complementary) rapidity gap tag, which has a background due to the low multiplicity of diffractive events, and allows the full characterization of the event in terms of t, ξ and M_X.

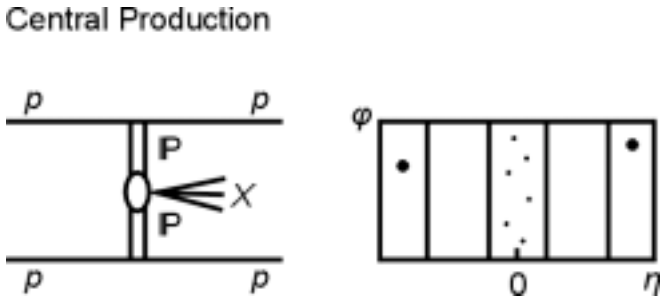

Fig. 38. Diagram of the Central Production (DPE) process in the t-channel

5.3.2 Hard and Soft Diffraction

The strength of the STAR detector: excellent charged particle identification in the central rapidity region and p_T resolution, coupled with ability to tag diffractive events with the forward protons with Roman pots, will allow measurements of single particle spectra as a function of t and ξ of the outgoing proton. STAR has established that using the leading particle, with highest p_T, one can characterize jet like phenomena in hadron-hadron collisions.

5.3.3 Central production of glueballs

The idea that the production of glueballs is enhanced in the central region in the process $pp \rightarrow pM_Xp$ was first proposed by [46] and was demonstrated experimentally [47]. The crucial argument here is that the pattern of resonances produced in the central region, where both forward protons are tagged, depends on the vector difference of the transverse momentum of the final state protons $\bar{k}_{T1}$, $\bar{k}_{T2}$, with $d\bar{P}_T \equiv |\bar{k}_{T1} - \bar{k}_{T2}|$. The so-called dP_T filter argument is that when dP_T is large ($\geq \Lambda_{QCD}$) $\bar{q}q$ states are prominent and when dP_T is small the surviving resonances include glueball candidates [45,46].

STAR has studied the geometrical acceptance of the proposed setup for both SDD and DPE processes, generating protons with t and ξ uniformly distributed in the regions $0.003 < |t| < 0.04$ and $0.005 < \xi < 0.05$ respectively. We assumed that the Roman Pots (RPs) are at least 12σ of the beam size at the detection point. The plot in Fig. 39 shows acceptance as function of M_X, the red dots indicating the location of the Roman Pots.

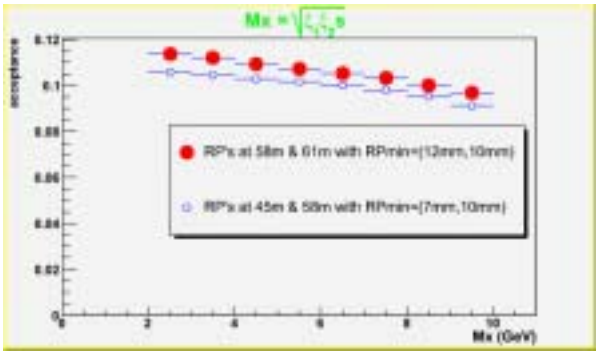

Fig. 39 Mass geometrical acceptance for DPE processes, red dots.

We conclude that there is good acceptance to measure inelastic diffraction DPE with β^*=20m. So while taking elastic data, a fraction of the trigger band-width could be dedicated to include events with two or one proton in the forward direction.

In what we are proposing large data samples of diffractive states can be obtained and analyzed as a function of diffractive mass and t ($d^2\sigma/dM_X^2dt$) for central production. As noted above, when dP_T between two out going protons is small the fraction of glueball candidates is enhanced and when the dP_T is big the qqbar states are enhanced. In

quantifying the limit WA102 experiment [47] found "small" $dP_T < 0.2$ GeV and "big" $dP_T > 0.5$ GeV.

With the expected luminosity one can collect about 450,000 triggered DPE events during the three days of running, with 40 hrs of useful beam time. One assumes a 10μbarn cross section within our acceptance for the DPE process, where it is required that two RPs on each side are used allowing reconstruction of the outgoing proton momentum. The number of events for which only one proton tag is used is factor of 4-5 higher.

The search for glueballs remains an experimental question and the proposed research will add significantly to the world body of knowledge concerning their possible existence.

5.4 Forward tagged proton implementation plan

The pp2pp Roman pots mounted on the outgoing beams, down stream from the STAR detector shall be used, Fig. 40. To achieve full azimuthal coverage for elastic events, at each location one Roman Pot station is horizontal and one vertical. RHIC accelerator magnets are used for momentum analysis resulting in forward proton taggers installed in the warm straight section between Q3 and Q4 magnets. The pp2pp Roman Pots are a moveable detector system allowing approach to the beam as closely as possible, thus extending the t and ξ ranges to the lowest values.

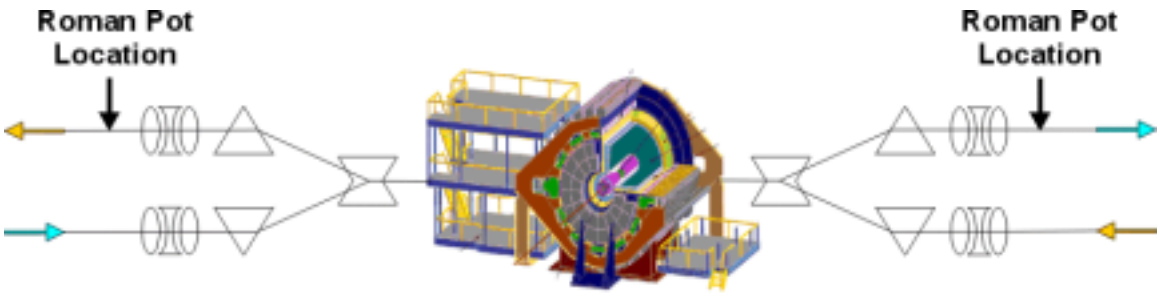

Fig. 40. The Roman pots of the pp2pp experiment in the STAR interaction region, with the arrows indicating proposed location. At each location one Roman Pot station is horizontal and one vertical.

5.5 Forward tagged proton beam use request

To maximize physics output, several days of efficient data taking are needed. The main reason is that in order to reach the t and ξ values needed for both diffractive and elastic data, beam scraping and special optics are needed. Hence, taking into account machine and detector uptime we are requesting ~ 1 week of dedicated running with longitudinal polarization in Run 8 and Run 9.

Using the capacity of existing power supplies optics of $\beta^* = 20$ m at $\sqrt{s} = 200$ GeV can be produced allowing the t coverage with 100% acceptance for elastic scattering for $0.003 < |t| < 0.024$. The setup time of the $\beta^*=20$ m optics is estimated by the C-AD to be 12 - 24 hours, leaving the remaining time for dedicated data taking.

5.6 Integration of pp2pp DAQ and trigger with STAR

The essential parts of the pp2pp DAQ system, both hardware and software, will remain unchanged and can be easily integrated into the STAR-DAQ framework. The current pp2pp DAQ was written as a detector extension to STAR. The pp2pp core DAQ system, Run Control, Data Monitoring & Online Q&A histograms are all exactly the same as in STAR-DAQ and as such can be easily integrated into STAR DAQ.

The STAR-pp2pp DAQ also retains the possibility of running pp2pp in a contained standalone fashion, which would allow pp2pp to test and debug its equipment without interference with STAR. It would also allow pp2pp to take data decoupled from STAR in the same manner as it did while it was at IP2, if the need arises.

The current pp2pp trigger is based on coincidences of a small number of (16) signals from scintillators, which can be adapted to the STAR CDB/DSM trigger scheme with only one pair of CDB/DSM STAR Trigger boards. Such a system is conceptually equivalent to many of STAR Trigger detectors (i.e. CTB, ZDC) and should not be a problem.

Once this has been done an opportunity naturally presents itself to run pp2pp's Roman Pots together with STAR central rapidity (or any other) detectors to enhance the inelastic physics program. At the same time the elastic physics can be run in parallel with only the Roman Pots being read out at a higher rate, in the so called "fast detectors only" mode.

In summary the physics program with tagged forward protons at STAR will:

1. Study elastic scattering and its spin dependence in unexplored t and $\sqrt{s}$ range;
2. Study the structure of color singlet exchange in the non-perturbative regime of QCD;
3. Search for diffractive production of light and massive systems in double Pomeron exchange process;
4. Search for new physics, including glueballs and Odderon.

The proposed studies will add to the world body of knowledge concerning QCD in the non-perturbative regime where calculations are not easy and one has to be guided by measurements. In this way the proposed program extends the physics reach of both STAR and RHIC.

6.0 Beam use proposal for Run 9

The STAR Collaboration proposes a low $\sqrt{s_{NN}}$ Au+Au run of (12+2) weeks duration to make a definitive search for the existence and location of the QCD critical point. This request incorporates a performance based goal, such that if the QCD critical point search is completed early enough, 2-3 weeks of data taking would be devoted to $\sqrt{s_{NN}}$ = 200 GeV Au+Au collisions to begin to take advantage of the upgraded PID capability provided by the TOF barrel to measure yields and spectra of charm, strange and non-strange mesons, baryons, and resonances. It is anticipated the completion of the DAQ1000 upgrade for this run will allow min-bias data to be taken 5-10 times faster than in previous runs.

The STAR Collaboration further proposes a $\sqrt{s}$ = 200 GeV polarized p+p run of (10+2) weeks duration to complete the measurement of $\Delta G(x)$ at this energy.

The near-term upgrades planned by STAR are a Forward Meson Spectrometer, a barrel TOF detector, DAQ1000 upgrade, and a micro-vertex detector. For Run 9 STAR expects to have completed the FMS (Run 7), the DAQ1000 upgrade, and the TOF barrel detector. An engineering prototype of the STAR Heavy Flavor Tracker is also expected to be operational. These upgrades will improve the performance of the STAR detector significantly by Run 9 (in some cases by an order of magnitude).

The hadron identification capabilities of the TOF over a large fraction of the full 2π STAR acceptance, combined with the newly implemented DAQ1000 ability to gather data an order of magnitude faster will allow the intermediate p_T region to be probed with unprecedented precision and detail. Correlation measures revealing complex structures in this p_T regime are already hinting at details of the dynamic evolution of the produced matter. These structures likely result from an interplay between the flowing medium, jet remnants, and the coalescence of constituent quarks into final-state hadrons. Hadron identification over a substantial portion of the high statistics correlation space possible with these upgrades will afford information key to disentangling the role of these effects.

Short wavelength (rare) probes such as measurement of the upsilon family of states, high pt direct photons, and direct photon + jet coincidences will benefit significantly from the DAQ1000 upgrade which, by increasing the available DAQ throughput by an order of magnitude, will afford essentially zero dead-time data acquisition for such probes. This means STAR will be able to sample the full RHIC luminosity resulting in an increase in throughput for triggered rare probes of a minimum of a factor two compared to present operation.

Based on simulations and demonstrated performance of the multi-gap resistive plate chambers that will used for the TOF barrel detector, there will be a significant reduction e.g. in the number of events required to obtain a statistically robust dataset for various charm particles and resonances. The combination of TOF information with specific ionization (dE/dx) information in the TPC will provide the ability to cleanly identify

electrons out to ~ 3 GeV/c. This capability, combined with the large acceptance of STAR, will allow detection of the leptonic decays of vector mesons to search for evidence of chiral symmetry restoration. This capability will also dramatically improve STAR's ability to measure non-photonic electrons from charm semi-leptonic decays, a key measurement for testing the coupling of charm quarks to the produced matter, and by extension, whether the matter is partonic.

6.1 The search for the QCD critical point

There is a growing body of theoretical and experimental evidence that the critical point on the QCD phase diagram (Fig 41), if it exists, should appear on the QGP transition boundary at baryo-chemical potential ~100 - 500 MeV, corresponding to heavy ion collisions with c.m. energy in the range 5 - 50 GeV/u.

Available results from LQCD [48] suggest that at non-vanishing chemical potential, as the temperature of dense hadronic matter increases it should undergo a rapid transition from a hadron resonance gas to a quark-gluon plasma signaled by a sudden change in the equation of state. As the baryon chemical potential is increased, the fluctuations on the cross-over line increase dramatically suggesting the existence of a critical point in the phase diagram. As Fig 42 shows, despite intense theoretical interest and effort using different LQCD approaches [49, 50, 51] which agree on the possible existence of a critical point, as yet there is no convergence on its possible location.

Verifying the existence of and locating this point with experimental measurements would be a major step forward in the world-wide effort to determine the properties of QCD at high temperature and density. Specifically, the discovery of the critical point would constitute the identification of a crucial landmark in the QCD phase diagram, key to understanding the phases of QCD and their quasi-particles.

In the vicinity of the critical point, critical fluctuations in parameters such as the baryon number density, quark number and charge occur. These should be reflected in the laboratory in observables such as hadronic yields and particle ratios (T, μ_B), the collapse of proton elliptic flow, fluctuations in v_2, K/π, p/π, $\langle p_T \rangle$ fluctuations and the scale dependence of the fluctuations which may reveal the source of the signal. The STAR detector, as a consequence of its large, uniform acceptance, and excellent PID capability with the inclusion of the TOF barrel upgrade has superb capability for carrying out the search for such effects and for providing definitive results on the existence and location of the QCD critical point.

Simulations have shown that the change in the kinematic distribution of secondaries for low $\sqrt{s_{NN}}$ Au+Au running would not require specialized trigger counters. As shown in Table 5 for example, the simulations indicate that STAR's existing beam-beam counters will be adequate for triggering, and that centrality can be determined from a reference multiplicity.

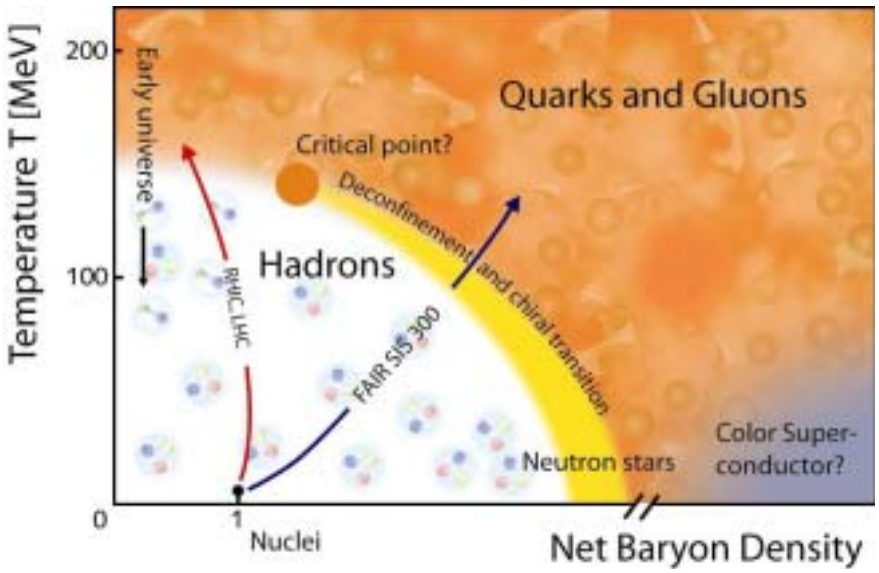

Figure 41. One of the major predictions of QCD in extreme conditions of high temperature or large baryon number density is the existence of a critical point at a particular temperature and density where a sharp distinction between the QGP phase and the hadronic phase first appears [52,53]. The QCD phase diagram, characterized by the temperature (T) and the baryon chemical potential μ_B, signifies the separation of QGP to hadronic phase. For physical values of quark masses the first order phase transition line rises from the μ_B axis and terminates at the critical end point T_C, beyond which there is a rapid cross over in quantities such as the quark condensate [49,50, 54,55]. Note that "focusing" in the μ, T plane by the hydrodynamic evolution of the system may cross many initial conditions to pass through the critical point region, broadening the signal region, and reducing the likelihood of sharp discontinuities.

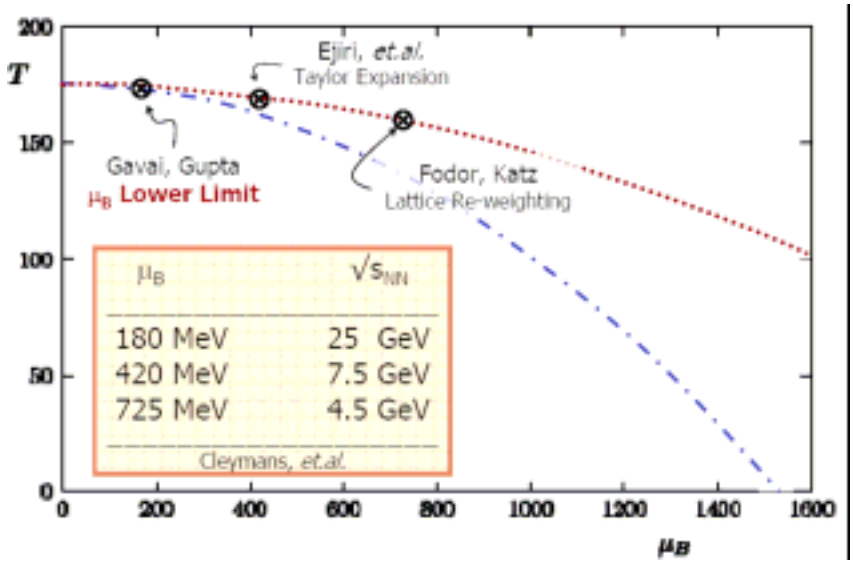

Figure 42. Comparison of three recent LQCD predictions on the possible location of the QCD critical point.

impact parameter	AuAu @ 5 GeV		AuAu @ 8.75 GeV	
	BBC Inner	BBC Outer	BBC Inner	BBC Outer
b<0	5	27	12	54
3<b<6	11	30	21	57
6<b<9	22	35	39	40

Table 5. Particle hit multiplicities in the STAR Beam-Beam counters for low $\sqrt{s_{NN}}$ Au+Au running

These simulations also demonstrate that the large 2π acceptance of STAR brings clear gains to this study as shown in the comparison of event plane resolution possible with STAR and NA49 (Fig. 43)

The desirability of full azimuthal acceptance is shown in Fig 44 where the apparent increase in the fluctuation measure $< \Delta p_{Ti} \Delta p_{Tj} >$ from failing to identify the underlying effects of a large scale correlation (in this case random orientation of the event plane for elliptic flow) is clearly evident. The conclusion is that a large 2π acceptance is essential for fluctuation measurements such as $<p_T>$ fluctuations. The utility of such measures has already been demonstrated at high energy where the variance excess for $<p_T>$ fluctuations has been inverted into p_T angular correlations which are then used to

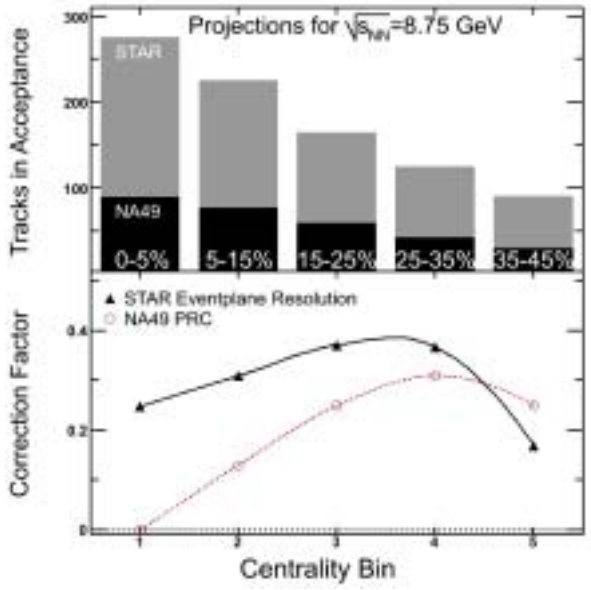

Figure 43. Simulation of the event plane resolution in STAR vs NA49 for comparable centrality bins ($\sqrt{s_{NN}}$ = 8.75 GeV Au+Au (Pb+Pb)). From [56]

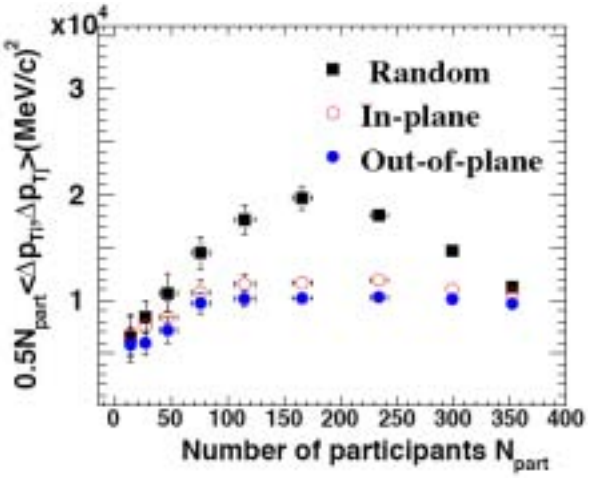

Figure 44. Contribution of elliptic flow to the apparent magnitude of $<\Delta p_{Ti}\Delta p_{Tj}>$ fluctuations for particles within 45 degrees of the event plane (red), 45 degrees of the out-of-plane direction (blue), and for a detector with partial angular coverage when the event plane is unknown (black). In the later case the fluctuations are overestimated because the event plane is fluctuating randomly in, out, and within the acceptance. From [56]

characterize elliptic flow and the near and away side medium response (Fig 45). These have proved an important tool for attempting to understand the role of elliptic flow, mini-jets, and medium response in producing the <pT> fluctuations forming an important baseline for the QCD critical point at lower energy as well.

As shown in Fig 46, it is also essential to have comprehensive particle identification capability within this acceptance to minimize the systematic error in searching for critical

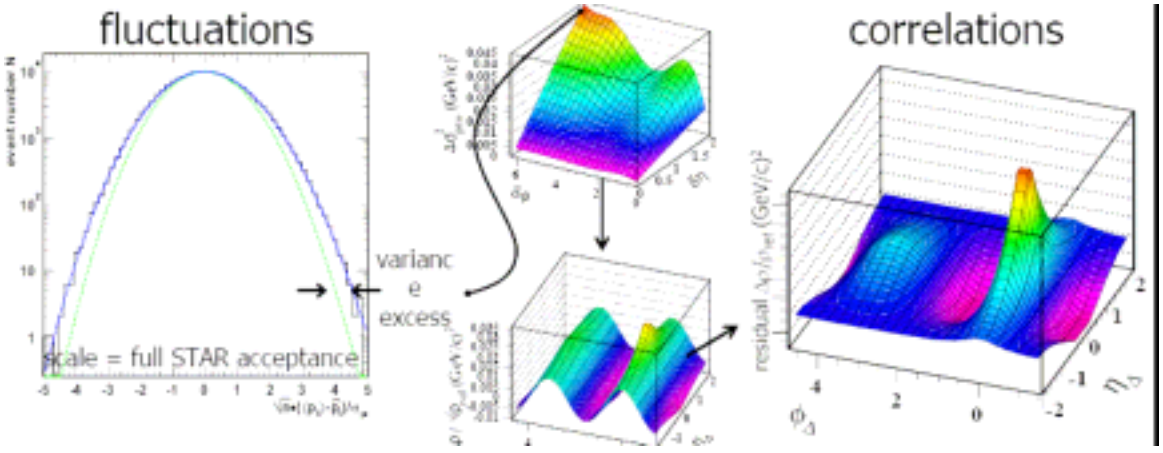

Figure 45. The variance excess from mean Pt fluctuations can be inverted to study the role of elliptic flow, mini-jets, and medium response to the correlations observed in Au+Au collisions.

fluctuations which might indicate the approach to the critical point. Systematic errors dominate the ultimate precision that is possible. As seen in the figure, based on simulation of 100,000 events at 40A GeV, the increase in statistical error without the full acceptance STAR TOF is from 5% to 11% (relative). However, a misidentification of only 1% leading to a swapping of pions for kaons reduces the width of the observed k/pi fluctuation distribution by 10%. A misidentification of 2% leads to a reduction in width of 20%. The conclusion is that it is essential to have the full acceptance TOF barrel in operation to perform a comprehensive search.

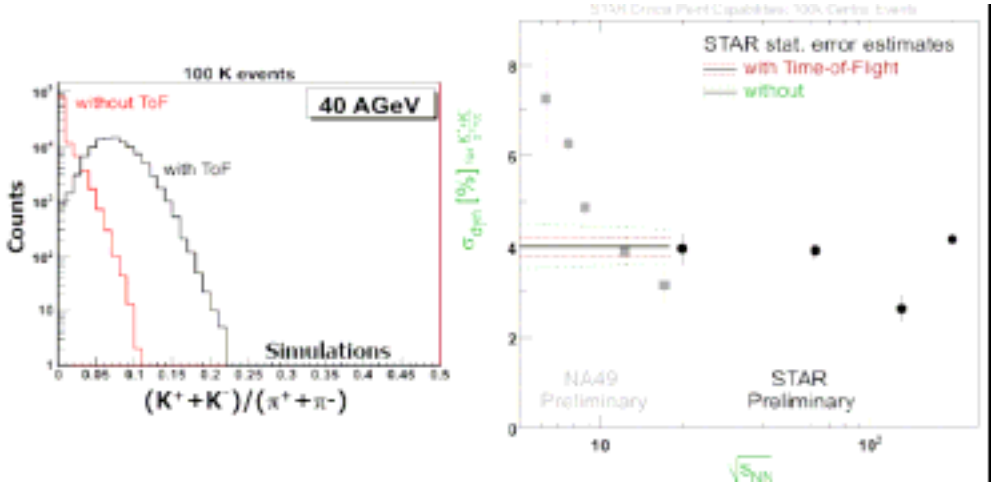

Figure 46. Study, based on 100,000 simulated events of the statistical and systematic uncertainties with and without the PID capability of the STAR TOF. From [56]

The conclusion from simulations such as that in order to optimize a comprehensive for the QCD critical point a large 2π acceptance with excellent PID capability is essential.

E c.m.	μ_B	BBC Coin Rate	#of days/1M (1day=10 hr)	#of events needed	#of days of beam
4.6	570	3	9	5M	45
6.3	470	7	4	5M	20
7.6	410	13	2	5M	10
8.8	380	20	1.5	5M	7.5
12	300	54	0.5	5M	2.5
18	220	>100	0.25	5M	1.5
28	150	>100	0.25	5M	1.5

Table 6: Strawman run plan for a QCD critical point search in Run 9 From [57]

For that reason, this study is performed most effectively once the STAR TOF Barrel upgrade is complete in Run 9. A strawman regarding the spacing of the energy points for such a scan, and the time necessary to acquire 5M events at each point is shown in Table 6. It suggests that a comprehensive search to determine the existence of a critical point in the QCD phase diagram can be completed by STAR in a data taking run of order 12 weeks long.

6.2 Polarized proton request in Run 9

Assuming sufficient progress in Run 8, the proton running proposed for Run 9 will likely constitute the conclusion of $\sqrt{s}$ = 200 GeV running dedicated to mapping the gluon polarization as a function of Bjorken x by measuring e.g. inclusive direct photons and γ + jet coincidences. Further data with $\sqrt{s}$ = 500 GeV will then be needed to study the flavor dependence of sea (anti) quark polarization and to extend the measurement of $\Delta g(x)$ to the lowest accessible x Bjorken accessible at RHIC in order to reduce uncertainties from extrapolating into this region. Based on projected progress in Run 8, the time expected to complete the $\sqrt{s}$ = 200 GeV running is 10-15 weeks.

7 Collaboration Readiness

The STAR Operations Group, as well as the STAR Collaboration membership have been participating in an extensive program of shut-down activities in preparation for Run 7, including the installation of the Forward Meson Spectrometer, implementation of an upgraded Vertex Position Detector, and the remoting of the readout boxes for the STAR Silicon Vertex Tracker (SVT). STAR will be fully prepared to begin the program outlined for Run 7.

Steady progress is being made toward the construction of the TOF barrel upgrade that will be substantially implemented in time for a high statistics Au+Au run in FY09. The DAQ1000 upgrade, which will increase STAR's data acquisition throughput by an order of magnitude will be operational by Run 9 as well. A prototype of a new micro-vertex detector designed to operate in tandem with the existing Silicon Strip Detector (SSD) is also planned to be tested during this beam time.

References

[1] W. Fischer *et al*., 'RHIC collider projections (FY2007-FY2008)', BNL internal document.

[2] M. Diefenthaler [HERMES Collaboration], talk presented at 13th Intl. Workshop on Deep Inelastic Scattering, Madison, Wisconsin, April 2005 [hep-ex/0507013].

[3] W. Vogelsang and F. Yuan, Phys. Rev. **D 72**, 054028 (2005).

[4] STAR, B. I. Abelev *et al*., hep-ex/0608030, submitted to Phys. Rev. Lett. .

[5] STAR, F. Simon et al., 'Inclusive Hadron Production in p+p Collisions at STAR', Parallel talk at Conference on the Intersection of Particle and Nuclear Physics CIPANP 2006, June 2006, Puerto Rico.

[6] B. Jager *et al.*, Phys. Rev. **D70**, 034010 (2004).

[7] J. Pumplin *et al.*, J. High Energy Phys. 0207, 012 (2002).

[8] S. Kretzer, Phys. Rev. **D62**, 054001 (2000).

[9] B. A. Kniehl, G. Kramer and B. Potter, Nucl. Phys. **B597**, 337 (2001).

[10] Q.H. Xu, Z.T. Liang, and E.P. Sichtermann, Phys. Rev. **D 73**, 077503 (2006).

[11] STAR, Q.H. Xu et al., 'Inclusive Hadron Production in p+p Collisions at STAR', Parallel talk at Particles and Nuclei International Conference PANIC 2005, October 2005, Santa Fe NM.

[12] M. Stratmann, 'How to extract ΔG from measurements of A_{LL}?', Talk given at the XIV International Workshop on Deep Inelastic Scattering DIS2006, April 2006, Tsukuba, Japan.

[13] S.J. Brodsky, D.S. Hwang and I. Schmidt, Phys. Lett. **B 530**, 99 (2002) and Nucl. Phys. **B 642,** 344 (2002).

[14] D.W. Sivers, Phys. Rev. **D 41**, 83 (1990) and Phys. Rev. **D 43**, 261 (1991).

[15] J.C. Collins, S.F. Heppelmann, G.A. Ladinsky, Nucl. Phys. **B420**, 565 (1994).

[16] R. Seidl, *et al*. [Belle collaboration], Phys. Rev. Lett. **96**, 232002 (2006).

[17] EMC, J. Ashman *et al*., Nucl. Phys. **B328**, 1 (1989); B. W. Filippone and X. D. Ji, Adv. Nucl. Phys. **26**, 1 (2001) and references therein.

[18] D.A. Morozov [STAR collaboration], talk presented at XI Workshop on High Energy Spin Physics, Dubna, September 2005 [hep-ex/0512013].

[19] J.Adams, *et al*. [STAR collaboration], submitted to Phys. Rev. Lett. [nucl-ex/0602011].

[20] STAR, J. Adams *et al*., Phys. Rev. Lett. **92**, 171801 (2004).

[21] D. Boer and W. Vogelsang, Phys. Rev. **D 69**, 094025 (2004).

[22] G. Bunce *et al*., Ann. Rev. Nucl. Part. Sci. **50** (2000) 525; C. Aidala, *et al.* Formal Report BNL-73798-2005 (2005).

[23] S. Albino, B.A. Kniehl, and G. Kramer, Nucl. Phys. B725, 181 (2005).

[24] B.A. Kniehl, G. Kramer and B. Potter, Nucl. Phys. B597, 337 (2001).

[25] I. Vitev, hep-ph/0603010; curves are calculations with initial gluon rapidity density 1150 in 0-10% Au+Au and between 100 and 150 in 40-80% Au+Au collisions.

[26] Preliminary data, J. Ulery (STAR Collaboration), talk presented at Hard Probes 2006 (no writeup as of yet).

[27] M. Cacciari et al, Phys. Rev. Lett 95 122001 (2005); FONLL calculations with CTEQ6M, m_c=1.5 GeV/c^2, m_b = 5 GeV/c^2, and $\mu_{R,F} = m_T$.

[28] J. Adams et al. (STAR Collaboration), nucl-ex/0602011, submitted to Phys. Rev. Lett.

[29] I. Arsene et al. (BRAHMS Collaboration), Phys. Rev. Lett. **93**, 242303 (2004).

[30] D. Kharzeev, Yu.V. Kovchegov, and K. Tuchin, Phys. Lett. B **599**, 23 (2004).

[31] A. Dumitru, A. Hayashigaki, and J. Jalilian-Marian, Nucl. Phys. A **765**, 464 (2006).

[32] D. Kharzeev, Nucl. Phys. A **715**, 35c (2003) ; D. Kharzeev, E. Levin, and L. McLerran, Nucl. Phys. A **748**, 627 (2005).

[33] S.S. Adler et al. (PHENIX Collaboration), nucl-ex/0603017.

[34] V. Guzey, M. Strikman, and W. Vogelsang, Phys. Lett. B **603**, 173 (2004).

[35] L.C. Bland et al., Eur. Phys. J. C **43**, 427 (2005). See also [37].

[36] S. Bültmann et al., Phys. Lett.**B579** (2004) 245.

[37] S. Bültmann et al., Nucl. Instr. Meth. **A535** (2004) 415.

[38] W. Guryn et al., RHIC Proposal R7 (1994) (unpublished).

[39] V. Barone, E. Predazzi, *High-Energy Particle Diffraction*, Texts and Monographs in Physics, Springer-Verlag (2002) ISBN: 3540421076.

[40] S. Donnachie, G. Dosch, P. Landshoff, *Pomeron Physics and QCD*, Cambridge University Press (1998) ISBN: B0006Z3XLM.

[41] A. Bravar, W. Guryn, S.R. Klein, D. Milstead, B. Surrow, J.Phys. G28 (2002) 2885.

[42] E. Leader, *Spin in Particle Physics*, Cambridge University Press (2001), ISBN: 0521020778.

[43] N. H. Buttimore, B. Z. Kopeliovich, E. Leader, J. Soffer, T. L. Trueman, Phys. Rev. **D59**, (1999) 114010.

[44] N.H. Buttimore, E. Leader, T.L. Trueman, Phys. Rev. **D64** (2001) 094021.

[45] E. Leader and T. L.Trueman, Phys. Rev. **D61**, (2000) 077504.

[46] F. Close, Reports on Progress in Physics **51** (1988) 833 and F. Close, A. Kirk and G. Schuler, Phys. Lett. **B477** (2000) 13.

[47] D. Barberis et al., WA102 Collaboration, Phys. Lett. **B479** (2000) 59.

[48] See for example, F. Karsch, "Lattic Results on the QCD Critical Point", RIKEN-BNL Workshop, "Can we discover the QCD Critical Point at RHIC", March 9-10, 2006, Brookhaven National Laboratory: https://www.bnl.gov/riken/QCDRhic/talks.asp

[49] Z. Fodor, S.D. Katz, JHEP 0203:014,2002, hep-lat/0106002

[50] R.V. Gavai, Sourendu Gupta, Phys.Rev.D71:114014,2005, hep-lat/0412035

[51] F. Karsch, hep-lat/0601013

[52] F. Wilczek, hep-ph/0003183

[53] F. Wilczek, Nucl.Phys.A663:3-20,2000, hep-ph/9907340

[54] M.A. Stephanov, K. Rajagopal, E.V. Shuryak, Phys.Rev.Lett.81:4816-4819,1998, hep-ph/9806219

[55] M.A. Stephanov, K. Rajagopal, E.V. Shuryak, Phys.Rev.D60:114028,1999, hep-ph/9903292

[56] P. Sorensen, *STAR Plans for Low Energy Running,* Workshop on Future Prosepcts in QCD at High Energy: A joint EIC2006 and Hot QCD Meeting, July 17-22, 2006, Broohaven National Laboratory: http://rhic.physics.wayne.edu/~bellwied/qcdfp/qcdfp-sorensen.ppt

[57] T. Nayak, "Experiments with STAR near the Critical Point", RIKEN-BNL Workshop, "Can we discover the QCD Critical Point at RHIC", March 9-10, 2006, Brookhaven National Laboratory: https://www.bnl.gov/riken/QCDRhic/talks.asp